THESIS FOR THE DEGREE OF DOCTOR OF PHILOSOPHY

# Automatic Condition Monitoring in the Swedish Power Transmission System Based on Data Analysis

ANDERS LINDSKOG


CHALMERS
UNIVERSITY OF TECHNOLOGY

Division of Electric Power Engineering
Department of Electrical Engineering
Chalmers University of Technology
Gothenburg, Sweden 2024

Automatic Condition Monitoring in the Swedish Power Transmission System Based on Data Analysis
ANDERS LINDSKOG



ISBN 978-91-8103-142-3
Doktorsavhandlingar vid Chalmers tekniska högskola
Ny serie nr 5600
ISSN 0346-718X

Division of Electric Power Engineering
Department of Electrical Engineering
Chalmers University of Technology
SE-412 96 Gothenburg
Telephone +46 31 772 1000

Printed by Chalmers Reproservice
Gothenburg, Sweden 2024

*Automatic Condition Monitoring in the Swedish Power Transmission System Based on Data Analysis*

ANDERS LINDSKOG
Division of Electric Power Engineering
Department of Electrical Engineering
Chalmers University of Technology

# Abstract

Following a campaign in which all energy meters in the Swedish transmission grid were replaced, over 40 high-quality, instantaneous values are continuously collected from each energy meter every three seconds. In 2014, a research project was launched to investigate how this data could be used. This thesis covers selected results from a journey of over ten years, using real-world data to improve the quality and efficiency of the Swedish transmission grid's maintenance (asset management) and operation. It refers to this process as automatic condition monitoring (ACM). Most of the results from the research are now in daily use by Svenska kraftnät, the state-owned transmission system operator in Sweden (Svk), in its operations.

Important results in this thesis includes:

- Development of a general methodology for ACM on how to use substation measurements. This methodology has been used to successfully develop algorithms that can detect specific equipment problems, as well as algorithms that detect previously unknown issues.
- Specific algorithms for automatically detecting individual punctures in capacitor voltage transformers (CVTs). These algorithms were verified over several years of real-world operation across the entire Swedish transmission system. The work led to lower personnel and operational risks, reduced maintenance costs and improved measurement accuracy in the revenue metering process. Over 74 individual punctures were detected using these algorithms. As of October 2024, Svk is monitoring 59 active punctures every day to ensure that the CVTs will not degrade further and explode.
- An in situ calibration algorithm for energy meters. This algorithm uses measurements from energy meters and can simultaneously detect non-linear measurement errors across all energy meters in a substation. It now forms part of an accredited verification process which is regularly used in the transmission system.
- A new $SF_6$ gas leakage detection algorithm has been developed, which offers unprecedented performance. This algorithm can detect small leaks within 15-25 days, unlike other reported algorithms that can take a year (or more) to accomplish the same task.
- Following a thorough investigation regarding the challenges and opportunities of implementing the process bus and digital metering into the substation

design, a new solution has been introduced that offers an efficient digital substation metering solution. The proposal is based on virtualising all accurate metering instruments and hosting them all in a single physical unit, rather than installing several tens of physical instruments in the control building.

**Keywords:** *algorithms*, *asset management*, *capacitor voltage transformer*, *capacitor puncture*, *CCVT*, *CVT*, *health*, *monitoring*, *unbalance*, *energy measuring systems*, *supervision algorithms*, *Kalman filter*, *measurement errors*, *IEC 61850*, *process bus*, *digital metering*, *digital substation*, $SF_6$, *circuit breaker*, *leak detection*.

# Preface

I would like to start by putting this thesis in perspective. Multiple individuals across various organisations have contributed to the overall work of automatic condition monitoring using substation measurements. Working in the real world with realistic problems is not always easy. The lead times for changing or implementing anything new in a transmission system are usually long. The process is also a costly one and involves many people. Thus, this thesis has taken a long time to produce.

The overall project is based, to some extent, on work done and decisions taken as far back as 30 years ago. This work would not have been possible without the replacement of energy meters and the introduction of a country-wide data collection system for those meters. Those two activities started some years before 2010. Shortly after energy meter measurement data became available (in late 2013 or early 2104), the first research project to explore that data commenced.

This thesis covers some of the automatic monitoring that takes place in the Swedish transmission system. It specifically targets what is done with accurate substation measurements acquired from all energy meters in the Swedish transmission system. The emphasis of our work has shifted over the years as different problems (such as instrument transformer failures or other problematic issues) have come to the fore. But the main question has never changed: How can substation measurements and automatic data analysis be used to streamline the daily operation of the Swedish transmission system?

Since it falls to me, Anders Lindskog, as the author, to defend this thesis, I have based it on a portion of the work for which I was the sole or lead researcher. Other activities may be studied in the reports from various research projects that have been conducted over the years. These reports can be accessed via the R&D Department at Svenska kraftnät.

Figure 0.1 gives an overview of how ideas and needs from daily operations have interacted with the research projects being conducted. Initially, there was no thought of writing a thesis. That idea formed around 2020, when I was employed at Svenska kraftnät. My Ph.D studies started in August 2020.

Other transmission systems are similar to the Swedish one but also differ in the type of measurement data that is available and the infrastructure behind that data. I hope this material may inspire other transmission system operators, even if their prerequisites might be slightly different.

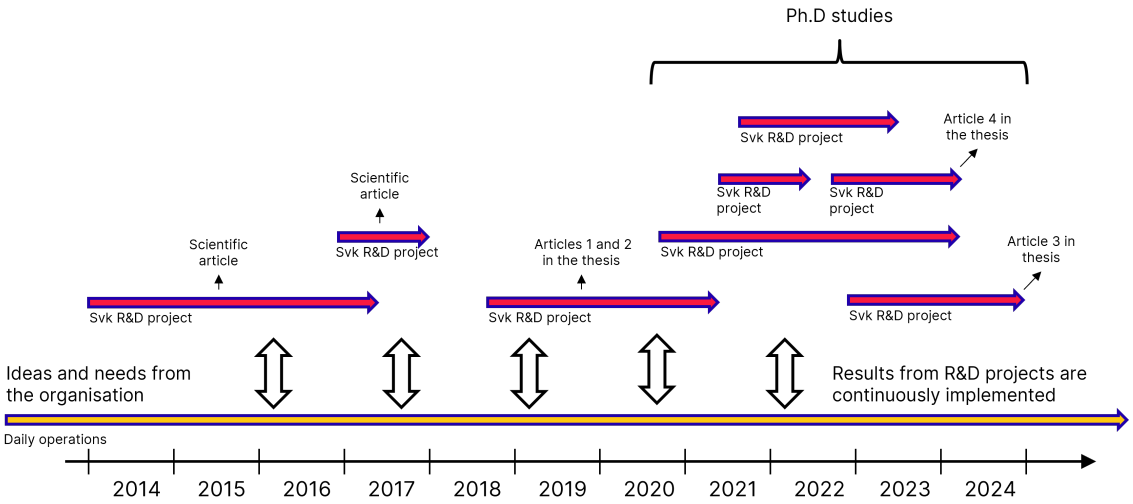


**Figure 0.1:** The background work to producing this thesis (and other reports) has gone on a long while. Ideas and needs from the organisation are developed into R&D projects and the results are implemented in the daily operations. Scientific articles and reports are produced to disseminate results to a wider audience. This is a cost-effective way of testing and implementing new technology and should be encouraged further.

Winston Churchill once said: "Now this is not the end. It is not even the beginning of the end. But it is, perhaps, the end of the beginning". This is my view concerning automatic condition monitoring in the Swedish power transmission system based on data analysis.

# Acknowledgements

Writing this thesis has been challenging and fun. Many people have supported and encouraged me in my efforts.

Firstly, I would like to thank my employer, Svenska kraftnät, for giving me the opportunity to write this thesis. I also want to thank the R&D organisation for supporting various projects over the years. Without the funding we received, our collective work would not have been possible.

Secondly, I want to acknowledge my excellent colleagues and co-authors. By this, I mean everyone at Svenska kraftnät and other organisations who contributed in various ways, large and small, to our quest to use substation measurement data more efficiently. There are well over 100 of you which precludes me from mentioning everyone by name here. However, there are three people I do want to name. Göran "Gotland" Eriksson, by defying gravity, you did things your way to enable this work. Without you, nothing of what we all accomplished would have been possible. Niklas Eriksson, you tirelessly structured the work and made things happen by sheer force of exceptional personality, whilst introducing many fruitful new ideas. Last but not least, my supervisor Torbjörn Thiringer. We have known each other for well over 20 years and I am increasingly enjoying your company. With your patience and vast knowledge, you succeeded where others have failed and got me to finish my thesis.

Thirdly, I have a great many friends who continually encouraged me to finish what I started over 20 years ago. Some of you dropped hints about me being the only one in the room without a Ph.D; that spurred me on to finish.

Lastly and most importantly, I want to thank my immediate family. Max and Albin, it makes me happy that you still want me to be a part of your lives. We play even more now than when you were young, which gives me great pleasure and strength. Jessica, without you, I would have been alone, totally lost in space. With over 30 years both lost in space together, I'm curious where our next chapter, the one we're now writing together, will take us. And of course, thank you to my mum, my sister and my extended family on Jessica's side. Love you all!

*Anders Lindskog*

# List of Abbreviations

| | |
|---|---|
| **AC** | alternating current |
| **ACM** | automatic condition monitoring |
| **AI** | artificial intelligence |
| **APP** | software application |
| **BIPM** | International Bureau of Weights and Measures |
| **CB** | high-voltage circuit breaker |
| **CVT** | capacitor voltage transformer |
| **CVD** | capacitor voltage divider |
| **CT** | current transformer |
| **DC** | direct current |
| **DEM** | digital energy meter |
| **DMP** | digital measurement platform |
| **DS** | digital substation |
| **EM** | energy metering |
| **GDMS** | gas density monitoring system |
| **GNSS** | global navigation satellite system |
| **GOOSE** | generic object-orientated substation event |
| **GUM** | Guide to the Expression of Uncertainty in Measurement |
| **IED** | intelligent electronic device |
| **IT** | instrument transformer |
| **IVT** | inductive voltage transformer |
| **JCGM** | Joint Committee for Guides in Metrology |
| **LPIT** | low-power instrument transformer |
| **NIC** | network interface card |
| **NMI** | National Metrology Institute |
| **NTP** | network time protocol |

| | |
|---|---|
| **PACS** | protection automation and control system |
| **PB** | process bus |
| **PDF** | probability density function |
| **PMU** | phasor measurement unit |
| **PQM** | power quality meter |
| **PRP** | parallel redundancy protocol |
| **PTP** | precision time protocol |
| **SAMU** | stand-alone merging unit |
| **SCU** | switchgear control unit |
| **SF** | software framework |
| **SI** | International System of Units |
| **SV** | sampled value |
| **Svk** | Svenska kraftnät, the state-owned transmission system operator in Sweden |
| **TAI** | International Atomic Time |
| **TSO** | transmission system operator |
| **UTC** | Coordinated Universal Time |
| **VIM** | International Vocabulary of Metrology |
| **VT** | voltage transformer |

# Contents

# Chapter 1

# Introduction

## 1.1 Background and previous work

Although metering systems have been used in transmission systems for many decades, the components within them are constantly changing. More importantly, the collection of measurement data and data analysis has increased dramatically in recent decades. Databases and computing tools are becoming more advanced and less expensive. This enables more efficient, continuous equipment monitoring through data analysis, something this thesis will refer to as ACM.

Svk has invested in data collection systems, databases and computing tools. Svk is continuously exploring different ways of using the collected data to enable more efficient workflows aided by data analysis. Over the last decade, energy-measuring systems have increased in importance, thanks to the accuracy of the data they supply. A nationwide data collection system for energy meters began rolling out in 2013. This system collects instantaneous, high-quality values from the meters every three seconds. The following year (2014), an initial research project was launched to explore how the data could be used to improve the maintenance and operation of the transmission system. The project was successful and revealed many different ways of using the data. Much of this thesis explores ideas originating from this initial research project. Some examples of the work are given below.

**Substation measurements** can be used in different ways. Normally, they serve as a basis for action; for example, when a voltage is too high or when sending an invoice to a customer. The data gathered can also be further processed to determine whether the condition of an equipment will develop into problematic and costly events. Events that are not easily detected using standard, manual, calendar-based maintenance activities. During the work for this thesis, a structured method was developed for applying algorithms to substation data. Many different, problematic events have been detected using methods described in this thesis. A selection of algorithms and events can be studied further in Chapter 4.

**CVTs** are commonly used in high voltage substations because they are cost-effective compared to other types of voltage transformers [1, 2]. These voltage transformers

provide important information for such things as SCADA measurement, protection devices, statistical measurements and revenue metering [2]; information that is vital for the safe and efficient operation of power grids [3].

Like any equipment, CVTs can fail. One common failure mode for a CVT (if not the most common) is punctured capacitor elements [3–5]. This occurs when a capacitor element in the capacitor stack is short-circuited. It starts with one puncture and can progress to several more. Eventually, the stress on the remaining capacitors causes an accelerating capacitor failure rate and, ultimately, the CVT can explode.

Although explosions are uncommon, they introduce risk to personnel, jeopardise system stability and can cause substantial repair costs. Furthermore, if one or more punctured capacitors go undetected for a long time, they can introduce major revenue metering errors that lead to incorrect billing, which is another serious problem.

The literature mentions several novel, online, data-driven algorithms that can be used to find energy measurement errors [6–9]. However, such algorithms do not discriminate between different error sources, such as finding an error in a specific CVT. As punctured CVTs can explode, it is important to monitor these particular components individually.

Using online monitoring to find all puncture events just as they occur provides a basis for implementing a risk-based asset management strategy for CVTs. There is plenty of literature proposing novel, online, data-driven methods for finding errors or error drift in voltage transformers [1–3, 10–15]. These methods can locate the actual component causing the measurement error and, thereby, potentially find the punctured CVTs. Unfortunately, there is a severe lack of available literature on how to monitor punctured CVTs and differentiate dangerous errors caused by punctures from the less dangerous ones caused by other issues.

This thesis considers the problem of finding *individual* punctures in CVTs. There seems to be no method of detecting all individual punctures that is suitable for online monitoring, works on all types of substations and can be implemented cheaply. To the author's knowledge, the only previous contribution addressing the specific problem tackled in this thesis is [5]. However, in that work, only the zero sequence voltage magnitude was used and not its angle. This led to (actual) missed puncture events. Furthermore, in this thesis, new algorithms are introduced that benefit from more sets of three-phase voltage transformers. Assisting algorithms are also introduced to find puncture events for which no continuous data was present when they occurred. This work can be studied further in Chapter 5.

**Revenue energy metering systems** are used to pay and charge market actors for the electric energy that is transferred. To create trust between market actors, such energy must be accurately measured. Therefore, revenue metering is surrounded by legal requirements. One such requirement is regular verification of the metering accuracy. Under Swedish regulations, this takes place in substations every six years. However, many things can degrade the accuracy between verifications. Thus, continual monitoring of revenue metering systems is also required, to ensure identification

of any problems that might degrade accuracy beyond the required levels. Traditionally, this has been a challenging task with low-quality results. The introduction of advanced data analysis has made this task more efficient and more accurate.

There is a large volume of literature covering voltage measurement errors in high voltage substations [1, 2, 11–13]. This is a good start but not sufficient to cover all energy measurement errors since energy meters and current measurement transformers also introduce discrepancies. In 2012, A. Korhonen released interesting work on how to monitor energy measurement errors and energy theft in distribution grids [16]. His work has been improved upon and expanded by several authors over the years [7, 8, 17, 18]. However, Korhonen's work mainly covered low-voltage grids, in which the accuracy requirements were lower and which featured both technical and non-technical losses (like theft). The work is also based on an accurate sum meter and usually contains many downstream meters. On the whole, this approach is not directly transferable to transmission systems, as these substations usually have few meters with similar accuracy. Therefore, previous work has been adapted to high voltage substations and new features are added. This work can be studied further in Chapter 6.

**Increasing awareness** of climate change has focused a lot of attention on fluorinated gases as these have a strong greenhouse effect. Electrical insulation in high-voltage switchgear is normally managed with $SF_6$, thanks to its electrical properties. $SF_6$ is also excellent for extinguishing arcs. Therefore, this gas is widely used in high-voltage high-voltage circuit breakers (CBs) [19–24].

Although $SF_6$ gas has admirable electrical properties, it is unfortunately also the most aggressive greenhouse gas known today [25], with extreme global warming potential. 1 kg of $SF_6$ gas is equivalent to between 22800-26700 kg of $CO_2$ [21, 23–28]. A high voltage substation often has many CBs, all containing $SF_6$. A normal 400 kV CB contains over 20 kg of $SF_6$ and, as an example, there are more than 2,000 CBs in the Swedish transmission system alone. As CBs age, they tend to start leaking, especially in corrosive environments and those operating at low temperatures [27, 29, 30].

Due to the environmentally harmful effects of fluorinated gases, both legislators and high-voltage equipment manufacturers are working hard to completely abandon the use of $SF_6$ gas [23, 25]. For example, the European Commission has proposed legislation that prohibits the use of $SF_6$ in new installations of high-voltage switchgear by the end of 2031 [31]. The manufacturers of switchgear are actively seeking alternate technologies. They have already had some success at lower voltages but higher voltage solutions are still pending [23].

Regardless of whether switchgear manufacturers can supply $SF_6$-free equipment or not, there will still be a large installed body of old equipment that needs to be maintained for 20-50 more years [23]. We can expect regulatory requirements for monitoring this old equipment will be increasingly stringent. The conclusion is that the grid owners will be expected to install supervision systems to detect $SF_6$ gas leakage as early as possible, thus reducing the amount of $SF_6$ gas that escapes into

the atmosphere [23].

Traditional manual monitoring of gas leakage is inefficient and has questionable performance. It is highly advantageous to monitor the gas automatically and quickly find any leaks. Early $SF_6$ gas leakage detection has several positive effects:

- Finding leaks long before electrical properties are (severely) degraded will lower the operational, personnel and equipment risks.
- Early detection of leaks will help to plan maintenance activities in the grid, making asset management more efficient.
- Rapidly finding leaks will reduce the environmental effects as repairs can then be made more quickly.

There are several commercial gas density monitoring systems (GDMSs) on the market that can be used to detect leakage, including sensors, data collection and data analysis products. This thesis favours no specific GDMS vendor and will only shed some light on different problems that may arise, regardless of which monitoring system is used. This thesis provides information that can be used when specifying, purchasing and installing a commercial system or if the grid owner wants to build parts of the system on their own, as was the case for this work.

There are several articles in the field of $SF_6$ gas leak detection [20, 21, 23, 24, 26, 32]. However, the performance of early $SF_6$ gas leak detection is poor and the few solutions that have been proposed are expensive and complicated. Chapter 7 of this thesis presents a novel algorithm for rapid leak detection in CBs.

Introducing **fully digital substations** (including process bus technology) will fundamentally change energy metering and other types of accurate metering in substations. The use of traditional meters must end, with new technology introduced into fully digital substations (DSs). Svk is now building its first DS with process bus (PB) technology compliant with the IEC 61850 standard. In the preamble design process for this pilot substation, it became clear that introducing the PB is problematic for the metering process in several ways. Although the available digital energy meter (DEM) products intended for use with PBs in DSs seem to meet all accuracy requirements [33–35], the lack of standards and legal requirements promoting new technology (such as digital revenue metering) make it even more challenging to use a PB [36]. Secondly, the available products are not yet mature and cannot provide the data that Svk relies on for the ACM activities developed over the years. Thirdly, the available solutions for digital metering using PBs do not take full advantage of the digital technology. To overcome these problems, Svk has developed a proof-of-concept "digital measurement platform" to explore opportunities for further exploiting the process bus. This is described in more detail in Chapter 8.

In summary, as indicated in the preceding text, there are several research gap issues related to automated supervision and the use of PB technology in DSs. In response to these gaps, the next section identifies a number of research questions for discussion in this thesis.

## 1.2 Research questions

Based on the problem overview and rationale of the thesis, the following research questions have been identified:

- **Overall research question:** How can substation measurements and automatic data analysis be used to streamline the operation of a transmission system?

  - **Research subquestion 1:** How can different types of problems be automatically detected using available substation measurements and algorithms? (Chapter 4)

  - **Research subquestion 2:** Is it possible to find equipment problems and pinpoint a specific problem using data analysis? (Chapter 5)

  - **Research subquestion 3:** Is it possible to develop accredited verification methods based on an analysis of energy meter data? (Chapter 6)

  - **Research subquestion 4:** In what way and how quickly and accurately can $SF_6$ gas leakage be detected? (Chapter 7)

  - **Research subquestion 5:** How can metering take advantage of the new opportunities afforded by introducing the process bus in fully digital substations? (Chapter 8)

## 1.3 Method

Model-based measurement relationships have been used to produce the algorithms presented in this thesis. They may entail modelling the behaviours of the three-phase grid or its components. These algorithms act on the measured data and supply one or more outputs that can be analysed in different ways. Three main analysis methods have been identified:

1. Output from general algorithms is analysed using a threshold type of alert.

2. A registered real-world event is compared against model behaviours.

3. Specific model-based algorithms are developed to target a specific use.

The first method is valuable when the subject of the search is unknown. The second is useful in discovering how to target a specific type of issue. The third is used when developing algorithms for specific uses. Often the research process starts with method 1 or 2 and continues with method 3.

The first method was primarily used at the beginning of the research when possible uses of the available data were being investigated. The measurements were used alongside many different models, with suitable alert threshold levels set so as to avoid too many alerts. Using this method enabled the discovery of multiple, previously unknown issues. Examples are provided in Chapter 4.

The second method is used when a real-world issue is found in the grid. The issue is correlated with the model outputs to assess whether the problem can be detected securely, hopefully well before it has a severe impact. An example of the use of this method is presented in Chapter 5.

The third method is used when there is some evidence that an issue can be addressed using a new algorithm. Enhanced models can be created for a specific use. Examples of when this has been used are described in Chapters 5, 6 and 7.

For the work presented in Chapter 8, the combined knowledge from previous work has been used to create a platform that can take ACM to a new level, in which the granularity of detection is much higher and provides a more efficient working platform.

It is important to point out that the research summarised in this thesis has been conducted on real-world measurement data in which all types of impurities can be expected. Therefore, the work is mainly experimental and is verified using real-world events in Svk's substations. Having said that, there is also a good proportion of theoretical verification. Practical work in Svk's substations requires lengthy preparation and is costly. This is why there is sometimes a long lead time between the start of research and its results.

## 1.4 Aims and main contributions of the thesis

This thesis aims to present some of the exploratory work carried out on measurement data from the Swedish transmission system. It aims to share ideas on how ACM can be implemented and used to make operating the transmission grid more safe and efficient. This thesis presents a selection of the total work that has been conducted.

Real substation measurements have been used in developing the algorithms presented in this thesis. These algorithms are used regularly to supervise the metering systems at Svk and have been shown to work in real-world situations. This may be the most important contribution of the work presented in this thesis.

The author hopes that his thesis may provide some inspiration to other transmission system owners and other industrial and academic stakeholders. Hopefully, it will also provide useful information for anyone wanting to follow a similar path to that of Svk.

The main contributions of this thesis are:

1. A discussion on strategies of how to analyse substation measurement data in a structured fashion. (Chapter 4)

2. Demonstration of data analysis methods that can securely detect single capacitor punctures in CVTs. (Chapter 5 based on Article I).

3. Implementation and verification of a data analysis method that can detect and quantify measurement errors and uncertainties in substations in which

all bays are measured. The method can support accredited verification of energy-measuring systems. (Chapter 6 based on Article II)

4. Implementation and verification of a data analysis method for quickly finding $SF_6$ gas leakage in CBs. (Chapter 7 based on Article III)

5. Introduction of a digital measurement platform that extracts more value when the process bus is introduced into a digital substation. (Chapter 8 based on Article IV)

## 1.5 List of publications

The following is a list of publications on which this thesis is based.

**Article I:** A. Lindskog, T. Lindquist, T. Thiringer, "A Data Driven Approach for Monitoring Puncture Events in Capacitor Voltage Transformers" in *IEEE Transaction of Power Delivery*, 2021.

**Article II:** A. Lindskog, P. Jarlemark, S. Svensson, "In Situ Calibration of Transmission System Power Grid Energy Meters Using Energy Measurements and Kalman Filter" in *IEEE Transaction of Power Delivery*, 2022.

**Article III:** A. Lindskog, K. Neandhers, T. Thiringer, "Early $SF_6$ Gas Leakage Detection Through a Novel Comparison Algorithm Based on Pressure Only" in *IEEE Transaction of Power Delivery*, 2024.

**Article IV:** A. Lindskog, N. Eriksson, M. Algehed, T. Arts, U. Norell, H. Svensson, P. Liedholm, D. Reimhult, A. Lööf, "A new value-adding approach for accurate measurements in digital substations using process bus" in *IEEE Transaction of Power Delivery*, 2024. *Submitted under review.*

**Additional related article produced outside the Ph.D studies and not included in this thesis:**

A. Lindskog, E. Viberg, T. Lindquist "Online monitoring of Capacitive Voltage Transformers using energy meters" in *CIGRE SESSION 47, Poster session A3, Transmission and distribution equipment, Paper A3-207*, Cigré, 2018.

## 1.6 Thesis outline

This thesis is organised as follows:

**Chapter 2** gives background information on measurement systems in the Swedish transmission system, to enhance the reader's understanding of this thesis.

**Chapter 3** discusses the basics of measurement errors and uncertainties. It also covers some specific information regarding uncertainties in high-voltage measurements.

**Chapter 4** discusses strategies for how substation measurements can be analysed and provides some examples of simple, general monitoring algorithms used regularly at Svk.

**Chapter 5** presents CVT puncture supervision based on Article I.

**Chapter 6** presents remote metering supervision and calibration based on Article II.

**Chapter 7** presents an SF6 gas leakage detection algorithm based on Article III.

**Chapter 8** presents the digital measurement platform based on Article IV.

**Chapter 9** discusses some general observations from the conducted work.

**Chapter 10** concludes the thesis.

# Chapter 2

# Measuring systems and their components

## 2.1 Introduction

Measuring systems play a vital role in a transmission system because decisions are continuously taken based on measurements. This chapter starts with a general discussion on measuring systems. Since this thesis is based primarily on high-voltage measurements, the components used in high-voltage measuring systems will be discussed in more detail. Since there is an ongoing transition to DSs incorporating PB technology, part of this chapter will be devoted to how this transition will affect high-voltage measuring systems. This discussion is based on common substation configurations in the Swedish transmission system and primarily deals with how to maintain high accuracy to provide high quality data metering data.

## 2.2 General measuring system layout

This section will discuss relevant parts of traditional general measuring systems. A measuring system is often regarded as a sensor connected to a measuring instrument[1]. This is, of course, true in one sense but, as indicated in Figure 2.1, for Svk, a measuring system generally includes at least the following parts:

1. Sensor.
2. Cables.
3. Measuring instrument.
4. Data collection system.
5. Data storage.

[1]Depending on what literature is studied one may find the expressions "measuring instrument", "metering instrument", "measurement instrument" or "instrument". The expressions are slightly different, but the meaning is the same. This is also true for this thesis.

6. Data analysis and presentation of results.

7. Time and time synchronisation.

All parts of a measuring system bring their own challenges and can degrade the accuracy of measurements. Below are some comments on each item listed above.

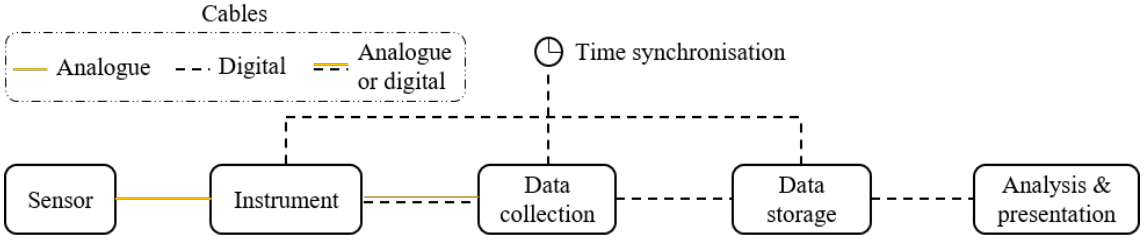


**Figure 2.1:** General measuring system layout.

### 2.2.1 Sensors

The sensor is the part that measures a physical quantity and converts that quantity into a signal that can be interpreted by a measuring instrument. Examples include:

- Instrument transformers (ITs). The two main categories of ITs are the voltage transformers (VTs) and the current transformers (CTs).
- Temperature sensors. One of the most-used temperature sensors is the PT100 element. This sensor changes its resistance according to a well understood function with temperature as its variable. The measuring instrument then converts the resistance to a temperature value.
- Pressure sensor. A pressure sensor often converts an absolute or differential pressure into a scaled 4-20 mA signal. This signal is then interpreted by a measuring instrument.
- Mechanical switch. Used to digitally indicate, say, the position of a circuit breaker as open or closed.

As indicated in Figure 2.1 above, sensors normally supply a signal through measuring cables to a measuring instrument, which then converts the signal into a measurement value. There is a strong trend for measuring instruments to be built into sensors, so they can supply the measured value directly through a digital communication channel. (The $SF_6$ gas sensors used in the work described in Chapter 7 are one example).

### 2.2.2 Cables

Measuring cables connect the sensor to the measuring instrument, allowing the sensor to supply a signal that the instrument converts to a measurement value. Cabling can include relays, screw connectors and other components that can alter a signal. The entire cable system is vital in assuring high accuracy in any measurement.

If a sensor is built into a measuring instrument, the interface is normally a communication cable. The design of the communication cable is not as critical to accuracy, as the digital communication normally does not alter the measured value.

### 2.2.3 Measuring instruments

The measuring instrument is responsible for converting the signal from the sensor into the desired value. Some important measuring instruments at Svk are:

- Measurement transducers.
- Phasor measurement units (PMUs).
- Energy meters.
- Power quality meters (PQMs).
- Digital I/Os.
- Temperature transducers.
- Remote terminal units.

Many types of measuring instruments will require multiple input signals to calculate their output values. For example, the energy meter requires three-phase current and voltage signals to calculate the total power and energy. Most measuring instruments will digitise the input signal and perform mathematical operations on the samples. These mathematical operations will introduce errors and uncertainties but the digitisers (A/D converters) usually introduce the largest ones.

Some measuring instruments (mainly the transducers) will convert signals into other signals which are then interpreted by another measuring instrument. This will add further error and uncertainty to the measured value. Transducers have traditionally been common but the current trend is away from multiple signal conversion steps and towards digitising the signal as early as possible in the measuring chain.

The measuring instruments must operate at a sufficiently high resolution to not introduce further (discretisation) errors.

### 2.2.4 Data collection systems

The value measured by the instrument is normally accessed by a data collection system that gathers the information through a digital communication channel. It might appear that the result is well-defined, if the prior measurement steps are done correctly. Unfortunately, not all measuring instruments attach a timestamp correctly to the values they measure. This makes the design of the data collection system important because it must collect the data and time stamp it. In general, from the perspective of this thesis, a measured value without time stamp cannot be used for further analysis because the uncertainty about when it was measured is too great.

### 2.2.5 Data storage

Since the cost of data storage has gradually come down, it is common for data to be stored for a very long time, in case there is a need to access it later. Provided it is properly designed, such data storage will not normally compromise the values that have been measured. Things like data truncation can occur when storing, compressing or decompressing data. It reduces the data resolution and can increase the level of uncertainty.

### 2.2.6 Data analysis and presentation

The primary goal of metering is to be able to take different kinds of decisions based on the measured values. Every so often, the data has to be processed to allow a decision to be made. Such processing can involve different kinds of measured values being combined through algorithms. The resulting uncertainty in the processed information clearly depends on the quality of the input data and it is important to evaluate the resulting uncertainty carefully. All calculated data must include an uncertainty evaluation and it must be possible to accompany all measured values with an uncertainty evaluation. This will be further discussed in Chapter 3.

### 2.2.7 Time synchronisation

Time synchronisation is often neglected or poorly managed. Since a large volume of measured values is stored, time stamps are important if the data has to be revisited and be sure that it is the correct set. For some analyses, the time of year is enough, while other types require an absolute timestamp better than 1 µs.

Time synchronisation between measurements being compared with each other is important. Poor synchronisation will lead to increased noise and poor convergence in calculations. As indicated in Figure 2.1, time stamps can be made in different parts of the measuring chain. It is advantageous to time stamp as early as possible in the measuring chain because communication delays can vary considerably and cause poor synchronisation accuracy. Given that time synchronisation is important, it is also vital to understand the internal delays within the measuring instrument.

Another common problem is that a measured value is most often calculated based on multiple discrete time samples. This can cause considerable problems if the time stamp setting is not well-defined. The recommendation is to set the time exactly at the middle of the analysed time period.

Time and time synchronisation will have increasing importance for accurate measurements. Time is especially important when designing DSs with PBs, because any synchronisation difference between the measured values will show up as a phase displacement between calculated phasors, which for example, will result in errors in power calculations.

## 2.3 Components used in accurate high-voltage measuring systems

Measurement errors and uncertainties are important factors for energy metering (EM) that are governed by legal requirements. Thus, the following text in this section will focus on high-voltage energy measuring systems. In most cases, this discussion is naturally applicable to other types of measuring systems (like PMUs and PQMs).

The components under discussion here are the ITs (sensors), cabling and energy measuring instruments, because this equipment will introduce most of the errors and uncertainties in the measuring system.

In the following sections, there will be a description of the different parts of a traditional EM system and a DEM system based on the PB using the sampled value (SV). The emphasis is put on those aspects that need to be considered if high accuracy is to be maintained in the measuring systems.

### 2.3.1 Instrument transformers

The purpose of an IT is to transform a primary voltage or current into a scaled copy of the signal, that can be connected to a measuring instrument.

It is impossible to construct instruments that can be connected directly to the primary signals. Therefore, the primary (high-voltage) signals are usually transformed into galvanically isolated proportional secondary signals in the order of tens of volt and a couple of amperes. The secondary signals can be connected directly to the measuring instruments that digitise the signal and perform mathematical operations to complete the measurement task. The goals are a) for the transformation ratio to be exactly as specified and b) for the phase angle to be exactly the same for the primary and secondary signals. Deviations are always present and will introduce errors. If these deviations are known, they can often be corrected for in the measuring instruments.

Instrument transformers are normally standardised and, usually, the transmission system operator (TSO) technical requirement refers to international standards. IEC 61869 is a widely used series of standards for instrument transformers. In the text below, the name convention and standard values will be taken primarily from that series of standards.

#### 2.3.1.1 Transformation ratio, ratio error, phase displacement, burden and accuracy class

Some definitions in the IEC 61869 standard relate to accuracy. The most important ones are described below.

The ITs are specified with a rated transformation ratio, $k_r$, that describes the amplitude relationship between the primary and secondary signals. For currents, the transformation ratio can be expressed as, say, 2000:2, meaning that a rated primary

current, $I_{pr}$, of 2000 A should be transformed into a rated secondary current, $I_{sr}$, of 2 A. In this case, $k_r = 2000/2 = 1000$. For voltages the ratio can be expressed as $k_r = 407\,\mathrm{kV}/\sqrt{3} : 110\,\mathrm{V}/\sqrt{3} = 3700$, meaning that a primary phase voltage of $407\,\mathrm{kV}/\sqrt{3}$ will be converted to a $110\,\mathrm{V}/\sqrt{3}$ signal. (The $\sqrt{3}$ is used to indicate that the voltage is a phase voltage and not the phase-to-phase voltage of the system).

As with all measuring equipment, there is always an error. The amplitude error can be expressed as a ratio error, $\varepsilon$. The ratio error for a CT, can be expressed according to:

$$\varepsilon_i = \frac{k_r I_s - I_p}{I_p} 100\ [\%]\ , \tag{2.1}$$

where $k_r$ is the transformation ratio, $I_p$ is the primary current and $I_s$ is the secondary current. The ratio error is expressed as a percentage.

Likewise, for the VT, the ratio error is expressed as follows:

$$\varepsilon_u = \frac{k_r U_s - U_p}{U_p} 100\ [\%]\ , \tag{2.2}$$

where the $k_r$ is the transformation ratio, $U_p$ is the primary voltage and $U_s$ is the secondary voltage.

A sinusoidal signal can be expressed as a vector (phasor) with a length and an angle related to a reference system. The angle difference between two vectors in the same reference system is called a phase displacement, denoted $\Delta\varphi$.

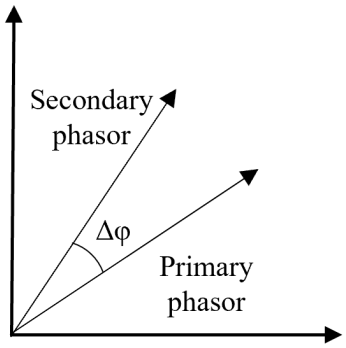


**Figure 2.2:** Phase displacement, $\Delta\varphi$, between primary and secondary phasors.

The phase displacement between the primary and secondary phasor is shown in Figure 2.2. In this case, the primary phasor lags behind the secondary phasor and the phase displacement is positive. The phase displacement is an angle often stated as (arc) minute (or sometimes centiradian) and is defined as: $\Delta\varphi = \varphi_s - \varphi_p$ .

The rated output design parameter, also referred to as the burden capability, states the power range an IT can supply to the secondary measuring circuit whilst remaining in its accuracy class. The burden is usually expressed in volt-amperes [VA] and can be measured on the secondary side of the IT. The burden can be resistive,

capacitive or reactive depending on the impedance in the measuring circuit. The burden will affect both the ratio error and the phase displacement.

Another important design parameter is the rated accuracy class and relates to the uncertainty of the secondary signal from the IT. The accuracy class information should be interpreted as if the IT is used within its stated design limits, the accuracy will also reside within its class limits. The accuracy class defines limits for both the ratio error and the phase displacement.

Apart from the specifications above, all ITs will normally be accompanied with a factory accuracy test report. For accurate measurement, it is possible to use the information to correct the individual measurements for the actual burden supplied by the ITs. Such corrections can be made for both ratio error and phase displacement.

#### 2.3.1.2 Traditional CTs

As described earlier, two main parameters for a CT are the primary and secondary rated currents, $I_{pr}$ and $I_{sr}$. The numbers will state the normal operating range of the CT and the transformation ratio. The primary value is chosen to fit the measured application, while the secondary value is chosen to suite measuring instruments.

Table 2.1 presents common accuracy classes, according to IEC 61869-2 and shows both the maximum allowed ratio error (amplitude error) and phase displacement. As indicated in the figure, the difference between the first four classes and the two "S" classes are that the "S" classes will maintain their accuracy further down in current amplitudes.

**Table 2.1:** CT standard accuracy classes according to the standard IEC 61869-2.

| CT accuracy classes | | | | | | | | | | |
|---|---|---|---|---|---|---|---|---|---|---|
| Accuracy class | Current ratio error ($\varepsilon_i$) ± % | | | | | Phase displacement ($\Delta\varphi_i$) ± minutes | | | | |
| | at current (% of rated) | | | | | at current (% of rated) | | | | |
| | 1 | 5 | 20 | 100 | 120 | 1 | 5 | 20 | 100 | 120 |
| 0.1 | - | 0.4 | 0.2 | 0.1 | 0.1 | - | 15 | 8 | 5 | 5 |
| 0.2 | - | 0.75 | 0.35 | 0.2 | 0.2 | - | 30 | 15 | 10 | 10 |
| 0.5 | - | 1.5 | 0.75 | 0.5 | 0.5 | - | 90 | 45 | 30 | 30 |
| 1 | - | 3 | 1.5 | 1.0 | 1.0 | - | 180 | 90 | 60 | 60 |
| 0.2S | 0.75 | 0.35 | 0.2 | 0.2 | 0.2 | 30 | 15 | 10 | 10 | 10 |
| 0.5S | 1.5 | 0.75 | 0.5 | 0.5 | 0.5 | 90 | 45 | 30 | 30 | 30 |

Figure 2.3 examines a model of a CT. It describes how the CT can be modelled and what to expect in terms of phase displacement and amplitude error.

The model consists of a primary and a secondary side. Between the two sides, there is an ideal transformer. On the secondary side, the magnetisation circuit with impedances $X_m$ and $R_m$ is modelled alongside the winding resistance $R_{CT}$. The CT is connected to an instrument that acts like an electric load (burden) to the CT, with the load modelled by $R_b$ and $X_b$.

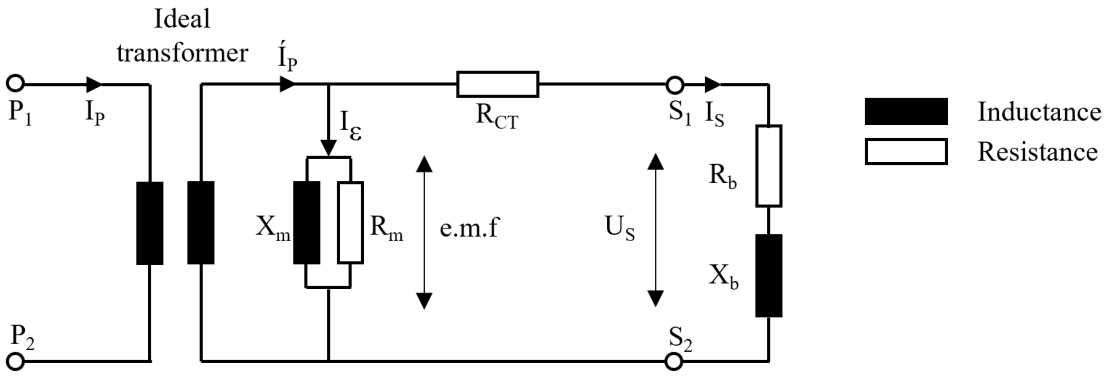


**Figure 2.3:** Simplified (linear) equivalent circuit of the CT.

The secondary current, $I_s$, is the sum of the magnetisation current, $I_\varepsilon$, and the transformation-ratio-corrected primary current, $I_p^{'} = I_p/k_r$. If the magnetisation current is low, both phase displacement and amplitude error will be low. The magnetisation current depends on the magnetic core characteristics, and a high-performance core material will make the CT more accurate. The model presented in Figure 2.3, makes it possible to study how the burden will affect the errors in the CT.

The simplified explanation of the working principle of a CT is that the load on the CT through $R_b$ and $X_b$ will create a voltage, $U_s$, over the secondary terminals, $S_1$ and $S_2$ . This voltage, added to the voltage over the winding resistance, $R_{CT}$, will sum up to the e.m.f, acting on the core. The e.m.f will create the magnetisation current, $I_\varepsilon$. It is now possible to analyse how both the amplitude and phase of the current through the burden will affect both the ratio error and phase displacement. The non-linearities in the core material cause variations in ratio error and phase displacement over the operating range of the CT. (Note that the linear model presented in Figure 2.3 will not describe the variations without having measured the non-linearities in the core material).

Table 2.2 presents the results of an accuracy test report. The test was performed under two different burdens. The first was 1 VA and a unity power factor (denoted PF) and the second was at 30 VA and a power factor of 0.8.

**Table 2.2:** Test report accuracy result for a 30 VA, 2000:2, 420 kV, 0.2S CT with an over-current capability of 200 %.

| Current (% of rated) | 1 | 5 | 20 | 100 | 200 | VA | PF |
|---|---|---|---|---|---|---|---|
| Ratio error [%] | 0.09 | 0.10 | 0.10 | 0.10 | 0.10 | 1 | 1 |
| Phase displacement [minutes] | -1 | 0 | 0 | 0 | 0 | 1 | 1 |
| Ratio error [%] | 0.03 | 0.04 | 0.05 | 0.06 | 0.05 | 30 | 0.8 |
| Phase displacement [minutes] | 1 | 1 | 1 | 0 | 1 | 30 | 0.8 |

Figure 2.4 presents the values from Table 2.2 as two graphs and includes the accuracy class limits. Figure 2.4a presents the ratio error, while 2.4b shows the phase displacement.

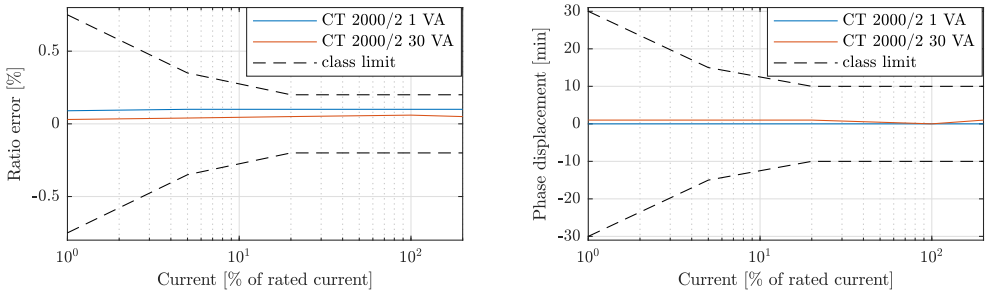


**(a)** Measured CT ratio error.

**(b)** Measured CT phase displacement.

**Figure 2.4:** Measured CT error and class limits according Table 2.2. (Note that the x-axis is presented as a log-scale).

In this particular case, the CT is exceptionally stable over the entire operation range and performs well, within the accuracy class limits. This CT is also not very burden-dependent. From the model, we should normally expect the ratio errors to move down with increased burden and the phase displacement to move up. However, this will depend on the burden's power factor and the non-linearities in the core material.

#### 2.3.1.3 Traditional VTs

The most common type of VT at Svk is the CVT, because of its favourable cost-performance ratio. The inductive voltage transformer (IVT) is the second most common VT in the Swedish transmission system.

The IVT is a traditional transformer with copper winding and a magnetic core, while the CVT has a capacitor voltage divider (CVD), to bring the voltage level down and is connected to a phase-compensating circuit and a traditional voltage transformer (as shown in Figure 5.1).

Important design parameters for a VT are the primary and secondary rated voltages, $U_{pr}$ and $U_{sr}$. The numbers state the rated transformation ratio. Another important parameter is the rated output (burden capability). The VTs are normally specified to measure within the accuracy class between two different burdens and should be zero adjusted at 50 % (Svk requirement) of the maximum specified burden.

The standard accuracy classes for a VT appear in Table 2.3. Unlike a CT, a VT will experience a small span of voltages around the nominal voltage and is also not very sensitive to voltage changes. Thus, there is no need for multiple calibration points at different voltages. However, the VT is burden-sensitive. A normal accuracy test report will have measured calibration points on at least two different burdens.

Figure 2.5 allows us to study multiple calibration points at different burdens and voltage levels on a class 0.2 CVT according to the standard IEC 61869-5. The blue markers are voltage calibration points (1 VA at unity power factor), while the red markers are calibration points at 50 VA, with a power factor equal to 0.8 (inductive). The figure also shows the class limits and when the burden changes, the ratio error evidently changes more compared to the phase displacement (relative to the class

**Table 2.3:** VT (IVT and CVT) standard accuracy classes according to the standards IEC 61869-3 and -5

| IVT standard accuracy classes | | |
|---|---|---|
| Accuracy class | Voltage ratio error ($\varepsilon_u$) ± % | Phase displacement ($\Delta\varphi_u$) ± minutes |
| 0.1 | 0.1 | 5 |
| 0.2 | 0.2 | 10 |
| 0.5 | 0.5 | 20 |
| 1.0 | 1.0 | 40 |
| 3.0 | 3.0 | Not specified |
| CVT standard accuracy classes | | |
| Accuracy class | Voltage ratio error ($\varepsilon_u$) ± % | Phase displacement ($\Delta\varphi_u$) ± minutes |
| 0.2 | 0.2 | 10 |
| 0.5 | 0.5 | 20 |
| 1.0 | 1.0 | 40 |
| 3.0 | 3.0 | Not specified |

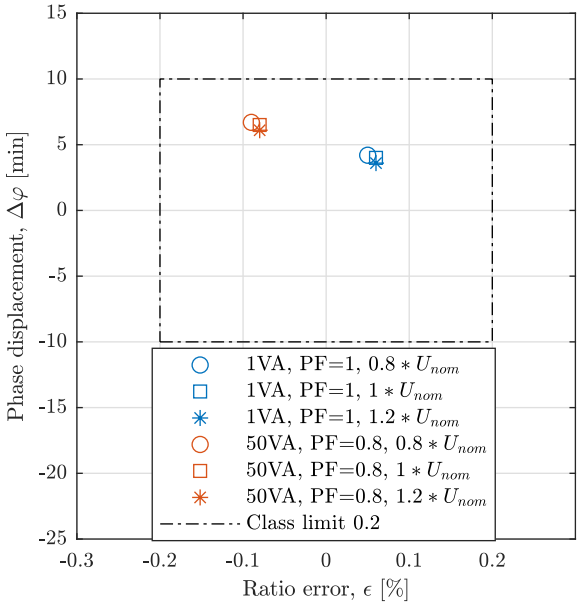


**Figure 2.5:** Measured ratio error and phase displacement at nominal voltage for a CVT in conjunction with its 0.2 class limits according to the standard IEC 61869-5.

limits).

### 2.3.2 Measuring cables

Traditional ITs are connected to measuring instruments via cables. Since the cabling between ITs and measuring instruments can be several hundred meters long and contain many different components (like screw connectors, fuses and relays), they can introduce major errors if not properly designed.

#### 2.3.2.1 Cables for CTs

The impedance connected to a CT should be as low as possible. A high burden will produce a high magnetisation current and, thereby, a greater ratio error and phase displacement. Often, the majority of the burden will come from the measuring cables. This is especially true when long cables are needed between a bay and the control building. It is important to design the cabling with enough cross-sectional area to not exceed the CT's burden rating.

In Sweden, the standard substation is a two-busbar, two-breaker design. This means there are two CTs per phase in each bay, which measure the currents to each busbar separately. To use a single measuring instrument for the two currents, they must be summed before entering the instrument, as indicated in Figure 2.8. This is done by connecting the two separate measuring cores in each CTs in parallel.

#### 2.3.2.2 Cables for VTs

The impedance connected to a VT should be as high as possible. This may seem a simple task for the measuring cables but, since the measuring instruments do not have infinite impedance, there will be a considerable voltage drop on the cables if they are not designed properly. The cables should have a low impedance to work well. In addition to the cable itself, there are also other components included in the cable circuit (like fuses and screw terminals) that can cause additional impedance and introduce major measurement errors.

To reduce the number of VTs in substations, one VT can be shared between multiple measuring circuits. In these configurations, there is also a voltage selection relay, that switches the voltage to the instruments between different VTs depending on the state of operation. This is not normally a problem, as long as the impedance in the secondary measuring circuit and the burden are kept under control. But it will create small voltage jumps that adds challenges for ACM.

### 2.3.3 Energy measuring instruments

#### 2.3.3.1 Traditional energy meters

Modern energy meters will digitise the analogue secondary voltages and currents in their internal A/D converters. The digitised information is then processed using different types of algorithms to finalise the measurement task.

There are standards, like IEC 62052-22, that put accuracy demands on the energy meter. In Figure 2.6, the measurement class limits for a 0.2S energy meter can be

studied, alongside typical calibration results of an energy meter used by Svk.

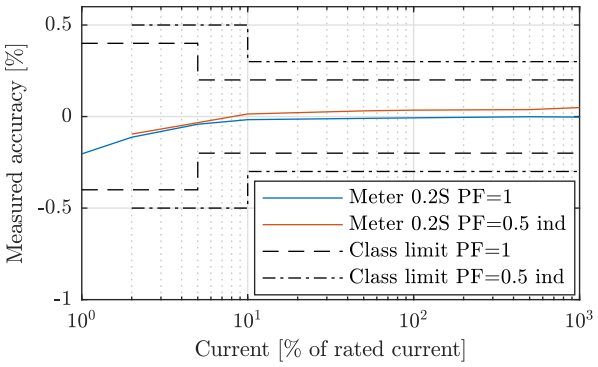


**Figure 2.6:** A 0.2S energy meter calibration with its accuracy class limits according to the standard IEC 62052-22.

Many advanced energy meters include the option to correct both the voltage and current ratio error and the phase displacement. In some meters, it is possible to introduce correction factors for multiple current amplitudes and thus correct the measurements of varying errors across the whole range of measured currents. Interpolation is carried out between the current correction points.

#### 2.3.3.2 Digital energy meters using SV

In a DS with PB, the measured quantity is digitised within or close to the ITs. The digitised signal is transmitted through a communication network to the digital energy meter.

Most of the inaccuracies in a traditional energy meter will appear during the digitisation of the analogue voltages and currents. Only a small proportion comes from the algorithms applied to the samples. This means that the old classification of the energy meter for a DS is no longer appropriate. The inaccuracies are split between an external digitiser and the calculation. There is evidence in the literature that the calculation errors can be as small as 0.01-0.02 % [34,35], while in reality meters can behave differently. Either way, there is a need for a well developed standard for DEMs using SV.

SV from an external digitiser, like a stand-alone merging unit (SAMU), is a discrete representation of an analogue signal. The most common way to work with discrete values is to move from the time domain to the frequency domain, using Digital Fourier Transform (DFT). In that process, a number of factors will affect the accuracy of the calculation. Some important reported factors in the literature are:

- Amplitude noise.
- Phase noise (time jitter).
- Discretisation.

- Spectral leakage.

Amplitude noise will normally create measurement errors on measurements with a high reporting rate, such as PMUs. Energy measurements suffer less from measurement noise because the noise will average out over the measurement period (normally 15 minutes or an hour).

The discretisation process of the analogue signal to SV normally produce integers with a scale factor. Scale factors according to IEC 61869-9 are 0.01 for voltages and 0.001 for currents in each discrete step. This will not have any practical implication in a high-voltage grid with high voltages and currents, but needs to be considered for measurements of very low voltages or currents [37].

Phase noise is due to the fact that the A/D conversion is not made at exactly the correct time and jitters back and forth between samples. High levels of phase noise will make the grid frequency determination inaccurate. This, in turn, will have a negative effect on the opportunity to compensate for spectral leakage.

There is a computational error called spectral leakage, caused by the grid frequency and the sample frequency not being adjusted to each other. In traditional high-quality measuring instruments, like energy meters and PQMs, the sampling frequency is normally locked to the grid frequency. In this way, the spectral leakage is more or less eliminated. SAMUs on the other hand always have a fixed sampling frequency governed by an accurate clock. If the frequency can be estimated properly, it is possible to compensate for spectral leakage by various methods [37].

#### 2.3.3.3 SAMU

As described in Section 2.3.3.2, the SAMU will take over some of the responsibilities of the traditional energy meter in order to produce high accuracy measurements. As demonstrated in Figure 2.7, the SAMU will convert a continuous analogue secondary signal into SV. However, while doing so it may introduce errors. The main errors are:

- Measurement noise.
- Amplitude error (ratio error).
- Phase error (time error).

Measurement noise has two components. The time component, that indicates that the actual SV time is jittering around the nominal SV time stamp and the amplitude component, which is noise in the registered value. The measurement noise is reduced by using a carefully designed SAMU. The amplitude error is a systematic error that can be reduced by calibration and correction. The phase error is a static time offset originating from a poor internal or external clock design and can also be reduced with a calibration and correction.

Different types of measurements require attention to different details. The SAMU has to perform well for all types of measurements because the produced SV will be

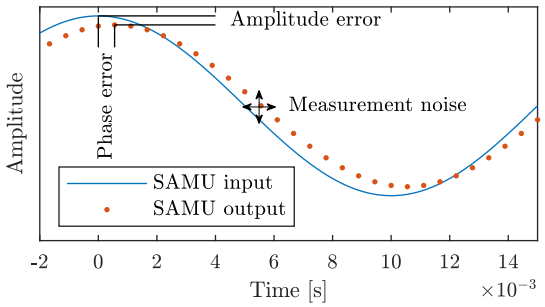


**Figure 2.7:** SAMU input and output based on a 50 Hz signal showing fictive errors and measurement noise.

used for several types of measurement tasks. This has been recognised and recently the standard IEC 61869-13 including important demands has been released.

The standard SAMU accuracy classes defined in IEC 61869-13 can be studied in Table 2.4. $K_{I_{min}}$ and $K_{I_{max}}$ are measuring class dynamic range lower and upper limit factors and are defined by the SAMU producer. They are stated as a percentage of the rated input current and define the dynamic working range of the SAMU.

**Table 2.4:** SAMU accuracy classes according to IEC 61869-13.

| SAMU accuracy classes | | | | | | | | |
|---|---|---|---|---|---|---|---|---|
| Accuracy class | Current ratio error ± % | | | | Phase error ± minutes | | | |
| | at % of rated current | | | | at % of rated current | | | |
| | $K_{I_{min}}/4$ | $K_{I_{min}}$ | 100 | $K_{I_{max}}$ | $K_{I_{min}}/4$ | $K_{I_{min}}$ | 100 | $K_{I_{max}}$ |
| 0.05 | 0.1 | 0.05 | 0.05 | 0.05 | 5 | 2,5 | 2,5 | 2,5 |
| 0.1 | 0.2 | 0.1 | 0.1 | 0.1 | 10 | 5 | 5 | 5 |
| 0.2 | 0.4 | 0.2 | 0.2 | 0.2 | 20 | 10 | 10 | 10 |
| 0.5 | 1.0 | 0.5 | 0.5 | 0.5 | 60 | 30 | 30 | 30 |
| 1 | 2.0 | 1.0 | 1.0 | 1.0 | 120 | 60 | 60 | 60 |

## 2.4 Substation high-voltage metering

Metering[2] in traditional substations has evolved over a long time and its accuracy is high. Measuring instrument providers have specialised in different types of product like energy meters, PQMs and PMUs. These instruments are normally delivered as separate units, in which the three-phase secondary signals from the ITs, are connected and converted to digital signals within each unit. After application-specific calculations have been performed to complete the measurement tasks, the processed values can be collected from the instruments.

### 2.4.1 Traditional metering configuration

In the Swedish transmission system, the most common substation is the double busbar double breaker design. The population of substations spans from one to twelve bays (soon also thirteen), averaging between five and six bays. The voltage is measured centrally in the bay. The current to the two busbars is led via circuit breakers. Measuring cables are connected between the ITs in the switch yard and routed to the instruments in the control building. As mentioned earlier, the cable length between the ITs and instruments can be several hundred meters.

Voltage is measured at a (central) position in the bay and the signal is supplied to both the protection automation and control system (PACS) IEDs[3] and the measuring systems (energy meter, PQM, PMU etc.). The currents to both busbars are measured, as seen in Figure 2.8[4]. The CT has five independent cores (not explicitly shown in the figure), comprising one measuring core and four protection cores. The protection cores are mainly used by the PACS, while the measuring core is connected to the measuring systems that require higher accuracy. Some functions in the PACS also use the measuring core.

Traditional measuring instruments usually only read three voltages and three currents. Therefore, the currents are physically connected in parallel to sum the current to the two busbars, before entering the instrument. There may be a large current flow between the busbars, which can result in that only a small portion of the current flow is supplied to the object being measured. This situation is unfavourable due to its large uncertainty. Another problem is that the measuring cores of the summed currents will interact with each other, introducing additional small errors and uncertainties. Summing the two currents introduces additional uncertainties in the measurement and is prohibited from use in revenue energy-measuring systems at Svk.

[2]This thesis commonly uses the word metering. It should be understood as accurate metering performed for other use than for the protection and control of a substation.

[3]The term intelligent electronic device (IED) is commonly used when discussing (digital) substations and PACS. It is normally understood as a micro-processor-based controller of power system components. IEDs perform measurement tasks for protection and control but can also carry out other types of measurement task. This thesis will subsequently use the term IED as a part of the PACS.

[4]This text introduces figures to show different measuring circuit configurations. For simplicity, the figures are single-line diagrams but, in reality, there are three phases.

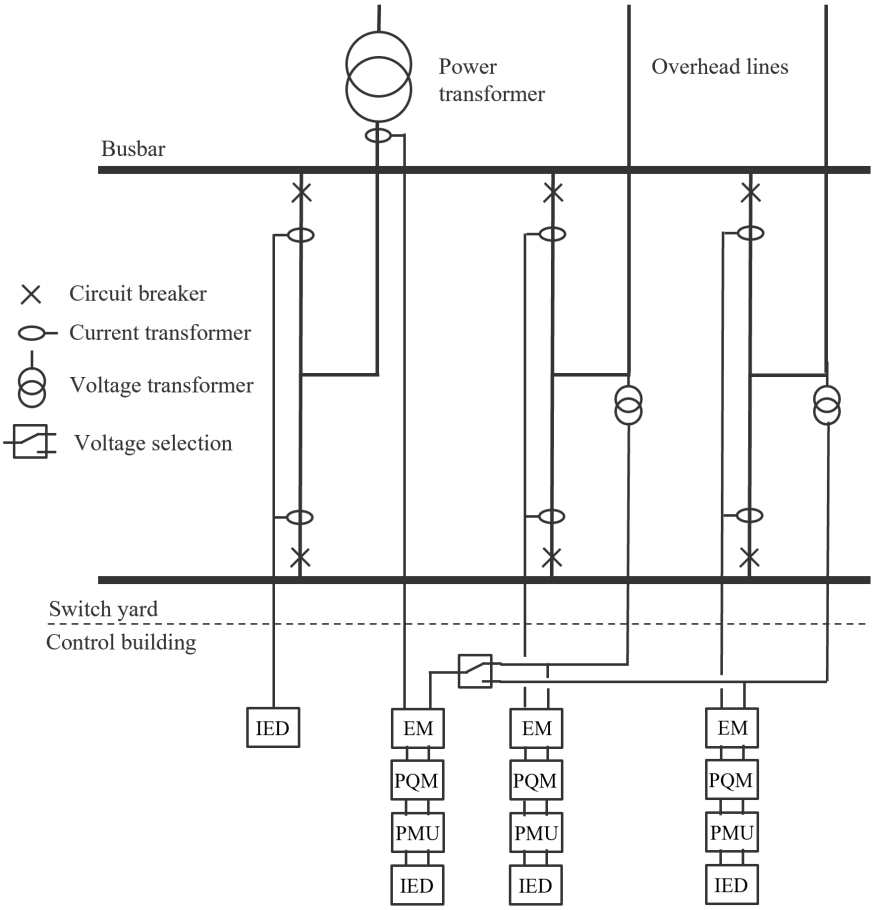


**Figure 2.8:** Conceptual traditional substation measuring design layout.

Since the procedure of summing the two busbar currents is not suitable for revenue metering, a single set of current transformers is used for this purpose. Usually, the revenue metering point is a power transformer connected between a high voltage (in Svk's case the TSO-level) and a lower voltage grid, using the measuring cores in the power transformer bushings. This is indicated in Figure 2.8.

A voltage selection scheme is often implemented to reduce the number of voltage transformers in a substation. This means that some bays are not equipped with voltage transformers and the measuring instruments receive their voltage from other sets of voltage transformers in the substation. The selection is made using a logic circuit that takes a decision based on whether the circuit breakers are in an open or closed state. The logic circuit manoeuvres one or more physical relays that direct the selected voltage to the measuring instruments. This is also indicated in Figure 2.8.

Normally, multiple measuring instruments are connected to both the voltage and current ITs. All instruments have their own A/D conversion and thus, contribute to the total burden (electric load) supplied by the ITs.

#### 2.4.1.1 Shortcomings of the traditional configuration

The practices used in designing the measuring systems of traditional substations have evolved over the years and satisfy both internal (operational) and external (legal) requirements. However, some flaws remain to be addressed to enhance the accuracy in measurements.

As mentioned in Section 2.4.1, the current summation adds errors and uncertainties to the measurements. These errors and uncertainties, introduced by summing the currents, make the connection design unsuitable and this is not allowed in revenue metering. Having said that, summing the currents does work well in normal operation. Summing the currents has two main negative effects: Firstly, the measurements in the bays with current summation will have higher uncertainties compared to when a single set of current transformers is used for metering. Secondly, another set of current transformers may have to be installed solely for revenue metering purposes.

The voltage selection scheme will switch voltages depending on the actual operation mode of the substation. Switching the voltages between VTs will change the burden on the voltage transformers. A change of burden will also change the voltage reading slightly. Moreover, after sustained operation, the selection relays can cause extra impedance. All this will decrease the accuracy and increase the uncertainty.

Since multiple instruments will be connected to the measuring circuit, the total burden imposed on the instrument transformers will increase for each instrument. This can normally be handled but if instruments are added, replaced or removed, the burden will be altered. This will alter the measurements and may require a re-calibration to retain high accuracy (which is sometimes omitted).

When there are long measuring cables for bays located far from the control building, these cables must be dimensioned with a large cross-sectional area not to exceed the

burden capability of the CTs. The cost will increase and, for metering purposes, it is impractical to install large cables.

### 2.4.2 Digital metering

It is challenging (but can also be very rewarding) to introduce the PB and SVs into the measurement tasks. This section includes a more detailed description of digital metering, together with some advantages and challenges of the technology. Chapter 8 will add further comments on how overall measurement efficiency can be enhanced by using the PB. Below the digital metering configuration is described in the context of the standard Svk substation design.

#### 2.4.2.1 Available digital metering technology

The introduction of the IEC 61850 digital substation standard, including the PB, fundamentally change accurate metering and has brought new advantages and challenges. The IEC 61850 standard was primarily designed for PACS and the accurate metering part has been neglected for many years. This has led to digital metering not yet being mature. Indeed, when it comes to development, both standards and equipment are still lagging behind [36]. This introduces challenges in terms of implementing PB in modern substations. The protection and control can be implemented according to IEC 61850 but traditional revenue metering may have to be implemented to meet legislative demands; something which is not optimal for the overall substation design.

In DSs including a PB, the use of low-power instrument transformers (LPITs) provides interesting advantages. LPITs, such as the optical current transformer, often digitise the measured primary values within the transformer, with the signal from the different ITs grouped into a merging unit. This merging unit will provide SV to the measuring instruments and other IEDs in the control building. When traditional ITs are used in a DS, the analogue signals are instead digitised in SAMUs often placed in outdoor marshalling cubicles, close to the ITs in the switch yard. The introduction of LPITs is ongoing. Many TSOs are reluctant to use such ITs since the technologies are still maturing and, as yet, there is no solid proof of performance over time for all such products. Like other TSOs, Svk is also hesitant to use LPITs. For these reasons, the digital pilot substation will use traditional ITs and SAMUs. Therefore, this thesis is primarily concerned with SAMUs and conventional ITs but the rationale should carry over naturally to LPIT designs as well.

#### 2.4.2.2 Important differences between traditional and digital energy metering in substations

The main difference between traditional and digital metering is that the digitisation of the analogue signal is made at the ITs and not in the measuring instrument as such. Figure 2.9 allows this difference to be studied. In a traditional measuring system, the secondary measuring cables from the ITs are routed all the way from the switchyard into the control building where the measuring instruments are mounted. Meanwhile, in the digital measuring system, the digitisation is made close to the ITs with a SAMU (or for some types of ITs directly within the unit). The SVs are sent

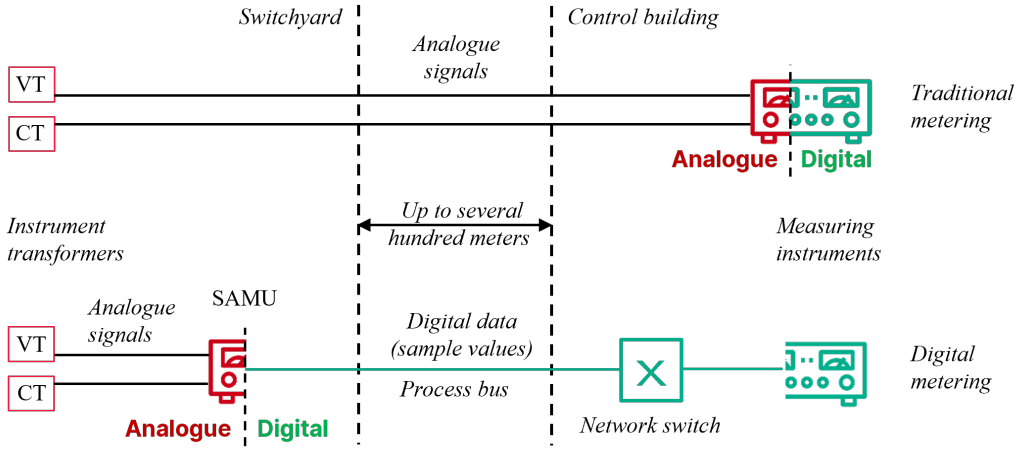


**Figure 2.9:** The figure indicates differences between traditional and digital measuring systems. The main differences are that the analogue signals are digitised already in the switchyard close to the ITs and that the measuring instrument is divided into a digitiser and computing unit for the digital measuring chain.

via the process bus to any instrument that wants to subscribe to the information.

The measuring task is split between the SAMU and the measuring instrument. In traditional measuring instruments, the digitisation of all relevant signals takes place within the instrument, making the time synchronisation between the signals easy. However, in a DS, there is no guarantee that the digitisation of all relevant signals will be made in one and the same SAMU. This means that time synchronisation is becoming more critical in a DS, as illustrated in Figure 2.10.

In a traditional substation, the current signals will be physically summed before entering the measuring instrument. In a DS, the currents to the two busbars will be measured separately and need to be summed (mathematically) during the calculation in the digital measuring instrument. Physical summation of currents is not allowed for revenue metering, which will require a further set of CTs in a traditional substation, which can potentially be avoided in a DS.

The differences between the traditional energy-measuring system and the proposed DEM system using SAMUs introduce a few different aspects that need to be considered:

- There is only one SAMU connected to any of the ITs, in contrast to multiple instruments in the traditional setup. This will lower the the total burden on the ITs.
- The SAMU will be installed in a marshalling cubicle close to the ITs and the cabling will be short compared to the traditional setup.
- The A/D-conversion of all voltages and currents are not necessarily made in the same SAMU. This means that the relative synchronisation between the measured values may not be as good as in a traditional meter.

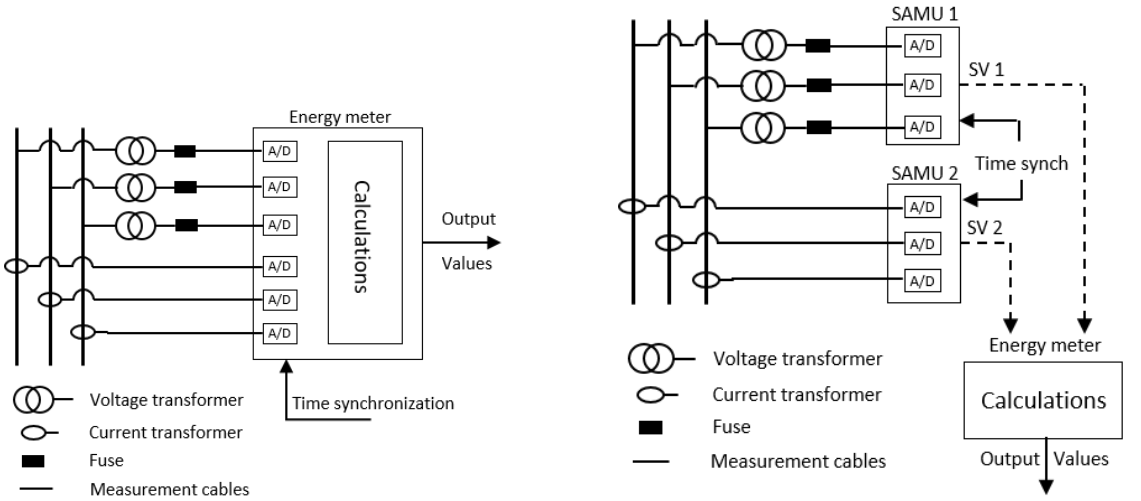


**(a)** In a traditional high-voltage energy-measuring system all A/D converters are synchronised within one instrument.

**(b)** In a digital high-voltage energy-measuring system the digitised signal can come from several units that are separately synchronized.

**Figure 2.10:** In a digital energy-measuring system time synchronisation efforts are more important, since poor synchronisation between between units included in the measuring chain can cause large measuring errors.

- The traditional energy-measuring task is split between the SAMU and the DEM in the digital metering chain.

In principle, the first two differences are positive for the overall stability and accuracy of the system because of the lowered burden on the SAMU, with reduced challenges concerning burden and the measuring cables. The second difference may introduce some problems since the SAMUs are placed in a cubicle close to the ITs, in which the temperature will vary more than inside the control building. This will create errors if the SAMU is not designed properly.

The traditional energy meter contains all (usually six) A/D converters that are synchronised to each other within the meter. The synchronisation in modern high accuracy energy meters is normally better than 100 ns, which enables high relative phase angle accuracy between current and voltages. This, in turn, makes it possible to accurately calculate active and reactive power. Since the voltage and current measurement in a DS may come from different SAMUs, the synchronisation between the A/D converters (in different SAMUs) will depend on the central synchronisation in the substation. Poor time synchronisation will introduce an extra phase displacement error.

The last difference is mainly a challenge because we are not used to splitting the A/D conversion and calculation into two separate units and there is not yet a standardised way of handling the configuration. A standard that defines the accuracy class for the calculation stage is needed.

#### 2.4.2.3 Digital metering configuration with available technology

As mentioned earlier, in a DS with a PB, the digitisation of the analogue secondary signals (from the ITs) is done close to the primary equipment. A SAMU will be installed in a marshalling cubicle placed approximately 10-20 meters from the ITs (as opposed to several hundred meters in a traditional substation). The burden on the ITs is low since only one SAMU is required to be connected to each IT and the cable lengths are short. The SAMU will publish the SV streams through a communication network to any IED or measuring instrument in the control building that needs to subscribe to the information. They can all share the same SV streams.

The SAMUs are often combined with a switchgear control unit (SCU) that manoeuvres the circuit breakers and registers whether they are open or closed. This information is also transmitted through the PB via generic object-orientated substation event (GOOSE) messages that can be received by any equipment connected to the PB.

PMU and simple PQM functions are sometimes virtualised within a protection and control IED, or can be supplied as separate units. The DEMs used with SVs, on the other hand, are still supplied as separate units. So far, the search for class A PQM using SV has not been successful.

Figure 2.11 presents a conceptual design layout of an accurate digital metering system. With the available technology, some measurement functions can be combined within other IEDs but since the DEMs are separate units not capable of summing the two busbar currents from different SV streams, two DEMs installed for each bay is needed, rather than one as in a traditional substation. This will increase the number of instruments that must be installed in the control building, compared to the traditional substation metering design. Thus, the digital design with available instruments has a number of disadvantages. Solutions to this will be discussed further in Chapter 8.

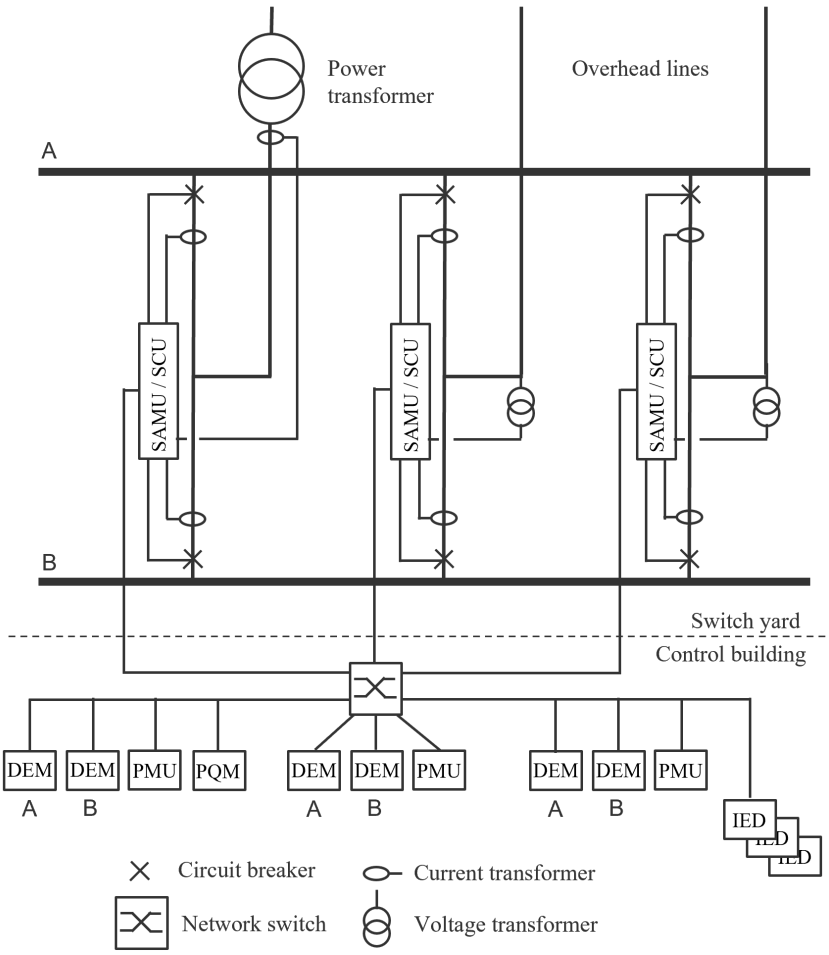


**Figure 2.11:** Conceptual digital substation metering design layout, using available products.

# Chapter 3

# Errors and uncertainty

*This chapter offers an overview and perhaps even a general understanding of uncertainty evaluation and how it is done, something generally missing from our industry. More specifically, this chapter deals with uncertainties in three-phase high-voltage measurements and the contribution of its components to the overall uncertainty.*

## 3.1 Introduction

Measurements are performed because we want to know something and perhaps take action. If we do not know how accurate a measurement value is, then what do we actually know? In other words, measurements help in decision-making, while measurement uncertainty helps in understanding the probability of making a correct action.

International Bureau of Weights and Measures (BIPM) is mandated to provide the basis for a single, coherent, worldwide system of measurements, traceable to the International System of Units (SI). As a part of its work, the Bureau participates in the Joint Committee for Guides in Metrology (JCGM). This body is responsible for two different documents: the Guide to the Expression of Uncertainty in Measurement (GUM) and the International Vocabulary of Metrology (VIM). These documents aim to create a consensus on the expressions used in metrology and the evaluation of uncertainty in measurements.

There are institutions in almost every country tasked with maintaining accurate references (measurement standards) for different measurement quantities. These are the National Metrology Institutes (NMIs) and their references are used to calibrate instruments that can be used later, in one or more steps, to calibrate the measurement equipment used in, say, a substation. A comparison is made between the reference and the instrument, and between the instrument and the next instrument until a comparison is eventually made with the measuring equipment used to gather the measurement values used in decision-making. Each step introduces new uncertainties but there is an unbroken chain of comparisons that presents a *traceable* calibration of our equipment. In Sweden, traceable calibration to national

or international standards (references) is compulsory for all components used in energy-measuring systems used in billing.

## 3.2 Errors and uncertainty in measurement

No measurement is correct. The question is, rather, how inaccurate it is. As stated in JCGM 100:2008 (GUM with minor corrections) [38], the results of a measurement are only an estimate of the true value being sought and a measurement value is only complete when accompanied by a statement of its uncertainty!

Measurement errors can never be completely known but they can be estimated. An important tool in estimating the size of possible measurement errors is uncertainty evaluation, according to the guides released by JCGM.

This section is based on the two documents JCGM 100:2008 (GUM 1995 with minor corrections) [38] and JCGM 101:2008 (Propagation of distributions using Monte Carlo Method) [39]. JCGM recommendations are written in general form and used for any measurement uncertainty evaluation. They must be adapted to the specific field of measurement.

This text discusses measurement errors and uncertainties in energy metering systems in high-voltage substations. The different parts of a measurement system will be briefly discussed but the focus will be on the ITs (VTs and CTs) and the measuring instruments, as these components introduce the largest errors and uncertainties.

There is a forthcoming change to digital substation technology that will change the structure of how measurements are performed. This change will require new ways of estimating the uncertainty in energy metering systems in digital substations, and will also be discussed in this chapter.

### 3.2.1 Terms and expressions

Below are some expressions that are either used later on or whose meaning it is worth knowing because they are common terms in metrology:

*Metrology* is the science of measurements and their application.

*Measurand* is the quantity intended to be measured.

*Measurement* is the process of experimentally obtaining one or more values that can reasonably be attributed to a quantity, alongside any other relevant information.

*Measured value* is the value of a quantity representing a measurement result.

*True value* is a value consistent with a quantity as it is defined.

*Measurement model* is the mathematical relation between all quantities known to be involved in a measurement.

*Measurement function* is the mathematical expression of the measurement model.

*Correction* is the quantity in a measurement model which compensates for an estimated systematic error.

*Measurement error* is a measured value minus a reference value (true value).

*Systematic measurement error* is a component of a measurement error that remains constant in replicated measurements or varies in a predicable manner.

*Measurement uncertainty* is the parameter characterising the dispersion of the values being attributed to a measurand, based on the information used.

*Standard measurement uncertainty* is the measurement uncertainty specified as a standard deviation.

*Combined standard measurement uncertainty* is the standard uncertainty obtained using the standard uncertainties associated with the input quantities in a measurement model.

*Coverage factor* is a number greater than one by which a combined standard uncertainty is multiplied to obtain an expanded uncertainty.

*Measurement standard* is a realisation of the definition of a quantity with a stated value and an associated measurement uncertainty which is used as a reference.

*Metrological traceability chain* is a sequence of measurement standards and calibrations used to relate a measurement result to a reference.

### 3.2.2 Basic theory

Most of the material presented in this section is taken from the document JCGM 100:2008 (GUM with minor corrections) [38] and JCGM 101:2008 (propagation of distributions using the Monte Carlo method) [39].

#### 3.2.2.1 Errors, error distributions, uncertainty and expanded uncertainty

An error is defined as:

$$\begin{aligned} e &= value_{measured} - value_{true} \ , \\ r &= \frac{value_{measured} - value_{true}}{value_{true}} \ . \end{aligned} \tag{3.1}$$

Errors can be absolute, $e$, or relative, $r$, as defined in (3.1). It is important to understand that the true value is impossible to find because all measurements have errors. Small or large.

Let us assume that we buy 10,000 multimeters and connect them to a perfect voltage source that has a true value of 100 V. If we take one *measurement value* from each and every one of these meters, not a single value would be the same. All of them would have errors. If we plot all the measured values, it might look like the left-hand

part of Figure 3.1.

The figure shows *random errors* for all measurements but also a mean value, $\mu = 100.5\,\text{V}$, which is 0.5 V above the sourced signal to the meters. This is a *systematic error*. Systematic errors can be corrected for, while random errors will remain as uncertainties. The *standard uncertainty*, $u$, is defined as the standard deviation of the measurement values, $u = \sigma_{measured}$. The standard deviation is indicated with dashed lines in the figure. The figure also shows that most of the values are close to the mean value, $\mu$. Further away from the mean value, the population is less dense. We have an error distribution centered around $\mu$. In the right-hand part of Figure 3.1, there is a histogram indicating how many measurements are placed within each bar (also called bin), showing how dense the population is for the various errors.

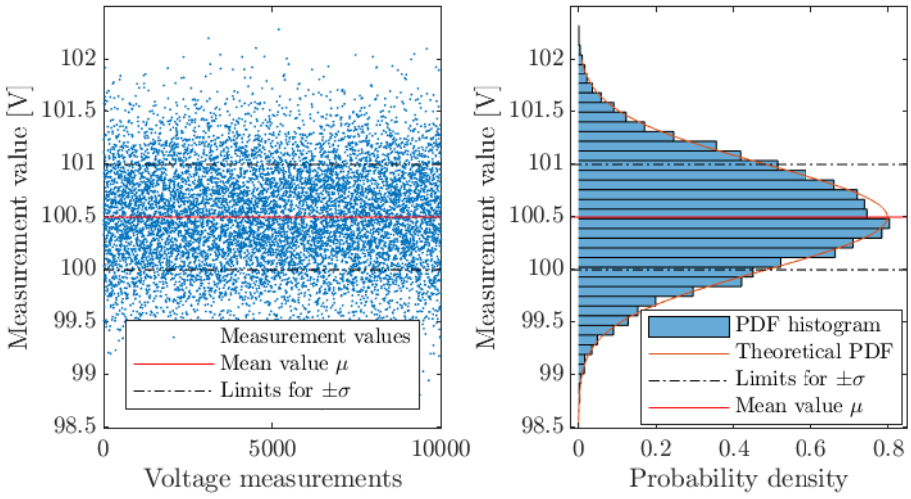


**Figure 3.1:** Left: Measurements from 10,000 randomly chosen multimeters that are all connected to a perfect 100 V signal. Right: The normalised histogram for the measured values and the corresponding probability density function for a normal distribution.

Every so often, it turns out that errors are *normally distributed*. This means that in a population of measurement values, the size of the errors will follow something known as the probability density function (PDF), called the normal distribution (also called a Gaussian distribution). The normal distribution is defined as:

$$p(x) = \frac{1}{\sigma\sqrt{2\pi}} e^{-\frac{1}{2}\left(\frac{x-\mu}{\sigma}\right)^2}, \tag{3.2}$$

where $x$ is the measured value, $\mu$ is the mean value (the expected value) and $\sigma$ is the standard deviation.

The simulated values in the example in Figure 3.1 are normally distributed, with a standard deviation of 0.5 V and a mean value of 100.5 V (i.e. $\sigma = 0.5\,\text{V}$ and $\mu = 100.5\,\text{V}$). The PDF of the normal distribution is also included in the right-hand part of the figure.

Even if the normal distribution is common, there are many other possible distributions. Another popular PDF is the triangular distribution, defined as:

$$p(x) = \begin{cases} (x - (\mu - a))/a^2, & \mu - a < x \leq \mu \\ ((\mu + a) - x)/a^2, & \mu \geq x < \mu + a \\ 0, & \text{otherwise} , \end{cases} \tag{3.3}$$

where $a$ is the half width of the distribution, as shown in Figure 3.2 and $\mu$ is the mean value. The standard deviation for a triangular distribution is $\sigma = a/\sqrt{6}$. A third useful PDF is the rectangular distribution, defined as:

$$p(x) = \begin{cases} 1/2b, & \mu - b < x < \mu + b \\ 0, & \text{otherwise} , \end{cases} \tag{3.4}$$

where $a$ is the half width of the distribution, as shown in Figure 3.2 and $\mu$ is the mean value. The standard deviation for a rectangular distribution is $\sigma = b/\sqrt{3}$. The number of possible distributions is infinite but the three distributions shown here are common when analysing measurements. The rectangular and normal distributions are the most important for high-voltage energy metering.

Figure 3.2 has histograms of the three distributions presented in (3.2), (3.3) and (3.4). All graphs in the figure have been created based on values with a standard deviation of $\sigma = 0.5$ and a mean value of $\mu = 100$. The histograms are normalised to display "relative" frequencies showing the proportion of cases that fall into each of several categories, with the integration of the heights over the measured value equaling 1. This means that the if the PDF is integrated over all values, then obviously, the probability is 100 % that we have included all values. If we integrate the function at close to the mean value, we will obtain another coverage of the number of measurements included.

For a normal distribution, it can be shown that roughly 68 % of the values will be found on one standard deviation either side of the mean value, $\mu$. Although the standard uncertainty can be universally used to express the uncertainty of a measurement result, sometimes an *expanded uncertainty* is used to cover a larger proportion of the measurements.

If we instead look upon two standard deviations on either side of $\mu$, we will cover approximately 95 % of the values. We define the *coverage factor*, $k$, which is multiplied by the standard uncertainty. In regulatory applications, like revenue energy metering, a coverage factor of $k = 2$ is normally used to state the uncertainty in a measurement. So, $U = ku = 2u$, where $U$ is the expanded uncertainty. We now have a *level of confidence* of 95 %. This means that we are confident of finding 95 % of all errors within the interval $\mu \pm 2u$. Sometimes other confidence levels are used, which will lead to other coverage factors.

Looking at the the rectangular distribution in Figure 3.2, it is evident that, if the same coverage factors are used for all distributions, it will lead to different confidence levels. For example, if a coverage factor of $k = 2$ is used for a rectangular

distribution, then "over 100 %" of the values will be covered because we will be outside the limits $\mu \pm b$ for the distribution as described in (3.4).

If multiple rectangular distributions, with similar standard deviations, are used to calculate the combined uncertainty, the result will be very close to a normal distribution. This means that in many practical applications, like high-voltage power and energy calculations, a coverage factor of 2 will give a confidence level close to 95 %, as indicated in Figure 3.4, Section 3.3.4.2.

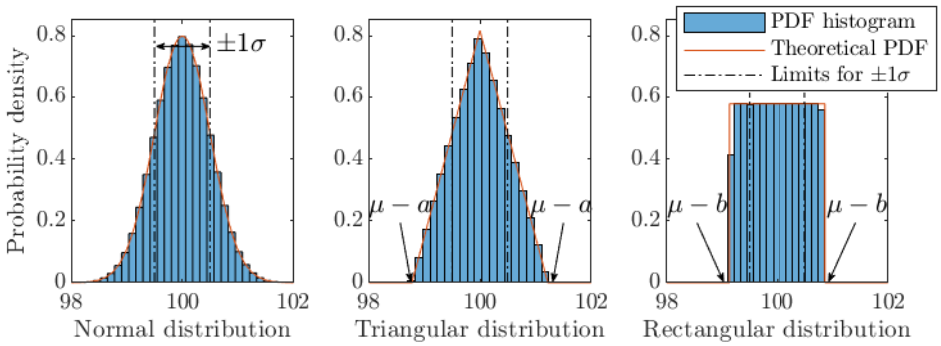


**Figure 3.2:** Three simulated common random error distributions. A mean value of $\mu = 100$ and standard deviation of $\sigma = 0.5$ is used for all distributions. The left-hand graph is normally distributed, the middle one has a triangular distribution and the right-hand one represents a rectangular distribution.

#### 3.2.2.2 Measurement function and combined standard uncertainty

If the measurand (the quantity intended to be measured), $Y$, is not measured directly and is determined by $N$ other quantities, $X_1, X_2, ..., X_N$, the general model of the measurement can be expressed as:

$$Y = f(X_1, X_2, ..., X_n) \ . \tag{3.5}$$

An estimate, $y$, of the measurand $Y$ can be obtained from (3.5) using the input estimates $x_1, x_2, ..., x_N$ for the $N$ quantities $X_1, X_2, ..., X_N$ according to:

$$y = f(x_1, x_2, ..., x_n) \ , \tag{3.6}$$

where $f(x_1, x_2, ..., x_n)$ is the *measurement function.*

If the input quantities are independent of each other (not correlated) the combined variance, $u_c^2(y)$, can be derived using the following expression:

$$u_c^2(y) = \sum_{i=1}^{N} [c_i u(x_i)]^2 \ , \tag{3.7}$$

where $c_i \equiv \partial f / \partial x_i$ and $u(x_i)$ is the standard uncertainty of the individual input quantities. The estimated standard deviation associated with the output estimate $y$ is called the *combined standard uncertainty* and denoted $u_c(y)$. The combined standard uncertainty is the positive square root of the combined variance, $u_c(y) = \sqrt{u_c^2(y)}$.

A special case is when the model of the measurement has the form $Y = cX_1^{p_1}X_2^{p_2}...X_N^{p_N}$ and the exponents $p_i$ are known positive or negative numbers with negligible uncertainties, the combined variance can be expressed as follows:

$$[u_c(y)/y]^2 = \sum_{i=1}^{N}[p_i u(x_i)/x_i]^2 \ . \tag{3.8}$$

The expression $[u_c(y)/y]^2$ is the *relative combined variance*. Often, the uncertainties of the input quantities (and the combined uncertainty) are expressed as relative uncertainties like $u(x_i)/x_i$.

The expressions in (3.7) can be used when the measurement function is linear (and (3.8) as a special case). If there is significant non-linearity, higher-order terms in the Taylor series should be used. Alternatively, the Monte Carlo method described in [39] can be used.

An interesting case in which the uncertainty evaluation is described as above is when the measurement function is the average of several, similar, uncorrelated measurement quantities. Let us consider averaging the measured phase voltage in a symmetrical three-phase grid. The measurement function would look like this:

$$U_{average} = \frac{1}{3}\sum_{i=1}^{3} U_{phase,i} \ , \tag{3.9}$$

where $U_{average}$ is the average voltage of the three phases and $U_{phase,i}$ is the individual phase voltage. This would lead to (3.7) being reduced to:

$$\begin{aligned} u_c^2(U_{average}) &= \sum_{i=1}^{3}[\frac{1}{3}u(U_{phase,i})]^2 \\ &= \frac{1}{3^2}u^2(U_{phase,1}) + \frac{1}{3^2}u^2(U_{phase,2}) + \frac{1}{3^2}u^2(U_{phase,3}) \ , \end{aligned} \tag{3.10}$$

and if $u(U_{phase,i})$ is equal for the three phases, it will be reduced to:

$$\begin{aligned} u_c^2(U_{average}) &= \frac{1}{3}u^2(U_{phase}) \\ u_c(U_{average}) &= \frac{1}{\sqrt{3}}u(U_{phase}) \ . \end{aligned} \tag{3.11}$$

The combined standard uncertainty for the average voltage is lower than the individual standard uncertainties for the phase measurements. The combined standard uncertainty, $u_c$, can be formulated as:

$$u_c = \frac{u_{individual}}{\sqrt{N}} \ , \tag{3.12}$$

where $u_{individual}$ is the standard uncertainty of the individual measurements and $N$ is the number of individual measurements that are averaged. Similarly, it can be shown that a sum of similar values also follows the same reduced uncertainty.

#### 3.2.2.3 Linear measurement function - example

If electric power is measured, there are two quantities included in the measurement - voltage and current. Both quantities have their own uncertainty. Let us consider a direct current (DC) power measurement function:

$$P = UI \ , \tag{3.13}$$

where the power, $P$, is equal to the voltage, $U$, times the current, $I$. Now, the measurement function is defined. If the uncertainties of the input quantities are known, the combined standard uncertainty can be calculated according to (3.7).

As an example, we have a voltage of $U = 100\,\mathrm{V}$ with a standard uncertainty of $u_U = 0.1\,\mathrm{V}$ and a current of $I = 10\,\mathrm{A}$ with an uncertainty of $u_I = 0.1\,\mathrm{A}$. Thus, the relative uncertainty is 0.1 % for the voltage and 1 % for the current. If (3.7) is used, the calculation of the combined standard uncertainty can be described as follows:

$$\begin{aligned}
y &= f(x_1, x_2) \\
y &= P = UI = 100 \cdot 10 = 10000 \\
f(x_1, x_2) &= UI \\
u(x_1) &= u_U = 0.1 \\
u(x_2) &= u_I = 0.1 \\
c_1 &= \partial f / \partial x_1 = I = 10 \\
c_2 &= \partial f / \partial x_2 = U = 100 \\
u_c(y)^2 &= (c_1 u(x_i))^2 + (c_2 u(x_2))^2 = (10 * 0.1)^2 + (100 * 0.1)^2 = \\
&= 1 + 100 = 101 \\
u_c(y) &= \sqrt{101} \approx 10.05 \ .
\end{aligned} \tag{3.14}$$

If (3.8) is used the calculation instead becomes:

$$\begin{aligned}
y &= c x_1^{p_1} x_2^{p_2} = 1 U^1 I^1 = 1 \cdot 100 \cdot 10 = 10000 \\
p_1 &= 1 \\
p_2 &= 1 \\
u(x_1) &= u_U = 0.001 \\
u(x_2) &= u_I = 0.01 \\
[u_c(y)/y]^2 &= (p_1 u(x_2))^2 + (p_2 u(x_2))^2 = (1 \cdot 0.001)^2 + (1 \cdot 0.01)^2 = \\
&= 0.000001 + 0.0001 = 0.000101 \\
u_c(y)/y &= \sqrt{0.000101} \approx 0.01005 \approx 1.0\ \% \ .
\end{aligned} \tag{3.15}$$

The relative combined uncertainty of the power measurement in (3.14) is $10.05/1000 \approx 1.0$ %. Unsurprisingly this is the same answer is found in the previous calculation (3.15). It is important to acknowledge that the largest relative uncertainties will be dominant in the combined uncertainty. With experience, it is possible to disregard small uncertainties when calculating combined uncertainties.

#### 3.2.2.4 Nonlinear measurement function - example

If we want to calculate (a sinusoidal) alternating current (AC) power instead, the measurement function will be:

$$P = UI\cos(\Delta\varphi) = UI\cos(\varphi_U - \varphi_I) \ , \tag{3.16}$$

where $P$ is the power, $U$ and $I$ the (RMS) voltage and current with their individual phase angles $\varphi_U$ and $\varphi_I$, while $\cos(\Delta\varphi)$ is the power factor. Equation (3.16) is in contrast to (3.13), a nonlinear equation. It is possible to evaluate the standard uncertainty of the power, $P$, using Monte Carlo according to JCGM 101:2008 (propagation of distributions using the Monte Carlo method) [39].

**3.2.2.4.1 The Monte Carlo approach** The main idea of the Monte Carlo method is to simulate combined errors and their distribution by using a large number of data points. The input quantities to the measurement function are simulated separately as a long array of data points with an appropriate error distribution. They are then merged using the measurement function to create an array of combined, fictive measurements. The fictive measurement array can be analysed in terms of uncertainties, distributions and coverage factor. As an example calculation, we use uncertainties that are close to the realistic values and which can be associated with commonly available current and voltage transformers. We use a relative standard uncertainty of 0.12 % for amplitude and 5.8 (arc) minutes for the phase displacement uncertainty.

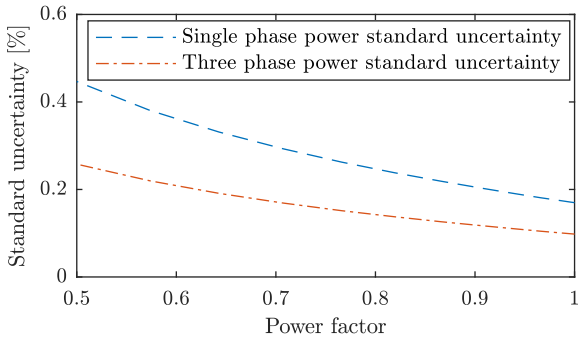


**Figure 3.3:** Calculated relative standard uncertainty for single-phase and three-phase power using the Monte Carlo method. The uncertainty is based on ITs, with a 0.12 % relative standard uncertainty in amplitude and 5.8 (arc) minutes of uncertainty in phase displacement.

We will sweep the difference in phase displacement angles, $\Delta\varphi$, between 0 to 60 degrees, giving a power factor of between 0.5 and 1. The results can be seen in Figure 3.3. As indicated in the figure, the relative uncertainty in the single-phase power will start at 0.17 % at a power factor of 1 and gradually increase to 0.45 % at a power factor of 0.5 (which is when the phase displacement between voltage and current is 60 degrees). The single-phase power uncertainty is $\sqrt{3}$ times higher than the three-phase power uncertainty, which can be expected as discussed in Section 3.2.2.2.

**3.2.2.4.2 Treatment of the AC power measurement function as linear**
It is possible to treat the measurement function for the AC power as linear. This can be done if the uncertainties are small and the *cosine* function and its partial derivative is still a good approximation. The expression in (3.7) would develop to:

$$\begin{aligned}
y &= f(x_1, x_2, x_3, x_4) \\
y &= P = UI\cos(\Delta\varphi) = UI\cos(\varphi_U - \varphi_I) \\
c_1 &= \partial f/\partial x_1 = I\cos(\varphi_U - \varphi_I) \\
c_2 &= \partial f/\partial x_2 = U\cos(\varphi_U - \varphi_I) \\
c_3 &= \partial f/\partial x_3 = -UI\cos(\varphi_U - \varphi_I) \\
c_4 &= \partial f/\partial x_4 = UI\cos(\varphi_U - \varphi_I) \\
u_c^2(y) &= (c_1 u(x_1))^2 + (c_2 u(x_2))^2 + (c_3 u(x_3))^2 + (c_4 u(x_4))^2 \\
&= (I\cos(\Delta\varphi)u(x_1))^2 + (U\cos(\Delta\varphi)u(x_2))^2 + ... \\
&... + (-UI\cos(\Delta\varphi)u(x_3))^2 + (UI\cos(\Delta\varphi)u(x_4))^2 \ .
\end{aligned} \tag{3.17}$$

If $\Delta\varphi = 0$, last two terms disappear since the difference in voltage and current angle is zero and the results are identical to those in the DC calculation. With another power factor, the calculation will not exclude the last two terms. If the power factor is zero (i.e. $\varphi_U - \varphi_I = \pm 90$ degrees), the first two terms will disappear and only the last two will be present. Any other power factor will cause all terms to be present.

The uncertainties, $u(x_1)$ and $u(x_2)$, are the absolute uncertainties for the voltage and current amplitude. We can express these uncertainties as relative uncertainties in per cent instead, giving:

$$\begin{aligned}
u_r(x_1) &= u(x_1)\frac{U}{100} \ , \\
u_r(x_2) &= u(x_2)\frac{I}{100} \ ,
\end{aligned} \tag{3.18}$$

where $u_r(x_1)$ and $u_r(x_2)$ are the relative uncertainties for the voltage and current expressed in per cent. If we use (3.18) to substitute the absolute uncertainties for voltage and current in (3.17), we can derive the following expression for the relative combined uncertainty (in per cent) for the phase power:

$$u_c(y)/y = 100\sqrt{(u_r(x_1)/100)^2 + (u_r(x_2)/100)^2 + (u(x_3)^2 + u(x_4)^2)\tan^2(\Delta\varphi)} \ . \tag{3.19}$$

In this particular case, when the uncertainties of the individual phase angles are small, the expression will not introduce any significant errors. For all practical purposes, the results of (3.19) will give the same result as the Monte Carlo simulation above.

## 3.3 Increasing accuracy and reducing uncertainty in high-voltage energy measurements

A manufacturer of components classifies their equipment according to a measurement class provided in a standard, as described in Section 2.3. Class information is used to understand the measurement uncertainty and is important when different equipment, from multiple manufacturers, is combined into a single measurement system. Aided by the uncertainties in the various parts of the measurement system, the combined uncertainty of the whole measurement system can be calculated according to the rules in JCGM 100:2008 (GUM, with minor corrections) [38], as described in Section 3.2. This process will help us to understand the probability of how large an error can be.

It is possible to reduce the uncertainties in a measurement system if more available information is taken into account. Reducing uncertainties will help in the quest to improve accuracy but will not necessarily help reduce systematic errors.

Svk mainly uses the following three activities to improve accuracy in measurement systems:

- Calibration and correction of systematic errors.
- Comparison of measurements to reduce uncertainty.
- Supervision of measurement systems.

The combination of calibrating and correcting for systematic errors and reducing uncertainty will improve the measurement accuracy. The supervision of measurement systems will help to maintain a high degree of accuracy over time. These activities are further outlined below.

### 3.3.1 Calibration

Systematic errors and uncertainties can be reduced by calibration and correction of errors in the energy meter. However, it is not always easy to calibrate equipment in a high-voltage substation, as access to ITs may be difficult. Gaining access to energy meters is normally not a problem.

Calibration is normally done as a part of the supplier's manufacturing process. The calibration equipment and process have inherent uncertainty. In principle, the uncertainty of adjusted equipment at the point of production is as low as for the factory calibration equipment. This can be of the order of 0.05 % for ITs and even lower for an energy meter. Depending of the specific type of equipment it will change its calibration status depending on internal or external factors. Internal factors may include long-term stability issues in any of the product's components, while external factors can include such things as temperature changes during operation.

When a measurement system first is installed and commissioned, it is possible to increase its accuracy by a few simple actions. As indicated in Section 2.3, ITs are

normally supplied with an accuracy test report. No test report is required to remain within the instrument's class, provided the IT is used as specified. However, it can assist in reducing systematic errors. As explained in Sections 2.3.1.2 and 2.3.1.3 the burden applied to the ITs, will change ratio error and phase displacement. If the burden is measured, an estimation for both ratio error and phase displacement can be performed for the actual measured burden. For VTs, it is also possible to measure the impedance in the measurement cables and calculate the voltage drop in them due to the actual burden. In modern meters, estimated errors can be corrected, allowing for a reduced systematic error. Having said that, it is also important to understand that using calibration results requires a deeper knowledge of both equipment and procedures.

#### 3.3.1.1 Voltage accuracy and uncertainty improvements

The factory accuracy test report for the class 0.2 voltage transformer presented in Figure 2.5 indicates that, depending on the applied burden, the VT will have varying error. If the actual burden is known (it can be measured during full operation), then both the ratio error and phase displacement at the applied burden can be calculated (estimated), using the calibration points in the test report. Thus, a previously unknown systematic error can now be estimated and corrected for. Thanks to this method, the resulting class of the VTs has been reduced to 1/2 of the stated accuracy class in the Swedish transmission system.

#### 3.3.1.2 Current accuracy and uncertainty improvements

As with the VT, the factory accuracy test report can also be used to lower the systematic error and uncertainty in a CT. The errors will depend on both the burden and the specific current amplitude. At low currents, the current transformer usually has larger relative errors compared to those of the nominal current. This is reflected in the class information in Table 2.1. Table 2.2 examines the results of a factory accuracy test on a 2000:2 420 kV CT. This test report suggests there is a positive offset (systematic error) on the ratio error.

In this particular case, the CT is wound with 999 turns on the secondary side and one turn on the primary side, giving an actual ratio of 1998:2. According to (2.1), this will create a positive error of 0.1 % if the transformer behaves as an ideal transformer, something which this transformer obviously does. If the burden is low, as in the case of a SAMU used in a digital substation, then the offset (systematic error) can be corrected for in the energy meter.

A CT is a very stable component with low temperature dependence and, if the ratio error and phase displacement are corrected for, the uncertainty can also be lowered. In this case, the difference in accuracy between a high and low burden is well below a quarter of the accuracy class. If the systematic errors are corrected for, the uncertainty of the class can be halved.

#### 3.3.1.3 Energy meter accuracy and uncertainty improvements

Energy meter calibration can normally be done in the substation without issue, because the meter is normally accessible even when the substation is in full operation.

Years of experience of calibrating the energy meters used in the Swedish substations have yielded enough operational history to be able to also lower the class of the energy meter to 1/3 of the original 0.2S class.

### 3.3.2 Comparison

When the measuring systems are in operation, there are a few measures that can be taken to reduce uncertainty and increase accuracy. One simple measure is to compare all voltages in the substation. This can be done by synchronously acquiring the voltages and averaging the result. Since the voltage drop within a substation is negligible, all measured voltages should be the same. An average of $N$ voltages with the same uncertainty, $U_{individual}$, will lower the uncertainty in the measured result by a factor of $U_{average} = U_{individual}/\sqrt{N}$, as indicated in (3.12). Voltage measurements can be corrected according to the deviation from the average voltage ratio and phase displacement. Since the uncertainty is now reduced, the accuracy is expected to be higher.

According to Chapter 6 [40], a similar procedure can be performed on energy measurements. This shows that it is possible to compare measurement data taken over a period of time in a substation where all bays are measured and also decrease the uncertainty by a factor of $1/\sqrt{N}$, where N is the number of bays.

Before any comparison is performed and deviations are corrected for, it is important to eliminate as many of the systematic errors as possible. Otherwise, the lowered uncertainty will not represent a true value.

### 3.3.3 Supervision

When a substation is built and commissioned for the first time and all measurement systems have been set up in the best possible way, we can normally trust our measurements and estimated uncertainties. For various reasons, the measurement systems can and will degrade over time. There are various ways of automatically supervising the measurement systems. Through supervision, which may be comparisons (like the ones described in Section 3.3.2) or other algorithms, it is possible to rapidly find and correct various different measurement errors. This is further discussed in the following chapters.

Over ten years ago, Svk started to use a supervision system that continuously monitors the energy metering system. During this time, it became obvious that fuses and screw terminals will often introduce severe voltage drops and major measurement errors into the measuring circuit. This is normally due to poor contact or the formation of oxide layers after a long period of operation.

Another fairly common problem with CVTs is capacitor punctures. Punctures introduce ratio errors that are higher than the class limit of the VT. Svk now successfully monitors all CVTs that are connected to the energy metering system and finds all punctures [41] (this is discussed in detail in Chapter 5). It is cost-effective to use automatic data analysis to continuously monitor the condition of measurement systems.

### 3.3.4 Uncertainty evaluation

This section will examine the uncertainty chain in the different setups described in Section 2.4, to obtain the combined uncertainty of the whole measurement system. The traditional metering setup is first examined and the DEM setup is then discussed. Since the DEM system using SV introduces interesting new possibilities, a third subsection has been included, with thoughts on how to further lower the uncertainty using DEM.

The process of finding the combined uncertainty can be done analytically through the measurement function, as described in Section 3.2.2.3 or by performing a Monte Carlo simulation, as described in Section 3.2.2.4. The latter is more straightforward and easier to use when the measurement function is nonlinear. Normally, all calculations are performed using one standard uncertainty. In the field of accurate measurements, the uncertainty evaluation is presented with an expanded uncertainty, at a coverage factor of 95 %. As described in Section 3.2.2.1, for a normal distribution of random errors, $\pm$ one standard uncertainty, $\pm u_c$, will cover approximately 68 % of the possible resulting errors. For accurate measurements, the result of an uncertainty evaluation should normally be given at a coverage of 95 %. For a normal distribution, the coverage factor, $k = 2$, which will be within $\pm 2u_c$. This means the results cover just over 95 % of the possible errors. This step is performed after the combined standard uncertainty is found.

#### 3.3.4.1 Uncertainty chain in a traditional energy metering system

This section brings together uncertainties from the different components of the measurement system into a combined uncertainty. The effect of the measurement cables has not been studied, as it is assumed they are designed to not affect the results.

We will also assume that the majority of the errors come from errors in the ITs and the A/D converters in the energy meter, and that very little of the uncertainty will come from the calculation within the energy meter.

Furthermore, if we know that we have implemented all equipment bearing in mind its limitations, we should interpret the class information as a rectangular uncertainty distribution according to JCGM 100:2008 (GUM with minor corrections) (Clause 4.3.7). This means there is the same probability that the error in the equipment lies somewhere within the class limitations. (We know this is not the case, since we have an accuracy test report from the manufacturer).

**3.3.4.1.1 Uncertainty within a traditional energy meter** Figure 2.6 allows the class information of a 0.2S energy meter to be studied. As can be seen, the class allow a maximum of 0.2 % deviation from a true value at power factor of 1. At a power factor of 0.5, the maximum deviation is allowed to be 0.3 %. (The deviations are only valid if the currents are sufficiently large as indicated in the figure). The larger maximum deviation at a lower power factor is because the phase displacement in the meter's A/D converters will increase the uncertainty. This is essentially the same effect that the ITs will have on the uncertainty.

As described in Section 3.2.2.4.2, we have an expression (3.19), that can be altered to take the fictive class information of the A/D converters into account. The following expression can be derived:

$$u_c(y)/y = \frac{100}{\sqrt{3}}\sqrt{(\frac{C_{AD_{U_r}}}{100\sqrt{3}})^2 + (\frac{C_{AD_{I_r}}}{100\sqrt{3}})^2 + ((\frac{C_{AD_{U_\varphi}}}{\sqrt{3}})^2 + (\frac{C_{AD_{I_\varphi}}}{\sqrt{3}})^2)\tan^2(\Delta\varphi)} \ , \tag{3.20}$$

where $C_{AD_{U_r}}$ and $C_{AD_{I_r}}$ are the fictive ratio error (amplitude) classes for the voltage and current A/D converters. Likewise the $C_{AD_{U_\varphi}}$ and $C_{AD_{I_\varphi}}$ are the fictive phase displacement classes for the A/D converters (expressed in radians).

The $\sqrt{3}$ underneath the class information in (3.20) is due to the fact that the class information should be interpreted as a rectangular distribution. According to GUM, to calculate the combined uncertainty, we need to convert the probability density functions for different equipment into one standard uncertainty, $u_{standard}$. The standard uncertainty of a rectangular distribution derived from the class limit is: $u_{standard} = class/\sqrt{3}$. The other $\sqrt{3}$ comes from the fact that we have summed three independent phase powers, as commented in Section 3.2.2.2.

There are endless combinations of uncertainties in the A/D converters in the energy meter. For the sake of argument, we assume that these uncertainties are the same for the voltage and current A/D converters. This is close to reality and the expression takes the following form:

$$u_{r_{meter}} = u_c(y)/y = \frac{100}{3}\sqrt{2(\frac{C_{AD_r}}{100})^2 + 2C_{AD\varphi}^2\tan^2(\Delta\varphi)} \ , \tag{3.21}$$

where $u_{r_{meter}}$ is the relative standard uncertainty (in per cent) for the meter and $C_{AD_r}$ and $C_{AD\varphi}$ are the fictive ratio error class and fictive phase displacement class for the A/D converters in the meter. At a power factor of 1, the last term under the root symbol will disappear. This makes it possible to calculate an appropriate equivalent A/D converter ratio error class, resulting in $C_{AD_r} = 0.245$. Using the $C_{AD_r} = 0.245$ class information at a power factor of 0.5, it is possible to calculate the equivalent phase displacement class to $C_{AD\varphi} = 5.434$ (arc) minute.

**3.3.4.1.2 Combined uncertainty for energy metering system including ITs and energy meter** Using the same argumentation as in the previous section, it is possible to derive a relative uncertainty expression (in per cent) for the ITs. This expression will be as follows:

$$u_{r_{ITs}} = \frac{100}{3}\sqrt{(\frac{C_{U_r}}{100})^2 + (\frac{C_{I_r}}{100})^2 + (C_{U_\varphi}^2 + C_{I_\varphi}^2)\tan^2(\Delta\varphi)} \ , \tag{3.22}$$

where $C_{U_r}$ and $C_{I_r}$ are the ratio class for the VTs and CTs and, likewise, $C_{U_\varphi}$ and $C_{I_\varphi}$ are the phase displacements for the VTs and CTs.

Now the relative standard combined uncertainty can be calculated for the measurement system that contains the ITs and energy meter, according to:

$$u_{c_{threephase}} = \sqrt{u_{r_{ITs}}^2 + u_{r_{meter}}^2} \ , \tag{3.23}$$

as described in Section 3.2.2.2.

If we use class 0.2 VT, class 0.2S CT and a class 0.2S energy meter and evaluate the system at a power factor of 1, we get an expanded uncertainty of the three-phase measurement system of $U_{c_{threephase}} = 2u_{c_{threephase}} \approx 0.298$ %. With the improvements discussed in Section 3.3.1 (in which the class of the ITs are both 0.1 and the class of the energy meter is 0.2/3), the above calculations will give an expanded uncertainty, $U_{c_{threephase}} \approx 0.122$ %. At a power factor of 0.5, the expanded uncertainties will, instead, become $U_{c_{threephase}} \approx 0.617$ % for the measurement system with no improvements and $U_{c_{threephase}} \approx 0.280$ % for the improved measurement system.

#### 3.3.4.2 Uncertainty chain in a digital energy metering system

For a traditional measuring system, uncertainties coming from A/D-conversion and the calculation are lumped together into a single uncertainty covered by the class of the energy meter. In this section, the SAMU introduced as an extra component with its own uncertainties in both amplitude and phase accuracy.

We examine the uncertainty in active power measurement and assume that the integration to the energy measurement value will add only a negligible uncertainty. We start with the expression of active, single-phase, power in an electric system:

$$P = UI\cos(\Delta\varphi) \ , \tag{3.24}$$

where $U$ is the voltage phasor length, $I$ is the current phasor length and $\Delta\varphi$ is the angle between the two phasors. As can be seen in (3.24), the function is non-linear. This means it is not recommended to use the the analytic approach described in JCGM 100:2008 (GUM with minor corrections). Rather, it is easier to use the Mote Carlo approach described in JCGM 101:2008 (propagation of distributions using Monte Carlo method). Both the voltage and current measurements will have uncertainties in amplitude and phase that come from both the IT and the SAMU.

In the Monte Carlo simulation, we create voltage and current samples where we add random errors, in both amplitude and phase, from the ITs and the SAMU. The samples are multiplied according (3.24). The function for the standard deviation is applied to the result. In the case of class 0.2 ITs and class 0.2 SAMU, the resulting standard uncertainty for the single-phase power is 0.231 % at unity power factor. When the three independent phase powers are summed to a total power, the standard uncertainty is 0.133 %. Figure 3.4 shows the resulting probability density for the errors in total active power.

It is worth noting that the ITs and SAMU all have a rectangular probability function, while the result is close to a normal distribution. Figure 3.5 shows the expanded uncertainties from the calculation and has three lines and four points. Line A is

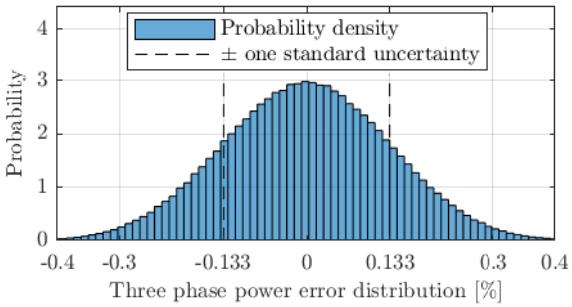


**Figure 3.4:** Probability density function of the simulated three-phase active power, using class 0.2 ITs and class 0.2 SAMU, where random errors have been introduced as rectangular distributions for both amplitude and phase errors for all components.

calculated with 0.2 class ITs and 0.2 class SAMUs. Line B is calculated with the improvements that are described in Section 3.3.1 for the ITs while the SAMU is class 0.2. For line C, the class of the SAMU is 0.1. The four points represent the results of the uncertainty calculations for traditional energy metering systems in Section 3.3.4.1. Points D and F are based on class 0.2 ITs and an energy meter at different powerfactors. Points E and G are the results of the improved traditional energy metering system, as discussed in Section 3.3.4.1.

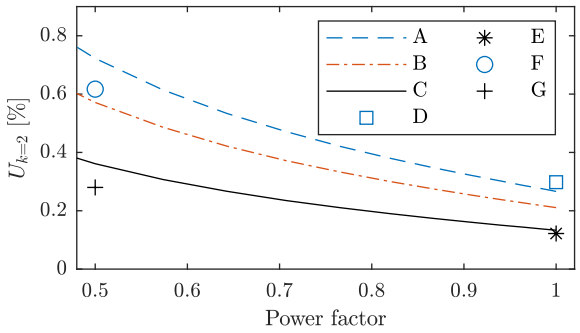


**Figure 3.5:** Expanded uncertainty ($k = 2$) depending on power factor for digital energy metering systems, with traditional ITs and SAMUs.

### 3.3.4.3 General comments

As can be seen in (3.23), the combined uncertainty is the root of the sum of the squared uncertainties of the different components in the system. This means that the largest component uncertainty will always have the most influence. Therefore, the largest uncertainty should be improved first, to reduce the combined uncertainty. Very small component uncertainties (one-fifth or lower compared to the largest component uncertainty) can normally be neglected.

The above SAMU example does not include the uncertainties in the calculation of power. There is evidence in the literature (as stated earlier) indicating that the error in the calculations can be lower than 0.02 %. Since the digital energy meter will have a low uncertainty compared to the ITs or a SAMU, such a small uncertainty

will only increase the combined uncertainty marginally and can therefore be omitted in the evaluation. However, there are also indications that the uncertainty can be much higher in the calculation, in which case it must be included. The quality of the SVs, as discussed in Section 2.3.3.3, will set some of the limitations on how accurate power and energy calculations will become. The uncertainty of energy calculations using SV needs to be proven.

# Chapter 4

# General supervision algorithms

## 4.1 Introduction

Svk uses accurate substation measurement data to find various problematic issues. In 2014, Svk initiated its first research project investigating how data from energy meters could be used for condition monitoring. In the Swedish transmission system, energy meters are installed in all substation bays. These meters are polled for instantaneous values every three seconds, with over 40 instantaneous values collected from each meter. The values create an excellent opportunity to use data analysis to investigate the state of both the substation and the grid. Since energy revenue measurements are governed by legal requirements, the energy-measuring systems are calibrated and corrected regularly. This results in high-quality data. Indeed, energy meters provide the highest quality data available at Svk today. Data from the energy meters is analysed continuously to evaluate the condition of both grid and equipment. Thus, problems are quickly detected and solved. Accurate measurement data from the energy meters has become invaluable to Svk.

This chapter will describe how energy meter data is used by algorithms (or manually) for structured supervision of Svk's substations.

## 4.2 Available data and relationships

According to Svk's substation design (described in Section 2.4.1), there are three-phase groups of VTs and CTs connected to the energy meters. Previously, not all bays in the transmission system were equipped with energy meters and, thus, certain information gaps remain. Several substations have only one bay and one energy-measuring system. From a measurement and analysis perspective, this gives Svk three main types of substation: Type A, with multiple bays all populated with energy meters; type B, with multiple bays but meters absent from one or more bays; and type C, with one measuring system. These are outlined in Figure 4.1.

From an analysis point of view, this creates various opportunities. Different types of relationships can be used to process the collected data, depending on the type of

substation. This is indicated in Figure 4.2.

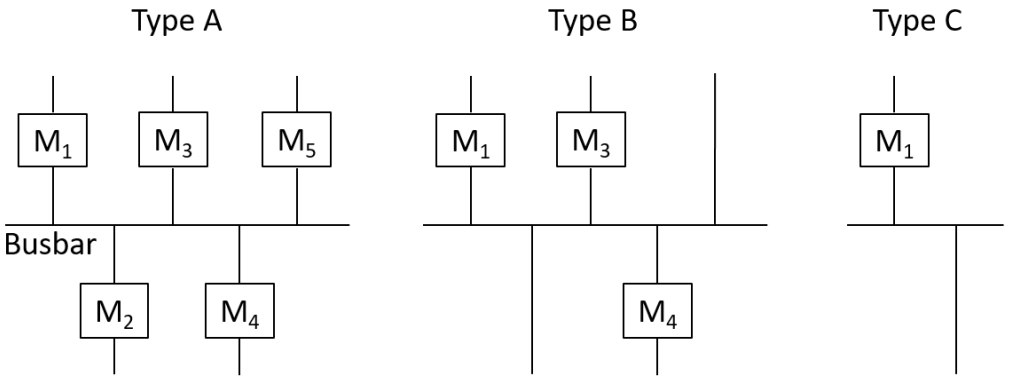


**Figure 4.1:** From a measurement perspective, there are three main substations types. In type A, all bays are measured. In type B, one or more bays lack a measuring system. In type C, there is only one measuring system (due to the size of the substation).

Measurement data from a single bay can be used in conjunction with certain models, while measurements from multiple bays can be used in other ways. There may also be more advanced models that can handle a combination of non-electric measurements (like CB position indications, temperature or moisture in the substation) and electric measurements. For example, the voltages within a bay (working horizontally according to Figure 4.2) can be used to investigate the symmetry of the measurements. This can indicate malfunctioning equipment. If all voltages on one particular phase are compared (working vertically according to Figure 4.2), it can give the same indication but in a different way. Using outdoor temperature and moisture plus measurements in the two connected substations can differentiate between corona losses on an overhead line and measurement errors.

Over 40 instantaneous values (apart from the energy values) are available from each energy meter in the Swedish transmission grid. Their values are collected every three seconds. There are detailed phase values and some values (like active power) are aggregated for the three phases.

So far, it seems that the following instantaneous values are adding the highest value for use in automatic supervision algorithms:

- Phase voltages.
- Phase currents.
- Phase symmetry values (angle between current and voltage vectors, all related to the phase one voltage).
- Active phase power.
- Reactive phase power.

Grid frequency and THD for currents and voltages can also be used to support some

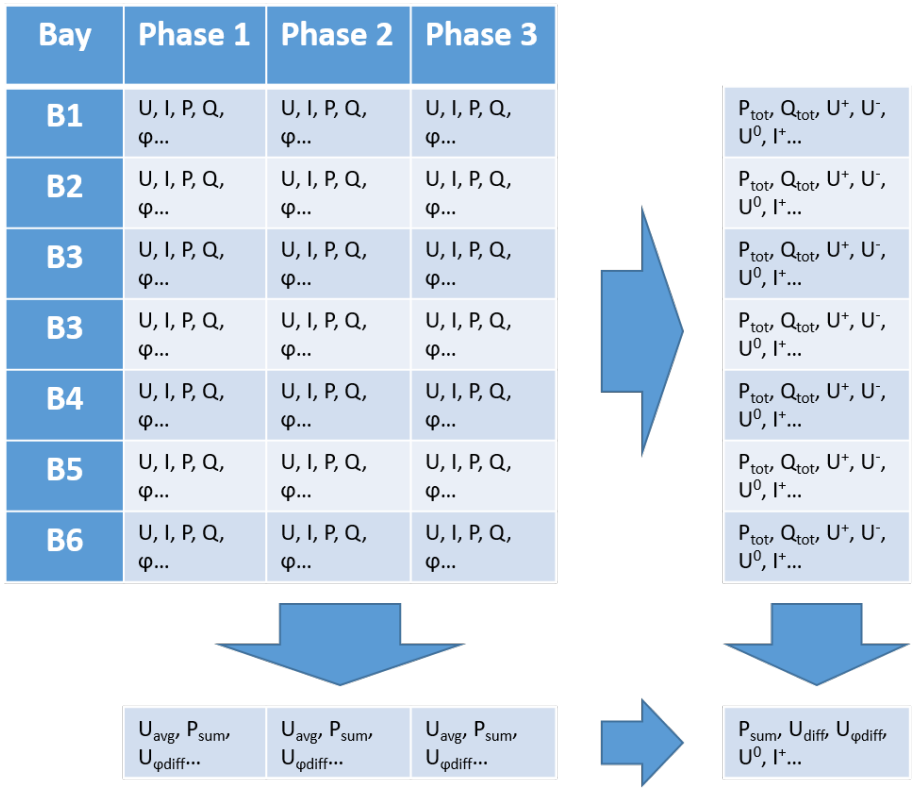


**Figure 4.2:** Each energy meter measures one bay. There are many phase values and a few aggregated values available. Further calculations can be made between phase values within a bay or between phase-specific values between bays, to derive further values for analysis.

investigations.

All instantaneous values are saved in a database and can be further processed in various ways. This allows the retrieval of new values for use in different algorithms. Values can be processed within a bay or between bays depending on the situation. With appropriate models, there are various opportunities to exploit relationships and compare data from substations located across a larger area.

## 4.3 Examples of supervision algorithms

For ACM, simple algorithms are preferred. These are easy to understand and can catch even rare or unexpected events effectively. A combination of multiple simple algorithms will enhance the understanding further and provide ways of isolating specific problems. The algorithms have one or more outputs that can raise an alert with a threshold value. Such thresholds may be fixed or can slowly adapt to varying signals, whatever is most suitable.

Svk uses a mixture of automatic detection and manual inspection. There are two reasons for this. Firstly, it is time-consuming (or even impossible) to write perfect algorithms that never produce false alerts. It is also quick to manually process the

few alerts that do occur. Initiating maintenance action can be very costly and, therefore, manual problem verification is necessary. Secondly, not all possible types of problems have been detected yet. It would be unfortunate to limit the number of alerts by increasing the thresholds so much that the algorithms avoided detecting unknown problems. There is still a lot to learn!

The next subsections give some examples of simple algorithms and discuss what might be analysed using them.

### 4.3.1 Comparison of voltages within the substation

Svk's long-term experience of using ACM indicates that the components included in voltage measurements are the most prone to causing problems. Thus, simple voltage supervision algorithms are valuable.

Most substations have multiple bays with energy meters providing data. A basic useful model is that all voltages on a specific phase must be the same (because the voltage drop on a substation's busbars is negligible). Any deviation between bays indicates a measurement error caused by poor error correction and/or malfunctioning equipment. As indicated in Chapter 2, the components affecting voltage data are: VTs, secondary voltage cabling and the energy meter. The components that most commonly fail in various ways are the VT and the cabling with its screw connectors and relays. On rare occasions, the energy meter may fail.

Figure 4.3 shows the voltages from three bays on phase one during a capacitor puncture (a short circuit on one out of some 250 capacitors in a CVT). A trained eye (or algorithm) might just catch such an event but they are easy to miss.

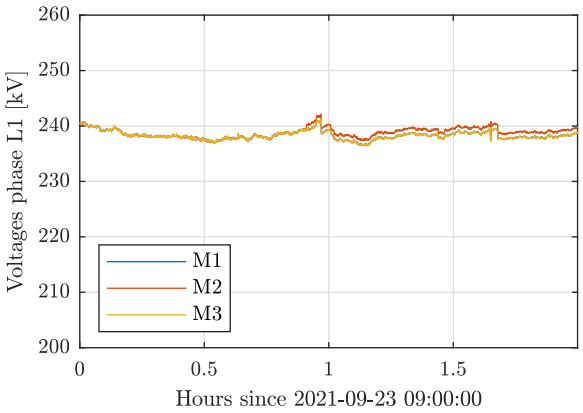


**Figure 4.3:** Example of three bays phase 1 voltages during a puncture event in a CVT in a substation with three independent energy measuring systems. As indicated, it is hard to actually see the differences. The voltages coincide with each other until the puncture occurs. Thereafter, M1 and M3 are still close to identical (the M1 voltage is hidden below the M3 voltage).

To increase the chances of securely detecting this event, it is possible to create a more sensitive signal by expressing a relative deviation between the voltages. This can be done by examining the difference between a specific phase-voltage value and

the average of all the other voltage values on the same phase. The relative deviation from an average voltage value for a specific measured voltage value, $U_{examined\,value}$, can be expressed according to the following equation:

$$Relative\ deviation = 100\frac{U_{examined\,value} - \frac{1}{n}\sum_1^n U_i}{\frac{1}{n}\sum_1^n U_i}\ , \tag{4.1}$$

where $n$ is the number of available measurements and $i$ denotes the value in a list of values against which a specific value will be compared. The *Relative deviation* is expressed in per cent. Relative values makes the algorithm useful for multiple voltage levels. Note that the algorithm uses measurement data along the columns in Figure 4.2.

Potential problems can be spotted by examining all the relative deviations for all voltages phase by phase and setting an alert level to indicate whether any of the deviations are larger than anticipated. Figure 4.4 allows the signature from the same puncture event as in Figure 4.3 to be studied. This time, the signal is clearer.

When a capacitor puncture occurs, the voltage will (in most cases) increase to a new static level (as will be further detailed in Chapter 5). It is evident from the figure that selecting a suitable alert level on all the signals from the algorithm would catch this event. It is quick and simple to investigate the event manually by automatically producing a plot with this figure and indicating that there is a new event in the alert list.

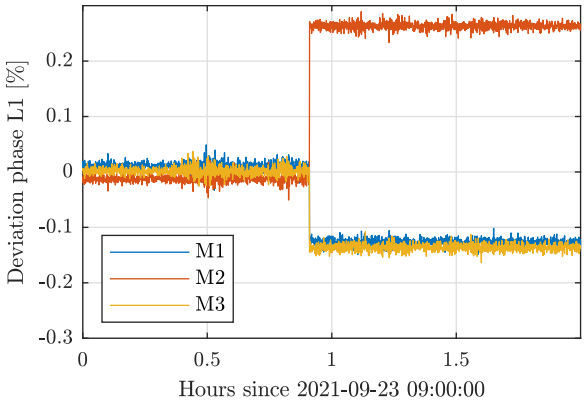


**Figure 4.4:** Example of a signature from a relative deviation of voltages during a puncture event. The puncture is a static irreversible event.

Figure 4.5 captures another event. This time, the issue is a bad connection in a screw connector located in the secondary voltage cabling. This bad connection cause a voltage drop that varies over time with, say, temperature.

Figure 4.6 catches another, similar type of event. This time, a corroded fuse (also located in the secondary voltage cabling) creates a similar signature to the one for the bad connection in the screw connector in Figure 4.5. It is hard to differentiate

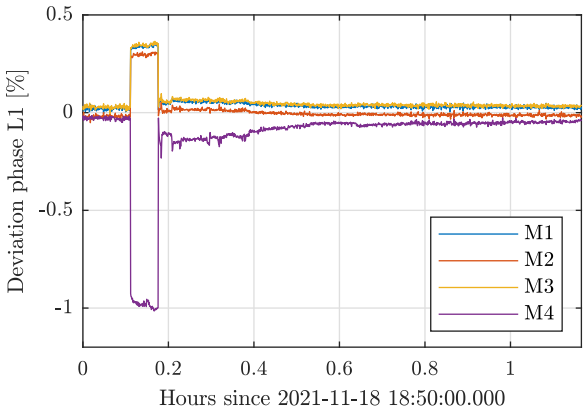


**Figure 4.5:** Example of a signature from a bad connection in a screw connector in the secondary voltage cabling on phase L1 (phase one). This bad connection creates abrupt voltage variations and also a slow one.

between these events and a manual inspection in the substation may be needed.

When a voltage variation occurs on one phase, the average value will change even if the other values are constant. This means that all voltages will vary but the most affected signal will vary more than the other. It is straightforward to automatically find the signal that varies the most and exclude it from the averaging process. Thus, a clearer picture can be gained of what is happening, as indicated in Figure 4.6b. If many measurements are present in the substation, the variations in the unaffected voltages will be smaller. When only two measurements are available, it may be hard to get an exact answer as to which phase voltage is affected and an on-site investigation may be needed.

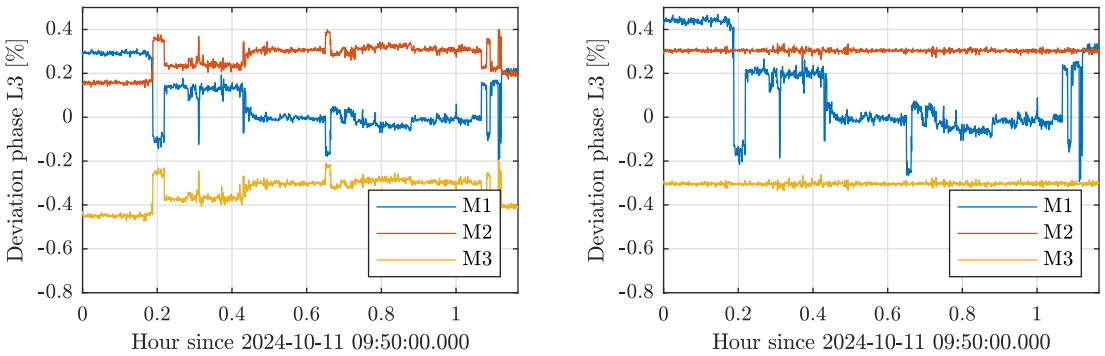


**(a)** Deviation based on average voltage from all three measuring systems.

**(b)** Deviation based on average voltage from measuring systems M2 and M3.

**Figure 4.6:** Example of signatures from a corroded fuse in the secondary cabling between the VT and the energy meter. In this case the phase L3 voltages from all measuring systems (M1-M3) in the substation is examined. In the sub-figure a all voltages are included in the average voltage, while in sub-figure b only voltages from measuring system M2 and M3 are used.

As can be seen from the examples in this subsection, it is possible to find different types of events and, sometimes, these need to be classified manually. There are various components in the voltage measuring circuit and events can have many possible causes. This means it is sometimes hard to understand the true cause of an event. When new types of events (new signatures) emerge, there is a need to investigate the true cause in more depth. This can sometimes be done using other supporting algorithms and revisiting underlying models. In other cases, someone needs to visit the substation, go through the circuits and find the reason for the problem. Once the problem has been identified, it may be possible to tailor-make an algorithm that can differentiate between different events, isolate the true cause and send a specific alert.

Statutory verification of energy-metering systems is performed every six years or when substations are new or refurbished. All possible errors in the energy meters are evaluated and corrected for. Figure 4.7 shows the voltage deviations before and after verification and correction of a substation with five interdependent measuring systems. To correct for known errors and use the ACM system in this way has a few advantages. Firstly, when all the measurements are trimmed to their highest accuracy, the algorithms can react to reasonable alert levels without producing false alerts. Secondly, the analysis can be made before the verification personnel leave the substation. Thus, any human error in the verification procedure can be found and amended without revisiting the substation. And thirdly, of course, the measurements will be more accurate!

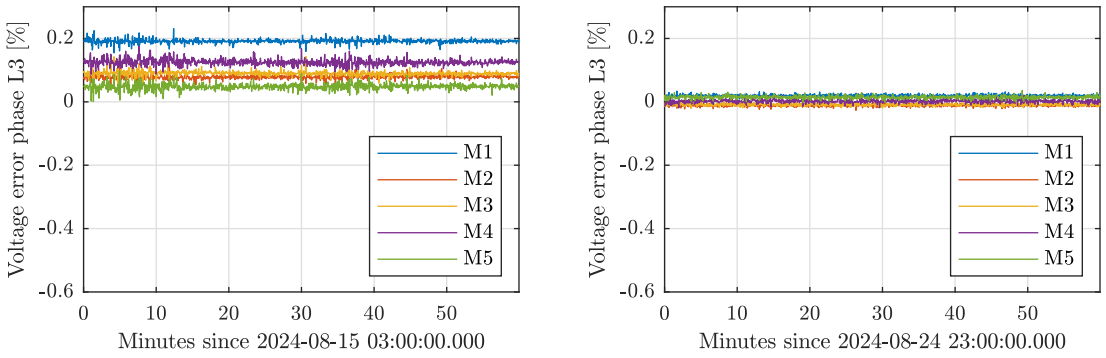


**(a)** Before verification and correction.

**(b)** After verification and correction.

**Figure 4.7:** When newly built or refurbished substations are brought into operation, the energy-measuring systems must be verified for accuracy. During the verification procedure, all known errors are corrected for. This figure describes a typical voltage error estimate before and after verification. In the left-hand part of the figure, there is a (collective) positive offset caused by the burden dependence of the CVTs, which is not yet corrected for.

Using the relative deviation between voltages in different ways has been a successful way of finding various types of problems, many of which were not previously known to exist. The relative deviation between voltages can be used in substations type A and B.

### 4.3.2 Finding measurement errors using sums

Type A substations offer further opportunities for data analysis. The losses within a substation are very small and can be neglected. Thus, if the true power in all bays is summed, the true sum will be zero. If the summed power value is not zero, it means there are measurement errors in the measuring systems, as shown by the expression:

$$P_{sum} = \sum_{1}^{n} P_i \ , \tag{4.2}$$

where $P_{sum}$ is the residual power sum from all bays and $P_i$ the individual power in each bay, while $n$ is the total number of bays. The power, $P_i$, can be the total power in the bay but also the power from a specific phase in that bay. Thus, by using a specific phase power, the granularity of error detection is increased. Note that the algorithm uses measurement data from the columns in Figure 4.2.

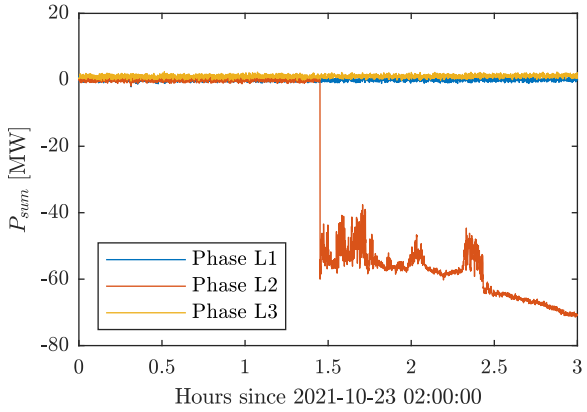


**Figure 4.8:** Example of a signature of the summed power for each bay and individual phase, in a substation during an event in which the secondary CT circuit in one of six bays experienced a partial short circuit on phase two.

Since the power (and residual power sum) will vary during operation, it is often inconvenient to examine $P_{sum}$ as such, because there is no reference. In the example seen in Figure 4.8, the error is unusually large. However, when the errors are much smaller and the power varies, it is hard to draw any conclusions from the summed power. Humans (and computers) will understand a relative value better. The question is which reference value to use? The power in each bay will vary considerably so they cannot be used as a reference. A more successful reference has been derived by formulating and using the power passing through the substation. This can be formulated according to:

$$P_{through} = \frac{\sum_{1}^{n} |P_i|}{2} \ , \tag{4.3}$$

where $P_{through}$ is an estimate of the power that passes through the substation and (as before) $P_i$ the individual power from each bay, with $n$ as the total number of bays in the substation. It is now possible to formulate the percentage value of total

measurement errors in the substation relative to the total power passing through the substation according to:

$$P_{err,\,percent} = \frac{P_{sum}}{P_{through}} \ . \tag{4.4}$$

We now have something that is easy to relate to. As Svk (normally) has excellent control over its energy-measuring systems, a value over 0.1 % indicates something wrong. Figure 4.9 shows the percentage errors for each phase and uses the same data as in Figure 4.8. Because the errors and, thereby, the residual power sum usually are very small, any measurement noise will give a noisy $P_{err}$ signal. Thus, careful filtering is normally required to get stable values that represent the size of the error. Depending on the instruments and time synchronisation noise, this filter can be set differently. Svk normally uses a moving average filter incorporating 20-40 three-second values. There is a trade-off between detecting quick events and getting accurate results.

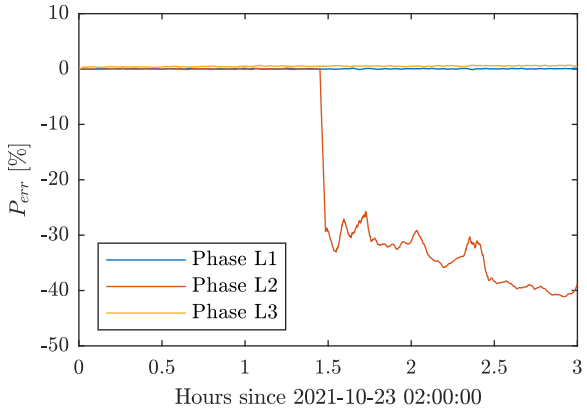


**Figure 4.9:** Example of a signature in the percentage value of total measurement values in a substation, during an event in which the secondary CT circuit experienced a partial short circuit on phase two. The data is filtered with a moving average of 40 values, equivalent to two minutes.

Figures 4.8 and 4.9 show that there is a considerable measurement error. But it also shows that it is impossible to know from which system or systems the problem arises. In such cases, a further analysis have to be conducted. In Figure 4.10, all individual currents from the measuring systems can be studied. This figure shows it was the current circuit in measuring system M3 phase two that caused the problem.

The advantage of using sums is that they make it straightforward to create a problem-detecting algorithm using a simple threshold alert. The disadvantage is that it cannot pinpoint which system is causing the problem. Usually, when the deviations are large, this procedure can be done manually by investigating the data in other ways. Smaller deviations can be found automatically using other algorithms. These will be further explained in Chapter 6.

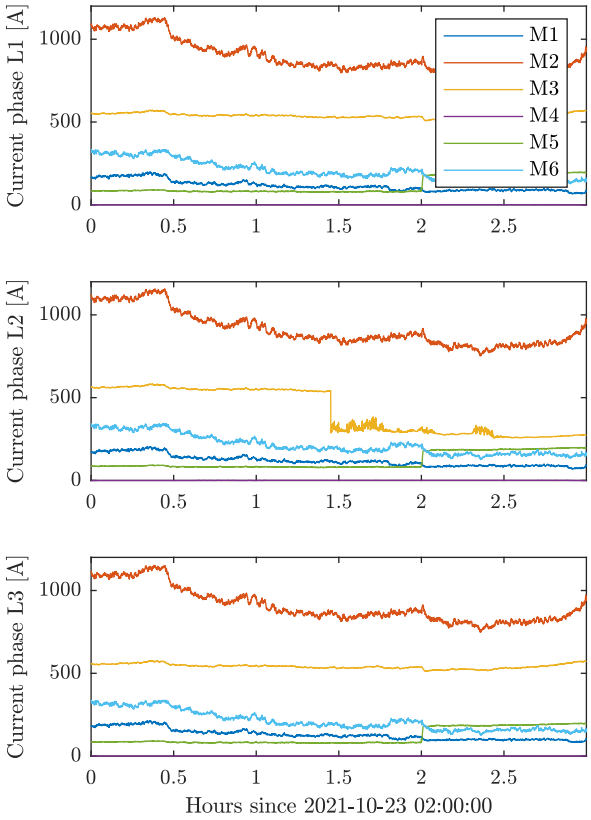


**Figure 4.10:** Individual currents on all phases in the substation during the short circuit event shown in Figure 4.8. The current from system M3 (yellow line in the middle of all three graphs) is evidently behaving differently on phase L2 (middle graph) compared to the other phases.

There are other ways of using sums when analysing a substation. One way is to observe the sum of all currents. The currents are phasors, having both a length and phase angle, information that is available from the energy-measuring systems. The current phasors can be summed to a resulting phasor from all bays, for each phase in the substation. A similar investigation to the one described above can be conducted, but there is a small capacitive leakage of current to the ground network due to the insulation capacitance in the ITs. Not all of this current is measured by the CTs connected to the energy meters.

Sums has pros and cons. As mentioned earlier, it can be hard to find a specific cause of a problem. It may be caused by any of the components in a measuring system, something which needs further investigation. One advantage is that it is a very simple and robust way to be alerted of a potential problem. Such problems may include human errors, which is common when commissioning meters for the first time or when equipment is changed. Svk has made substantial savings by using this method while personnel are working in the substation. Thus, such problems can be quickly solved without the need for a subsequent visit (which is costly).

### 4.3.3 Algorithms using data from a single measuring system

In type B or C substations, some methods (like using sums) are not possible. The remedy is to use other algorithms that rely on models focusing on the symmetry between phases, working along the rows in Figure 4.2. Some opportunities are lost by doing this but since the symmetry in a transmission system is usually good, there are various other opportunities to find small errors efficiently using ACM.

The main methods for type C substations used by Svk entail working with zero sequence unbalance. Zero sequence is calculated as follows:

$$\vec{U}_{zero\ sequence} = \frac{\vec{U}_{L1} + \vec{U}_{L2} + \vec{U}_{L3}}{3} \ . \tag{4.5}$$

The zero sequence voltage, $\vec{U}_{zero\ sequence}$, is calculated by adding the three voltage vectors, $\vec{U}_{L1}$, $\vec{U}_{L2}$ and $\vec{U}_{L3}$ together and dividing by 3. The same can also be done with currents.

The unbalance value is hard for a human eye (or a computer) to digest, while a relative unbalance value is more useful. The zero sequence unbalance is calculated as follows:

$$\vec{U}_{zero\ seq.\ unbal.} = \frac{\vec{U}_{zero\ sequence}}{|\vec{U}_{positive\ sequence}|} \ , \tag{4.6}$$

where the positive sequence, $\vec{U}_{positive\ sequence}$, is used to normalise the zero sequence unbalance, $\vec{U}_{zero\ seq.\ unbal.}$. Note that the zero sequence unbalance is not usually expressed by a vector but as will be seen later, it has some positive and useful

effects.

Revisiting the event presented in Figure 4.4 above and using the data with (4.6), we obtain another result that can be used also for type C substations. Figure 4.11 shows the unbalance vectors for the substation.

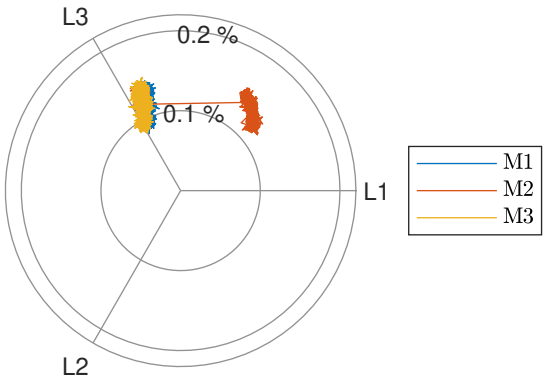


**Figure 4.11:** The figure represents the same event and data used in Figure 4.4 but is now presented as a zero sequence unbalance.

In the figure, we can see that an unbalance is present in all measuring systems in the substation. This can be caused by measurement errors but, in this case, is more likely due to a small unbalance in the grid. This is because all three unbalance vectors are positioned on top of each other before the event. The important point is that when the puncture occurs, the zero sequence unbalance belonging to one of the measuring systems will move abruptly to the right. The phase one voltage on that system has increased and thereby given the unbalance vector another direction. The change is in the zero-degree direction, which corresponds to phase one. Thus, with the unbalance vector, rather than the absolute value of the vector, it is possible to know which of the three phases is affected by the problem.

Zero sequence unbalance has proven to be an especially useful tool for type C substations. It is also useful in type A and B substations as a backup for other, more precise algorithms. The zero sequence unbalance has been used successfully in a method that can detect individual capacitor punctures in CVTs, as will be further detailed in Chapter 5.

### 4.3.4 Further use of substation measurement values

#### 4.3.4.1 Comparison between substations

Several examples add focus on analysis using data from a single substation. As indicated in the text above, there are limitations to what can be done in substations with only one measuring system (type C substations).

The remedy is to use data from multiple substations across a larger area alongside overhead line models. It is possible to use a state estimator that includes multiple substations, or use the line model between two substations to "*transfer*" the measurement from one to the other substation. The calculated values can be compared with the measured values to explore any potential discrepancy.

Small deviations can normally be detected but the main drawback is that the available line models at Svk are single-phase. Thus, it is challenging to be absolutely sure that the results on the individual phases are correct. This is especially pronounced for long and/or poorly transposed overhead lines. If three-phase models of the overhead lines were available, it would most certainly be possible to produce accurate statements on the condition of the measuring systems using this method.

#### 4.3.4.2 Measurement redundancy

There is a great deal of redundancy in substations where all objects are being measured (measuring each bay). On more than one occasion a measurement transducer connected to the measurement core of CTs in a bay has been exchanged, causing the loss of all accurate measurements from that bay for several hours. The main problem is that revenue meters cannot register the energy flowing through the bay, a fact which disturbs the billing process. Having measurements in all bays provides a redundancy and allows the energy from all the other bays to be used to recreate the lost measurement. The total value of lost revenue data (that could be recovered by the redundancy) exceeded EUR 30,000 on only one of these occasions.

#### 4.3.4.3 Wrongly mounted CVTs

CVTs are tall units and, for transportation reasons, are usually delivered in two pieces. During factory calibration, these two pieces are calibrated together. Mixing up the parts from different CVTs will create errors of a few tenths of a per cent. If mounting personnel are not aware of the importance of pairing the correct parts together, measurement errors will occur. This has happened several times when subcontractors have built or refurbished substations at Svk.

On one occasion, multiple units were wrongly paired, which directly showed up as voltage deviations between the measurements. By studying the factory test reports, which include capacitance for each part of a CVT, it was possible to construct a model describing the anticipated errors of any wrongly paired combination. By using the measured data, it was possible to theoretically determine how all the parts were mixed up. This was later verified by checking the serial numbers of all units. This example adds strength to the argument for having accurate substation measurements available for analysis.

#### 4.3.4.4 Influence on the neutral conductor

The voltage signal ground reference for the measuring instruments is collected from the substation ground close to the VTs. Sometimes, when using voltage selection relays (described in Section 2.4.1), the ground signal can be mistakenly connected to the ground signal from another group of VTs. This will cause a large "antenna" that reaches from the control building out into the switch-yard. The antenna is affected by the magnetic fields from currents flowing in the substation. A minor current (caused by induction) will flow in the ground signal cables, producing a small voltage that will slightly offset the neutral point for the instruments. This will cause the voltage reading to change according to the current flow in the substation. This was noticed in multiple substations, by alerts caused by variations in the voltage

readings. Since the grid is symmetrical the total energy measurement accuracy was not affected but it did produce irritating alerts from the ACM system.

## 4.4 Conclusions and discussion

There are drawbacks to the present measurement and data collection infrastructure. Firstly, the time synchronisation, as mentioned in Section 2.1, can be poor (this is a relative statement), adding to the noise when data is analysed between bays (because time synchronisation between instruments may differ slightly). Secondly, there is the drawback that data must be transported to a central location for processing, adding to the communication bandwidth needs. Thirdly, as described in Section 2.4.1, the summation of currents to the two busbars introduces limitations on how granular analysis can be made in a substation. Yet another drawback is that the instantaneous values typically average 200 ms collected only every three seconds. This leaves gaps where events might occur between the samples and will thus go undetected. These drawbacks can be eliminated in DSs, as described in Chapter 8. Even with these drawbacks, the supplied data is high-quality and can be used to find many different kinds of problematic issues.

The simpler the algorithms, the better! Simple algorithms are easy to develop and understand. The output from such algorithms can often be used to produce an alert for situations that might be caused by a problem, without too many false alerts. It is normally a question of how the alert criteria are implemented. At the start of using a new algorithm, the alert levels should be set in a way that creates plenty of alerts. Following investigation, the alert criteria can be modified to limit the number of alerts. By using various different algorithms, it is normally possible to limit the number of false alerts and discriminate between different types of problems. In certain situations, it is possible to construct special algorithms that target a specific type of problem. This can normally be done as a post-mortem analysis when a problem has occurred and data for the event is available. This is why it is important to gather as much data as possible all the time. We never know when it may be useful. As a result of the early findings, Svk quickly decided to install energy meters in every bay in all substations, as it will enhance the supervision of the substations and the grid overall.

The experience is that a model-based, compared to an artificial intelligence (AI) approach, will give results that are simple to understand and the algorithms are easier to make. Another reason not to use AI is that such approaches often require training data. This is hard to come by in transmission grids, because of the small number and diversified problems that appear. Some types of investigation, like the one described in Chapter 6 are not possible with AI, since the output will not contain an uncertainty. Having said this, there are also examples in the transmission grids that could benefit from an AI approach. However, such examples are not included in this thesis.

There is an endless number of possible use-cases for ACM purposes using substation measurement values. Some of them are more valuable than others, which requires

a focus on the working process.

# Chapter 5

# CVT punctures

## 5.1 Introduction

In 2014, a number of CVTs in the Swedish transmission grid exploded. Data-driven methods of continuous monitoring CVTs were then developed to address this problem. Thanks to these methods, CVT capacitor punctures are now routinely noticed and addressed before they can cause serious damage. This chapter describes the algorithms used to make this possible.

Detecting all CVT capacitor punctures as they occur increases the transmission system's stability, avoids equipment damage, lowers the risk to personnel during substation visits and allows measurement errors in energy measuring systems to be corrected.

Automatic supervision scripts using energy meter data are in continuous operation and will alert maintenance personnel when problems occur. Using the algorithms proposed in this chapter, Svk has been able to detect many old punctures and it is anticipated that no future capacitor punctures will go undetected. Detecting all new punctures will allow Svk to save substantial sums in future, as planned actions are now possible.

The purpose of this chapter is to provide a novel approach to monitoring CVT punctures using existing data or which can be collected from existing systems in the grid. The methods are sensitive and simple to implement. They monitor the CVTs continuously and can detect old punctures for which there is no measurement data when they occurred. The main contribution of this chapter lies in the algorithms it has developed. The work is strengthened by performance validation that uses real-world data and actual events. This provides proof of the algorithms' usefulness in detecting CVT punctures. Some of its specific contributions include:

- Section 5.2. A proposed theory that can be used to successfully detect all individual punctures in CVTs.
- Sections 5.4.1 and 5.4.3. An introduction to new algorithms that can detect

single punctures in CVTs and solve some deficiencies with state-of-the-art monitoring.

- Sections 5.4.2 and 5.4.4. An introduction to assisting algorithms that can be used if, for some reason, no data is available during a puncture event.

## 5.2 Theory

Punctured capacitors change the ratio between the primary and secondary voltages. Figure 5.1 shows a functional diagram of the most important components in a CVT.

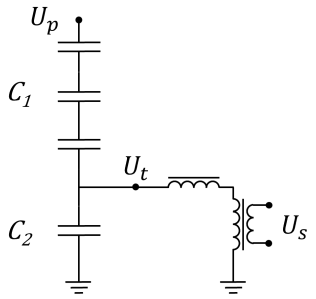


**Figure 5.1:** Functional diagram of a CVT. The relationship between the primary voltage, $U_p$, and the measured secondary voltage, $U_s$, depends on the number of capacitors in the top stack, $C_1$, and bottom stack, $C_2$.

If a puncture occurs in the top part of the capacitor stack, $C_1$, the measured voltage will increase slightly. With a small number of punctured capacitors, the phase angle will not change noticeably [4]. If a capacitor in the bottom stack, $C_2$, is punctured, the voltage will decrease several per cent and there will be a noticeable change in phase angle [4].

The relationship between the tap voltage, $U_t$, and primary voltage, $U_p$, depends on the number of capacitors in $C_1$, $n_1$ and $C_2$ stack, $n_2$. The measured voltage, $U_s$, is proportional to the tap voltage, $U_t$, by a factor $k$. With $p_{C_1}$ being the number of capacitor punctures in the $C_1$ stack, the relationship between the measured secondary voltage and the primary voltage can be written thus:

$$U_s = U_p k \frac{n_2}{n_1 - p_{C_1} + n_2} \ . \tag{5.1}$$

The percentage voltage change if a capacitor in $C_1$ is punctured can be written as:

$$\begin{aligned} U_{change\,percent} &= 100\left(\frac{U_{s,\ after\,puncture}}{U_{s,\ before\,puncture}} - 1\right) \\ &= 100\left(\frac{U_p k \frac{n_2}{n_1 - p_{C_1} + n_2}}{U_p k \frac{n_2}{n_1 + n_2}} - 1\right) \\ &= 100\left(\frac{n_1 + n_2}{n_1 - p_{C_1} + n_2} - 1\right) \ . \end{aligned} \tag{5.2}$$

The number of capacitors in a CVT depends on the voltage level and is also manufacturer-dependent. According to available CVT data, the design voltage over each capacitor is approximately 0.8-1 kV. This means that for a 420 kV (phase voltage 242 kV), there are some 240-300 capacitors in total, across both stacks. One punctured capacitor in the top stack will increase the phase voltage reading by approximately 0.3-0.4 %, while a puncture in the bottom stack will decrease the voltage reading by approximately 5-10 %. Likewise, for a 245 kV CVT with 140-175 capacitors, the increase is about 0.6-0.7 % when a puncture occurs in the $C_1$ stack and the decrease is about 5-10 % when a single puncture appears in the $C_2$ stack.

A CVT can have more than one independent secondary output. Connecting a spare output from each CVT in a three-phase group according to Figure 5.2 creates an open delta connection. Measuring the voltage in this open point indicates an unbalance between phases. A high (open delta) voltage is commonly used as an indicator of voltage transformer problems, including punctures.

$$\vec{U}_{Open\ delta} = \vec{U}_{L1} + \vec{U}_{L2} + \vec{U}_{L3}$$

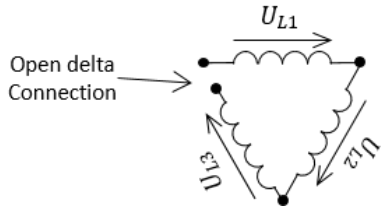


**Figure 5.2:** An open delta voltage is created by adding the three-phase voltage vectors to each other. The three secondary voltages of the CVTs are connected by one open point that can be measured.

The open delta voltage is three times higher than the zero sequence voltage. The zero sequence voltage is calculated by adding the three voltage vectors together and dividing by 3, according to the following expression:

$$\vec{U}_{zero\ sequence} = \frac{\vec{U}_{L1} + \vec{U}_{L2} + \vec{U}_{L3}}{3} \ . \tag{5.3}$$

The zero sequence unbalance value is created by normalising the zero sequence voltage magnitude with the positive sequence voltage magnitude [42],

$$U_{zero\ sequence\ unbalance} = \frac{|\vec{U}_{zero\ sequence}|}{|\vec{U}_{positive\ sequence}|} \ . \tag{5.4}$$

To demonstrate how registered voltage and zero sequence unbalance change when capacitors in a CVT are punctured, the author simulated an output from an energy measuring system in which three consecutive punctures occurred. The simulated punctures were achieved by abruptly increasing the phase voltage amplitude reading by 0.35% for each phase, 15 minutes apart. The results are presented in Figure 5.3 (top and bottom). The system was in perfect balance at the start of the simulation.

Figure 5.3 (middle) shows how the registered unbalance, according to (5.4), will increase as the first puncture occurs in phase one. When the second puncture occurs in phase two, the zero sequence voltage will change direction but the amplitude will not change. Therefore, the unbalance will not change. Finally, when the third puncture in phase three occurs, there is a perfect balance again and the zero sequence voltage will return to zero.

This clearly indicates that merely exploring the difference in unbalance between samples (as was the case in the earlier approach [5]) is not a reliable way of detecting a puncture. If the phase angle information is kept when calculating the zero sequence unbalance (not using the absolute value in the nominator in (5.4)), it is possible to study both the amplitude and direction of the zero sequence voltage jump.

The following relationships may be used to calculate the change in zero sequence vector:

$$\vec{U}_{zero\ seq.\ unbal.} = \frac{\vec{U}_{zero\ sequence}}{|\vec{U}_{positive\ sequence}|} \tag{5.5}$$

$$\vec{U}_{i,\ diff} = \vec{U}_{i,\ zero\ seq.\ unbal.} - \vec{U}_{i-1,\ zero\ seq.\ unbal.} \tag{5.6}$$

The zero sequence unbalance vector, shown in (5.5) and the difference between successive samples, $i$, are calculated for each time sample. Figure 5.3 (bottom) permits the amplitude of the differences according to (5.6) to be studied. In contrast to the zero sequence unbalance (middle), all three punctures can now clearly be identified.

According to (5.6), a puncture in stack $C_1$ will create a jump in the $\vec{U}_{i,\ diff}$ vector in the same direction as the corresponding phase vector angle. The angle of the jump clearly indicates what phase is affected by the puncture. As Figure 5.4 indicates, the direction of the vector jump (in this case, puncture number three at t = 45 minutes) coincides with phase three, as would be expected.

In the above theoretical example, only information from a single (simulated) measuring system is used. This is relevant in substations with a single group of three-phase voltage transformers. More data is available in substations with two or more groups of transformers. This facilitates another type of reliable detection which, instead, calculates the deviation from an average voltage on each phase.

Figure 5.5 shows a (simulated) difference between the average voltage and all individual voltages for a substation with six groups of three-phase CVTs. The difference is calculated according to:

$$Diff = 100\frac{U_{examined\,phase\ voltage} - \frac{1}{n}\sum_1^n U_{i,\ phase}}{\frac{1}{n}\sum_1^n U_{i,\ phase}}\ , \tag{5.7}$$

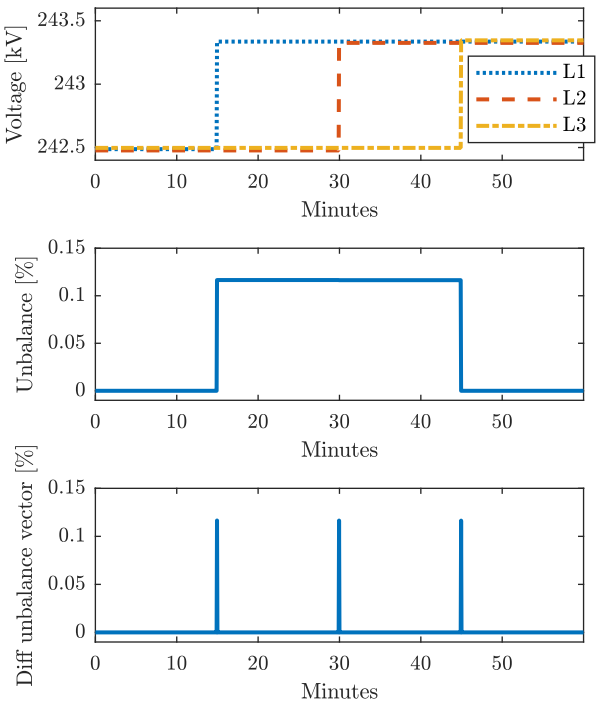


**Figure 5.3:** Theoretical registered phase voltages (top) for one hour, with a single capacitor puncture in the $C_1$ stack on each phase, 15 mins apart. Theoretical registered zero sequence unbalance (middle) and changes in normalised zero sequence vector between samples for the theoretical CVT puncture events (bottom).

where $n$ is the number of available measuring systems and $i$ denotes the sample used. (The equation is essentially the same as (4.1)).

A punctured $C_1$ capacitor in a 420 kV CVT with 288 capacitors in the total stack, will increase the measured voltage by approximately 0.35 % according to (5.2). If only two independent CVTs for each phase are compared, the average voltage will raise by half the increase in the punctured CVT, or approximately 0.17 % according to (5.7). The examined voltage reading will increase by 0.35 % compared to the other intact voltage readings. This means that the puncture will only indicate a 0.17 % raise from the average voltage. With further measurements available, the system suffering from the puncture will be raised by more than the decrease in the other systems. If there were an infinite number of CVTs to compare, the increase would be 0.35 %. Unaffected phase measurements will indicate a negative change from the average voltage.

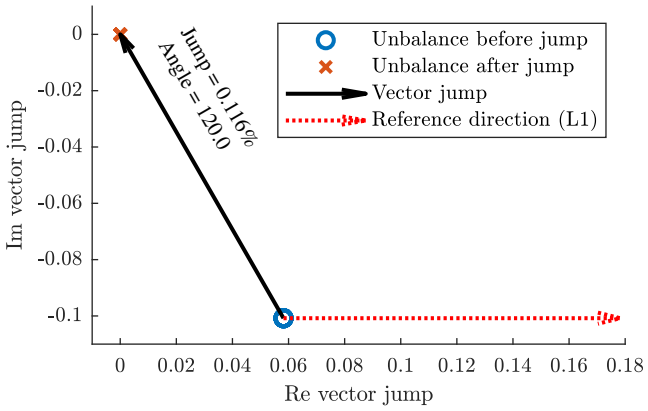


**Figure 5.4:** Vector jump for the third theoretical puncture at t = 45 minutes.

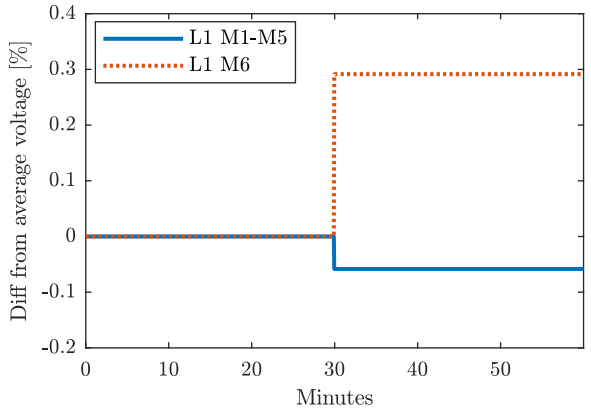


**Figure 5.5:** Comparison between six available voltages and the average of all voltages for phase one in a theoretical 420 kV substation. The simulated voltages are nominal for 30 minutes, at which point the measuring system M6 suffers a theoretical puncture in the top stack, $C_1$, in phase one.

## 5.3 Traditional and state-of-the-art monitoring methods for CVTs and new demands

A commonly used method for supervising CVTs is to measure the open delta voltage during service. Since this voltage can vary considerably in normal operation, the acceptance limit must be significant to safely indicate a problem. It is not normally possible to distinguish between a few punctured capacitors and a normal unbalance. A high open delta voltage may also indicate other types of problems than punctured capacitors.

Oil sample analysis is another way of monitoring CVTs. Samples during service visits and subsequent analysis may indicate a potential problem. The method requires a substation visit and the results cannot pinpoint specific problems, such as punctures.

The model-based method proposed by Freiburg *et al.* [4] is accurate and capable of

finding the root cause of different types of CVT failures. However, it is unsuited to online monitoring as it requires bulky equipment, manual intervention and service visits to substations.

One interesting automatic method using protection devices has been proposed by Kasztenny *et al.* [3]. They describe a method that is well-suited to continuous monitoring and can be used on only one group of three-phase CVTs. However, the stated accuracy is not high enough to detect individual CVT punctures. The article also introduces the idea of implementing algorithms in intelligent electronic devices (IEDs), an area of increasing interest as the industry gradually moves towards programmable digital equipment.

Feng *et al.* [1] do discuss several issues related to CVTs and suggest a data acquisition system very much like that of an energy meter or protection IED. It proposes methods that can be used in substations with only one group of three-phase CVTs. There is no mention of algorithms for achieving the proposed "Risk Early Warning Technology" and no evidence that single punctures can be detected. Therefore, it is hard to evaluate its performance.

Zhang *et al.* [14] propose a very interesting and promising approach to detecting ratio error drift in a single group of three-phase CVTs, which improves on earlier work [15]. Error simulation using real-world data has been made and it shows potential for achieving the necessary accuracy for detecting single-puncture events. However, no attempt has been made to discriminate a puncture from a similar step change in ratio error. Further data analysis of the detected rapidly changing error drift would certainly establish the true cause, if it was a puncture.

There are numerous articles relating to calibration or error estimation of voltage transformers and CVTs. Some examples are [2,10–13]. Most of these articles present interesting and accurate error evaluation but they all fall short in discriminating single-puncture events from other measurement errors. Most of them might be further developed to target puncture events. But even if it were possible to adapt the methods for targeting punctures, they all have limitations because they require more independent measurements than are normally available in substations. These methods cannot detect CVT problems in a substation with only one group of three-phase CVTs.

The author's earlier contribution [5] only monitored changes in zero sequence unbalance and not changes in its vector. This actually led to a real puncture event being missed, as described in Section 5.2. Moreover, the method does not use the information available in the measurement data when two or more three-phase groups of CVTs are measured in the substation.

Traditional CVT testing is normally calendar-based. Some testing and monitoring methods are more advanced than others but are performed during infrequent yet costly service visits. Therefore, partially failed CVTs can go undetected for a long time. Previously developed methods for continuous monitoring do not detect individual punctures, or are not accurate enough, or require special set-ups that cannot

be done in all stations or are costly. The work in this section allows new demands to be formulated. These may be summarised as follows:

- The method must automatically detect all individual puncture events as they occur, and provide a time stamp.
- The method must work in all types of substations.
- The method should use existing infrastructure to keep implementation costs down.

## 5.4 Continuous monitoring of CVTs

Long periods when CVTs go unchecked will increase the risk of the CVTs failing dramatically (exploding). Continuous monitoring of CVTs will reduce personnel risks, improve system stability in the transmission system and limit incorrect customer billing.

After the CVT explosions in 2014, it was evident that a new continuous monitoring method was needed; one accurate enough to find every punctured capacitor. To keep supervision costs down, such a method needs to be automatic. Computerised data-driven methods seem to offer the only hope of achieving this.

For a method to be low-cost, it should (if possible) reuse existing infrastructure. Svk uses real-time values sampled every three seconds. These values are already collected from high-quality energy meters [5]. Similar data can be found in IEDs, such as modern protection systems or other substation control equipment.

Two main, data-driven methods to monitor CVTs in the transmission system are presented:

1. A method for substations with a single three-phase group of CVTs.
2. Another method for substations with two or more independent three-phase groups of CVTs

The purpose of splitting the methods in this way is that both are required but work in fundamentally different ways. These methods are also divided into dynamic and static monitoring. Furthermore, the dynamic part needs continuous data and will analyse changes, while the static part can estimate the state of the CVTs with data from a single measured time sample.

The reason for having both dynamic and static approaches is that the dynamic approach is more sensitive than the static one, while the static approach can evaluate the current situation without historic data. The latter is important to capture events that happened before continuous data became available or for situations in which continuous data has been interrupted for some reason.

The methods described below will disregard punctures in the lower stack, $C_2$. There

are two reasons for this. Punctures in $C_2$ are much less frequent than in $C_1$ and $C_2$ punctures are easily detected due to the large measurement errors [4]. However, following the presented logic, it is simple to modify the algorithms and catch $C_2$ punctures as well. Other methods for $C_2$ puncture detection are currently used by Svk.

### 5.4.1 Dynamic monitoring - substations with only one group of CVTs

Experience has shown that punctures occur abruptly [5] and that the voltage reading will change rapidly. However, abrupt changes are common in electric grids. They can occur, for example, when a shunt reactor or shunt capacitor bank is energised. Therefore, it is impossible to examine each phase voltage separately to detect a puncture.

Taking inspiration from an open delta measurement, one may examine changes in the zero sequence voltage according to the theory described in Section 5.2. Figure 5.6 shows information from an energy measuring system and three punctures and a disturbance can be seen. As shown in the figure's bottom section, a disturbance can easily be mistaken for another puncture.

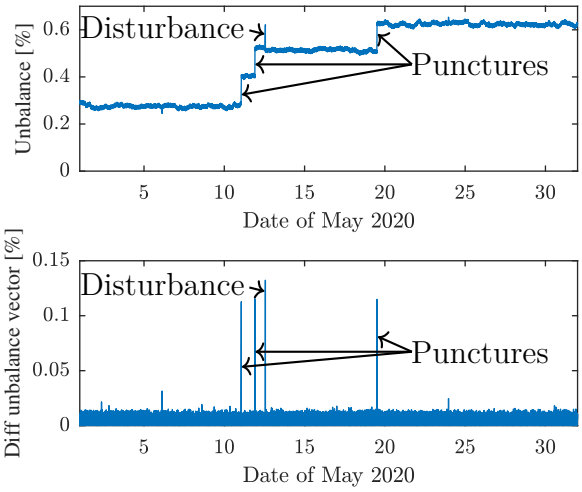


**Figure 5.6:** Zero sequence unbalance (top) and changes in normalised zero sequence vector between samples (bottom) for three CVT puncture events in May 2020.

According to (5.6), calculating the change in the zero sequence vector between each set of sampled values allows identification of the abrupt changes that occur when capacitors are punctured. The amplitude and angle of the changed zero sequence vector accurately differentiate between disturbances and punctures. Figure 5.7 shows both the amplitude and angle of the vector jump. Both values are very close to the anticipated theoretical values.

To reduce measurement noise, the difference is calculated by averaging some zero sequence vector values before and after the recorded high difference value. The

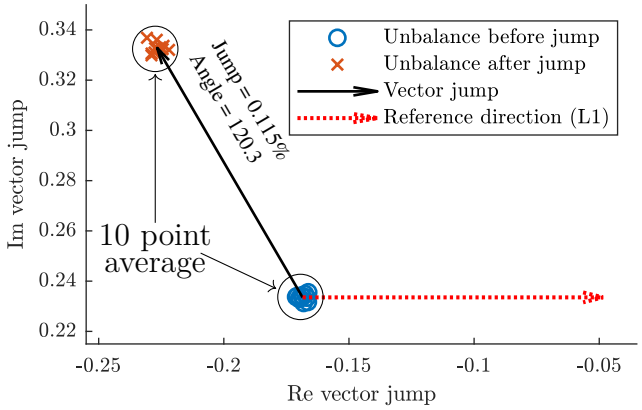


**Figure 5.7:** Vector jump for the first puncture in May 2020

difference between the two average vectors is the vector jump and is illustrated in Figure 5.7.

The novel algorithm for a single group of three-phase CVTs is presented as a flowchart in Figure 5.8 and consists of the following steps:

1. When new data is available, calculate zero sequence and positive sequence vectors. Normalise the zero sequence vector with the absolute value of the positive sequence (keep angle relation in zero sequence), according to equation (5.5). Calculate the change in the normalised vector between each sample, according to equation (5.6). If the calculated amplitude value is higher than a predefined threshold value, go to the next step and continue the investigation.

2. Average the unbalance vectors before and after the recorded high value. Calculate the vector jump between the two sets of averages.

3. Check that the amplitude and angle are within the correct range. If the angle is within a certain tolerance relative to 0, -120 or +120 degrees, the change indicates a puncture in phases one, two or three respectively. The tolerated range for amplitude and angle can be chosen in different ways depending on, say, voltage level and measurement noise. Checking that the vector jump is within certain tolerances will discriminate between a persistent change in unbalance, a puncture and a transient change such as an unbalanced that will disappear between the consecutive three-second samples.

In the Swedish transmission grid, there are only two voltage levels (220 kV and 400 kV). There are identical measuring instruments for all supervised CVTs. The experience is that it is sufficient to examine the data manually and choose reasonable algorithm settings that eliminate false alerts. Thus, settings are possible to find that work for both voltage levels. However, other grids with different voltage levels, measuring instruments and daily unbalance variations may require different settings.

A scientific methodology to find suitable algorithm settings involves using information on the CVTs and carefully examining the data. The recommendation is to

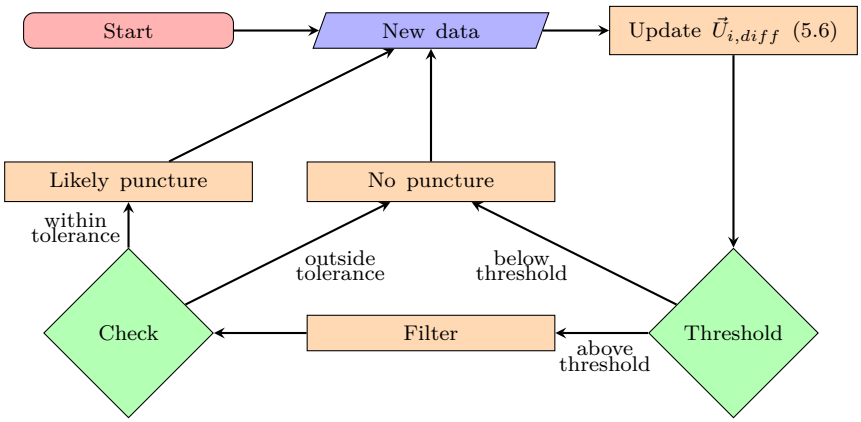


**Figure 5.8:** Algorithm flowchart for detecting punctures in substations with a single three-phase group of CVTs.

consider mainly the voltage level and measurement noise.

#### 5.4.1.1 Threshold

The threshold in Step 1 above is only used to alert high values in the vector jump, $\vec{U}_{i,\ diff}$, according to (5.6) and to discriminate a potential puncture from measurement noise or other minor disturbances. A suitable way of choosing the threshold is to examine the standard deviation of the noise. Figure 5.6 (bottom) illustrates how the standard deviation of the difference in the unbalance vector is equal to approximately 0.0046 %. Choosing a threshold value 4.9 times higher than the standard deviation, approximately 0.023 %, would theoretically give a false registration only once per million cases, as the noise is normally distributed. A value of 0.05 % has been selected for this work, which makes the algorithm very robust. The threshold must be well below the anticipated vector jump; this will depend on the number of capacitors in the CVT. The higher the number (depending on the voltage level), the smaller the anticipated jump. This means that the combination of measurement noise and voltage level will limit the opportunities for discriminating noise from a puncture.

#### 5.4.1.2 Average filter

In Step 1, a vector jump is calculated between two samples. The averaging in Step 2 will help calculate a more accurate vector jump. The averaging before and after the high value in Step 2 will increase the accuracy of the vector length and angle between the averaged values before and after the recorded event. The standard deviation of the mean value will decrease by a factor of $1/\sqrt{N}$, where $N$ is the number of values that are averaged. In other words, the effects of the measurement noise is reduced by the averaging filter. The recorded unbalance can also change over time. Averaging considerably more values is possible but, at some point, the averaging time will be so long that normal variations in the grid can negatively affect the result. There is a trade-off between a high number of averaging points and the risk that the unbalance will change due to normal variations in the grid. This can be investigated dynamically but the author determined empirically that an average of

10 recorded unbalance vectors before and after the recorded jump (as seen in Figure 5.7) gives robust results.

#### 5.4.1.3 Tolerances

Through the averaging step, a vector jump is determined. According to the theory, a puncture should produce a vector jump that coincides with the phase direction of the CVT with the punctured capacitor. Due to the measurement noise and slow natural variations of the zero sequence unbalance vector, neither the angle nor magnitude will perfectly match the phase direction or anticipated amplitude. A suitable tolerance between measured and anticipated values can be established by examining the standard deviation of the averaged values. The standard deviation will add uncertainty at both ends of the vector jump. The uncertainties perpendicular to the vector jump plus the length of the vector will produce an uncertainty in the angle; this can be used to find a suitable tolerance. The measured phase angles are normally very close to 0, -120 and 120 degrees in the grid. In some cases though, there are small deviations that must also be added to the anticipated tolerance. In Svk's case, a 2.5-degree tolerance has provided a robust algorithm for both voltage levels. Also, the length of the vector jump is examined and compared to the anticipated jump. Tight tolerances can be calculated using the same logic as for angles. If tight length tolerances are used, the algorithm has to be adopted for individual substations and cannot be used on mutiple voltage levels without different settings. Practical tests have proved that the algorithm is robust without using tight length tolerances in Step 3.

The bottom part of Figure 5.6 shows the amplitude difference in the zero sequence unbalance vector between samples.

For the particular group of CVTs, the anticipated change in the zero sequence vector amplitude is approximately 0.11 %. In Figure 5.6, it is evident that the noise level is low compared to the signal when a capacitor is punctured. The smaller disturbances can be disregarded (due to their size) but there is one disturbance in the same order of magnitude as the three punctures. This one is disregarded because the angle is not close to any of the phase directions and no increased level of unbalance remains. Figure 5.9 shows a printout from the algorithm for the puncture events in May 2020.

The first high peak in Figure 5.6 corresponds to the second row in Figure 5.9. The "likely CVT puncture" matches perfectly with what would be anticipated from a puncture in phase three. The change in phase voltage is $3 \cdot 0.115 = 0.345$ % and the phase angle is very close to 120 degrees. Row 4 is the next puncture and corresponds to the next high peak in Figure 5.6. The next two rows relate to the third high peak in Figure 5.6; the disturbance. The peak almost matches the amplitude change but the angle is unlike any of the three phases and the amplitude of the vector jump is too small, which distinguishes this peak from a puncture. The last peak relates to the third puncture.

Since punctures seldom occur, it is no great effort to manually check that the algorithm has made a correct determination (disturbances sometimes indicate other

```
Start time: 2020-05-01 00:00:00
CVT puncture C1 2020-05-11 01:25:45 on L3 Angle=120.3 Diff=0.115
Large unbalance 2020-05-11 23:43:42 Angle=124.4 Unbalance=0.52
CVT puncture C1 2020-05-11 23:43:42 on L3 Angle=120.1 Diff=0.115
Disturbance 2020-05-12 13:24:06 on L1 Angle=-178.9 Diff=0.002
Disturbance 2020-05-12 13:24:09 no phase Angle=-12.9 Diff=0.010
CVT puncture C1 2020-05-19 12:04:42 on L3 Angle=120.6 Diff=0.119
```

**Figure 5.9:** Print-out from algorithm developed for substations with only one group of CVTs.

problems in the measuring circuit).

### 5.4.2 Static monitoring - substations with only one group of CVTs

In substations with only one set of three-phase CVTs, the proposed static monitoring scheme is to set an alert level for the zero sequence unbalance.

Due to poorly transposed overhead lines, unbalanced loads and other circumstances that do not depend on punctures in CVTs the zero sequence unbalance can change substantially during normal operation.

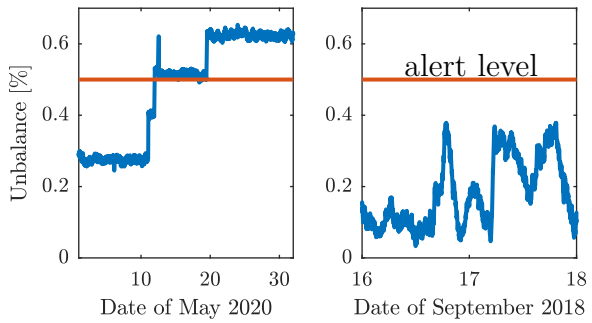


**Figure 5.10:** Unbalance in a substation during punctures (left) and an example of a normal (but high) daily unbalance variation in the transmission system (right).

The right-hand part of Figure 5.10 shows the zero sequence unbalance variation for a substation. In most areas in the Swedish transmission grid, the zero sequence unbalance varies by no more than 0.1-0.2 %. However, in other areas, it can be 0.5 % (or sometimes even higher). The unbalance normally varies with system load and will change during the day. Theoretically, a 0.5 % unbalance means that a single voltage reading has increased by 1.5 %. Such an increase would require multiple punctured capacitors (but still would not increase the stress on the remaining capacitors to a critical level).

Row three in Figure 5.9 is a static alert indicating an unbalance exceeding 0.5 %. In the left-hand part of Figure 5.10, the unbalance level at the second puncture exceeds the alert level. This appears because the CVT already had two damaged capacitors before the first puncture in May, as described later in Section 5.4.4.

This indicates that the static alert can only be used for puncture detection when

multiple punctures have already occurred. Furthermore, according to the above theory, it may fail to detect problems when several punctures have occurred in all phases.

Setting an unbalance alert level at 0.5 % would normally still catch a potential problem that could develop into a complete breakdown and possibly an explosion.

### 5.4.3 Dynamic monitoring - substations with two or more independent groups of CVTs

In substations with multiple three-phase voltage transformer groups, it is possible to compare amplitudes with other voltage transformers on the same phase. The algorithm primarily compares each measured amplitude with the average from all voltage transformers connected to the same phase.

In theory, a punctured $C_1$ capacitor in a 420 kV CVT, with a total of 288 capacitors, will increase the sampled voltage by approximately 0.35 %. If (5.7) is parametrised with a 0.35 % increase in voltage for one out of six voltage measurements, the increase would be approximately 0.30 %, as indicated in Figure 5.5.

The data in Figure 5.11 contains three punctures on phase three in system M6 during May 2020. This data comes from the same event as presented in Figure 5.6 above. However, Figure 5.6, presented only the data from measuring system M6.

The top part of Figure 5.11 shows the deviation between the average voltage and all individual voltages on phase three for all six available measuring systems in the substation, according to (5.7). There are several things worth pointing out in this part of the figure:

1. Because there are very small voltage drops within a substation, it is anticipated that all available voltages on each separate phase will be the same [2]. In Figure 5.11, there is a considerable difference between the voltages. In the Swedish transmission system, burden dependence in voltage transformers is corrected for, voltage drops in measuring cables and phase errors in the energy meters. Any differences should normally be less than a few hundredths of a per cent. The differences between systems M1-M5 are caused by poor (or no) voltage adjustment in the energy meters.

2. Right at the beginning of the data set, there is an even larger deviation on measuring system M6. As will be shown later, this is because the CVT has already experienced two previous punctures.

3. There are also variations and disturbances present in Figure 5.11. These variations are mostly due to temperature dependence and most of the disturbances originate from poor time synchronisation of the data from the different measuring systems.

4. Even from a brief examination of Figure 5.11, it is clear when the punctures occurred.

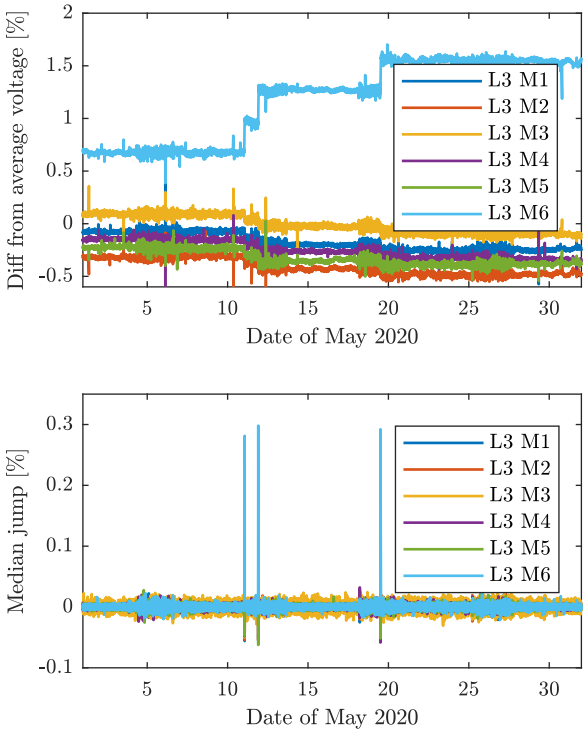


**Figure 5.11:** Comparison between average voltage of all measurements and each available phase voltage for phase three (top). Jump in median voltage deviation for all six measuring systems in the same substation (bottom). The data originates from a substation which had three punctures in May 2020.

The data used to examine CVTs is limited to the time stamp and phase voltage magnitudes. This data is collected from the energy meters every three seconds. The time synchronisation is within approximately +/-100 ms [5]. (Time synchronisation deficiencies will create noise).

The proposed novel algorithm for substations with several groups of CVTs is presented as a flowchart in Figure 5.12 and comprises the following steps:

1. When new data is available, calculate the phase-wise deviation from the average voltage for each measuring system in the substation. Normalise the deviation with the average voltage to a percentage value. This is done by using (5.7).

2. Filter the deviation to reduce some of the effects of time synchronisation issues and measurement noise. In this case, median values are created for 10 samples at a time (30 seconds of data). Median filtering effectively reduces the impact of the noise.

3. Compare the last median value with the new one. If any of the measuring systems have increased their deviation (jumped) suspiciously, continue investigating the event.

4. Compare the size of the step change with an anticipated puncture change. The increased deviation depends on the number of voltage measurements, as described earlier. If the change is within the anticipated range, indicate a potential puncture.

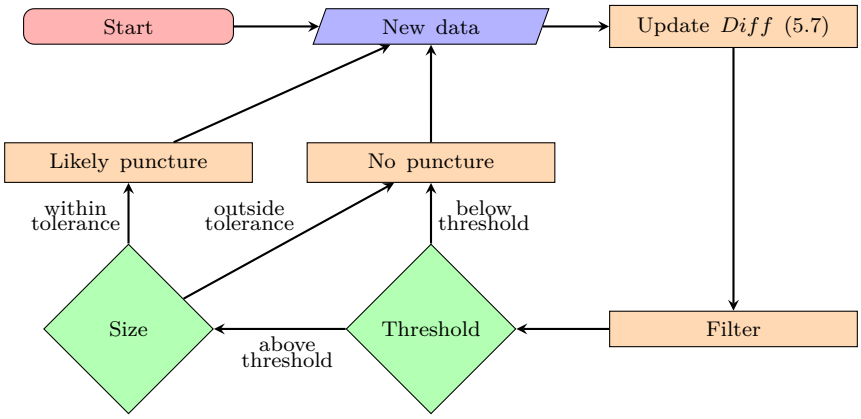


**Figure 5.12:** Algorithm flowchart for detecting punctures in substations with several groups of three phase CVTs.

The choice of algorithm settings depends on the voltage level, how many independent measuring systems are available and the measurement noise level. As discussed in Section 5.4.1, the voltage level will determine the approximate number of capacitors in the CVTs which, in turn, will determine how much the measured voltage level changes when a capacitor punctures. Equation (5.7) can be used to estimate the voltage jump.

The advantage of comparing several voltage transformers on the same phase is that any unbalanced disturbance appearing outside the substation will affect all voltage readings on the same phase. Therefore, such outside events or an unbalance between phases will not provoke any jumps in voltage, while a puncture in one CVT will change the relations between the voltage transformers and create a persistent change. The median filter, used in Step 2, will effectively eliminate short internal substation measurement noise and disturbances. Since a voltage change from a puncture event will be constant, the filter length is not critical and can be chosen freely. Using a very short filtering time will increase the noise in the median jump calculation in Step 3. Using long filtering will reduce the time accuracy for the actual puncture event. In practice, a minimum of 10 samples has proved a reasonable trade-off.

A large median voltage jump indicates a potential puncture. A minimum level can be estimated via the standard deviation, similar to the discussion on threshold values in Section 5.4.1. Obviously, the minimum level must be smaller than the anticipated median voltage jump.

As discussed earlier, so as not to miss any punctures, the threshold of deviation rise has to be well below 0.17 % for a 400 kV substation with only two independent CVTs on one phase. It should also be well above the noise level. The level can be chosen individually for specific substations, depending on how many groups of

voltage transformers are available for analysis. A setting of 0.1 % has been selected, which works for substations with two or more independent sets of three-phase voltage transformers and both voltage levels in the Swedish transmission system.

Analysing the change in voltage deviation rather than just levels eliminates the risk of mistaken alerts for variations like temperature dependence or poorly calibrated systems. Having a large span for a step change means the algorithm can also pick up other potential problems or find instances when several capacitors are punctured at the same time. The bottom part of Figure 5.11 indicates that the signal-to-noise ratio is high. Figure 5.13 shows the print-out from the algorithm.

```
CVT puncture C1 2020-05-11 01:25 on L3 system no 6 Diff=0.281
CVT puncture C1 2020-05-11 21:43 on L3 system no 6 Diff=0.298
CVT puncture C1 2020-05-19 12:04 on L3 system no 6 Diff=0.292
```

**Figure 5.13:** Print-out from algorithm using multiple measuring systems to detect CVT punctures.

### 5.4.4 Static monitoring - substations with two or more independent groups of CVTs

Although it is valuable to find new events as quickly as possible, it is also important to find capacitors that have already been punctured. The CVTs will normally be replaced after 30 or more years. This means that it will take a very long time to get rid of all CVTs which have suffered capacitor punctures before continuous data was available. The static monitoring scheme is a suitable aid for finding old puncture events. It is generally not possible to find individual, old punctured capacitors if there is only one group of three-phase CVTs in a substation. However, having multiple groups of independent CVTs makes this task easier.

As shown in the top part of Figure 5.11, there was a considerable offset from the average voltage for measuring system M6, even before the first puncture event in May 2020. This indicates that punctures had already taken place before the new events. Over two years' worth of data was examined but it was not possible to trace back and determine when these events took place.

When a capacitor in one of several groups of CVTs punctures, the deviation from the average voltage for each CVT voltage will change for all measuring systems. The voltage registered by the punctured CVT will increase and all the rest will decrease slightly (if the puncture is in Stack $C_1$). The changes will depend on how many independent voltage readings are available in the substation. If the system voltage is known, it is possible to estimate how much the change will be. This information is used to estimate how many capacitors are punctured in each system with the following novel algorithm.

The algorithm consists of the following steps:

1. Calculate the amount of deviation from the average voltage for all measuring systems. This can be done by calculating the Euclidean norm for all deviations (the norm effectively estimates the spread between all the voltages). Perform

this procedure for each phase individually.

2. Make a fictive correction of the voltage for the first system by reducing the voltage by the voltage value that one punctured capacitor would have.

3. Calculate the amount of deviation for the new set of voltages as in Step 1 above.

4. If the amount of deviation is lower than the previous one, there is likely at least one broken capacitor.

5. Continue to test whether further capacitors are broken by reducing the voltage by further fictive capacitor punctures until the amount of deviation starts to rise again. Store the number of fictive capacitor punctures needed to minimise the amount of deviation.

6. Perform the same procedure for the other systems and all three phases.

This procedure will produce the results seen in Figure 5.14. In this example every hundredth available sample is used.

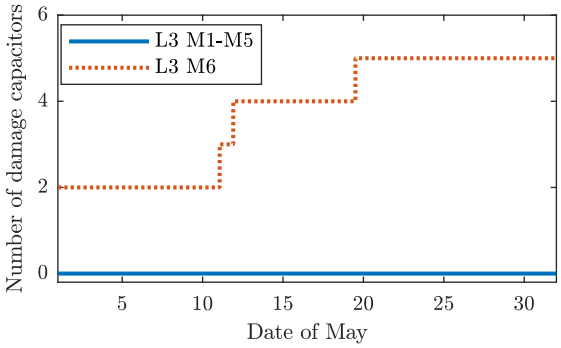


**Figure 5.14:** Result of the static monitoring approach performed on voltage measurements on phase three from the May 2020 puncture events.

The method depends on there being no other large voltage errors in the substation, such as very poorly calibrated measuring systems. It also depends on using a reasonably good estimate for the voltage change in punctured capacitors. Since the amount of anticipated voltage change depends on the total number of capacitors in the stack (which can vary), the algorithm can potentially misinterpret the information when the exact number of capacitors is unknown. Although the method is not perfect, it will still produce a reasonably good static estimation of partially broken CVTs in a substation with multiple measuring systems.

## 5.5 Results

During an initial campaign the algorithms were applied to data from approximately 100 substations. A total of 37 punctured capacitors were found, across 11 substations. In addition to the three punctures already presented in Section 5.4.3, a further

four punctures were detected as they occurred.

Furthermore, 30 old punctures (for which data was unavailable during the events) have been found using the static algorithm presented in Section 5.4.4. To date, no known false alerts have been produced.

Table 5.1 is a summary of punctures discovered using the static monitoring algorithm in Section 5.4.4. The dynamic monitoring algorithms could not be used for these punctures since continuous data was not available when the punctures occurred.

**Table 5.1:** Examples of punctures found with the static algorithm.

| Substation | measuring system | Phase 1 | Phase 2 | Phase 3 |
|---|---|---|---|---|
| SS1 | M1 | 2 | 2 | 1 |
| SS2 | M1 | 1 | 0 | 0 |
| SS3 | M1 | 0 | 0 | 3 |
| SS3 | M1 | 0 | 1 | 0 |
| SS4 | M1 | 0 | 0 | 3 |
| SS5 | M1 | 0 | 1 | 0 |
| SS6 | M1 | 0 | 1 | 2 |
| SS7 | M1 | 4 | 1 | 0 |
| SS8 | M1 | 1 | 0 | 0 |
| SS8 | M6 | 0 | 0 | 2 |
| SS9 | M1 | 0 | 1 | 1 |
| SS9 | M2 | 1 | 1 | 1 |
| SS9 | M3 | 1 | 0 | 0 |
| | Total | 10 | 7 | 13 |

Table 5.2 is a summary of punctures discovered using the dynamic monitoring algorithm described in Section 5.4.1 and 5.4.3. The static monitoring algorithms have also been successfully applied to these events.

**Table 5.2:** Examples of punctures found using the dynamic algorithms.

| Substation | Measurement system | Date and time | Affected phase |
|---|---|---|---|
| SS10 | M1 | 2016-10-24 08:08:54 | 3 |
| SS11 | M1 | 2017-11-18 21:08:03 | 2 |
| SS9 | M3 | 2018-09-18 05:30:06 | 3 |
| SS9 | M3 | 2018-09-18 05:32:03 | 3 |
| SS8 | M6 | 2020-05-11 01:25:45 | 3 |
| SS8 | M6 | 2020-05-11 21:43:42 | 3 |
| SS8 | M6 | 2020-05-19 12:04:42 | 3 |
| | Total | 7 | |

## 5.6 Conclusions and discussion

The automated monitoring system based on the above-described algorithms has proven to work according to Svk's needs. The algorithms have revealed many old punctures and continue to reveal new ones regularly. Until October 2024, Svk has found 74 individual punctures and currently monitors 59 active ones on a daily basis.

A CVT can survive for many years with one or two punctures without increasing the risks even to a moderate level. Knowing the number of punctures enables us to assess the risk and take relevant action. For example, Svk can immediately correct for the error that has been introduced rather than replacing the voltage transformer. Svk can plan a replacement or decide to keep the CVT in service. This procedure will enable a high degree of measurement performance and considerably reduce the cost and stress associated with planning for outages caused by equipment replacement.

Svk use available data from high-quality energy meters. This data is highly accurate and enables robust output from the algorithms. Svk anticipates that the proposed algorithms may be used with data from other measuring instruments, like IEDs in digital substations. This will work, provided the IEDs can provide reasonably high resolution and accuracy for both phase voltage and phase angles. If measurements from multiple IEDs are used together, the time synchronicity between measurements is important. Most advanced IEDs can be set up to either perform calculations internally or automatically transmit data to another IED that can do it. This can provide for low-cost, continuous supervision of CVTs, as pointed out in [3].

# Chapter 6

# Remote calibration of energy meters using Kalman filter

## 6.1 Introduction

Correct energy measurement is vital to electric energy trading. There are often stringent legal requirements on revenue metering that require periodic in situ substation verification. Traditional energy metering test methods are not possible in IEC 61850 DSs using a PB. This chapter will show that it is possible to use data analysis to verify the accuracy of energy-measuring systems in substations. The algorithms can be used as part of the legal verification and run remotely, online. Thus, some of the periodic accuracy verification (including substation visits) can be eliminated. These online algorithms make it possible to decrease the errors in both revenue metering systems and other energy-measuring systems in the Swedish transmission system. Measurement errors are now detected and amended much faster, which reduces incorrect billing. The algorithms also provide a solution to bridge the problem of verifying measurements in future, fully DSs.

energy-measuring systems play a vital role when trading electricity. Ensuring the high-accuracy measurement of traded electricity builds trust between market players [9, 17, 43]. Even measurement errors as small as 0.1 % in a single strategic measurement point in a transmission system can lead to incorrect billing running into the tens of thousands of EUR every month. Hence, the stringent legal requirements regarding accuracy and verification of revenue metering in transmission systems.

In Sweden, the required accuracy is stated as +/-0.5 % (including any uncertainty in the accuracy verification method) for all revenue metering systems exceeding a nominal measuring power of 10 MW. This applies to all measuring points in the Swedish transmission system. All revenue metering systems are subject to periodic verification at an interval of maximum six years. There is also a legal obligation to continuously monitor the accuracy of the measuring systems to ensure they meet the requirements.

Periodic verification is normally conducted on site and is costly. In the six-year

interval between visits, many different events can degrade the performance of a measuring system. It is difficult to monitor measuring systems between verification visits and, too often, degradations in performance go undetected.

An additional challenge is the introduction of the IEC 61850 DSs with a PB and LPITs. The energy-measuring system functionality is fundamentally different in such substations and will require new verification methods [44].

To overcome these challenges, it is worthwhile having a verification methodology that uses data analysis to continuously monitor the performance of energy meters and fulfils the legal requirements for verification. Such algorithms will lower the cost of verification and detect measurement errors as they occur. Corrections can be made immediately, leading to a fairer energy sector and greater public trust in the electric energy market.

The use of data analysis in transmission systems is becoming more popular, as more data from substations is made available each year. Energy meters are not alone in being able to supply high-quality measurement data from substations. PMUs, PQMs and IEDs are contenders in accurate measurement and can help monitor the array of energy-measuring equipment.

This chapter presents a unique, in situ calibration method for energy-measuring systems in substations in which all objects are measured (measurement in each bay). This means that all active power entering or leaving the busbars is measured, as mentioned in Section 4.2. The method is based on an analysis of energy measurement data and can be used as part of a traceable, accredited verification procedure.

Thus, the purpose of the work presented in this chapter is to develop algorithms suitable for transmission systems in which the requirement for verification accuracy is greatest and then prove their effectiveness. This aim is achieved by deriving and demonstrating algorithms that can factor in non-linear behaviour and present solid mathematics to give an uncertainty evaluation of the method. This is necessary if the algorithms is to be used as a part of an accredited verification method for energy-measuring systems in high-voltage substations.

The main contributions of this chapter are:

- Section 6.2. A theory that can be used for successful, continuous monitoring of the accuracy of measuring systems in high-voltage substations in which all objects are measured. The theory may be used as a part of an accredited verification procedure for energy meters.
- Sections 6.2.3 and 6.2.4. Algorithms that estimate measurement errors based on the most probable error distribution, based on *a priori* information from each measuring system.
- Section 6.2.5. A theory that also handles non-linear error behaviour in the measuring system.

This work closes the gap regarding what must be in place to use algorithms as part of the legal verification of energy meters. This is highlighted as a current problem in [17].

## 6.2 Theory

No measuring system is error-free. As mentioned in 3.2, the question is, rather, how inaccurate its measurements are. The theory developed here focuses on quantifying measurement errors and their associated uncertainties.

The algorithms presented in this chapter are specifically developed for substations in which all objects are measured, as illustrated in Figure 6.1. This requirement may seem a limitation but many existing substations (and all new ones in the Swedish transmission system) are built to facilitate it. The transition towards fully DSs will also allow for this condition, as all bays are measured.

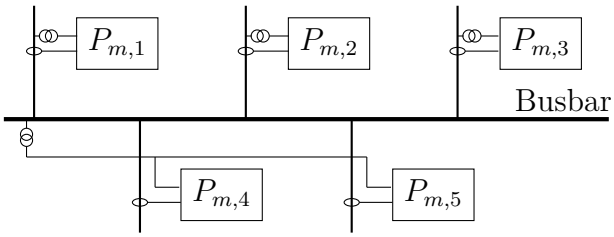


**Figure 6.1:** Schematic description of a substation in which key quantities from all objects (such as transformers, overhead lines, shunt reactors etc.) are measured.

Since the losses in a high-voltage switch yard are very low, they can be disregarded and set to zero in subsequent discussions [13] (as mentioned in Section 4.3.2). This assumption means that, if measured correctly, the sum of measured power should be zero. There are always measurement errors that will create a small residual power term when the sum of the measured power is calculated. This residual power term is the sum of all individual power measurement errors. The task is to split the residual power term (the total error) into portions that belong to each measuring system and convert this to individual measurement errors. An estimate of the uncertainty in the errors is included in the task.

### 6.2.1 Least Squares formulation

It is not possible to split the residual power term into each measurement error using only a single time-sample of power from all the measuring systems in the substation. However, under certain conditions, it is possible to do so by using multiple power samples.

To start with, we assume that all measurements have a relative linear error according to the following expression:

$$P_{m,i}(t) = (1 + r_i)P_i(t) + v_i(t) \ . \tag{6.1}$$

In (6.1) $P_{m,i}$ represents the measured (index $m$) power, $r_i$ is the fractional error for each power measurement, $P_i$ is the true power, $v_i$ is measurement noise and $t$ is the time at which the measurement sample is taken. The index $i$ refers to the specific measuring system. The sum of the registrations from all $n$ measuring systems, $z(t)$ can now be formulated as follows:

$$z(t) \equiv \sum_{i=1}^{n} P_{m,i}(t) = 0 + \sum_{i=1}^{n} r_i P_i(t) + \sum_{i=1}^{n} v_i(t) \ . \tag{6.2}$$

The "0" in the equation comes from the fact that the true power summation is exactly zero. If the last measuring system is excluded from the sum in (6.2), the equation can be rewritten:

$$\begin{aligned} z(t) &= \sum_{i=1}^{n-1} r_i P_i(t) + r_n P_n(t) + v(t) \\ &= \sum_{i=1}^{n-1} r_i P_i(t) - r_n \sum_{i=1}^{n-1} P_i(t) + v(t) \\ &= \sum_{i=1}^{n-1} (r_i - r_n) P_i(t) + v(t) \ , \end{aligned} \tag{6.3}$$

where

$$v(t) = \sum_{i=1}^{n} v_i(t) \ , \tag{6.4}$$

is the noise term. The last error, $r_n$, is now used as a reference for all other errors. Equation (6.3) can be rewritten:

$$z(t) = \sum_{i=1}^{n-1} \rho_i P_i(t) + v(t) \approx \sum_{i=1}^{n-1} \rho_i P_{m,i}(t) + v(t) \ , \tag{6.5}$$

using the formulation $\rho_i = r_i - r_n$ and the fact that there are small measurement errors indicates that $P_i \approx P_{m,i}$. This approximation will introduce errors in the $\rho$ estimates of the order of $\rho^2$ (in other words, negligible for systems with a small $\rho$). (For systems with a larger $\rho$, the calculations can be improved by taking corrected power values from the first calculation and use them in a second estimate). In the Kalman formulation below, it is possible to compensate for estimated errors as they start to become available and, thereby, improve the accuracy of the estimate.

By rewriting the equations in vector form we get:

$$z(t) = \boldsymbol{H}_{line}(t)\boldsymbol{\rho} + v(t) \ , \tag{6.6}$$

where vector $\boldsymbol{H}_{line}$ is

$$\boldsymbol{H}_{line}(t) = [P_{m,1}(t) \ P_{m,2}(t) \ ... \ P_{m,n-1}(t)] \ , \tag{6.7}$$

and the relative error vector $\boldsymbol{\rho}$ is:

$$\boldsymbol{\rho} = [\rho_1 \ \rho_2 \ ... \ \rho_{n-1}]^T \ . \tag{6.8}$$

With multiple measurements at different times, $t_k$, we will get an equation system:

$$\begin{cases} z(t_1) = \boldsymbol{H}_{line}(t_1)\boldsymbol{\rho} + v(t_1) \\ z(t_2) = \boldsymbol{H}_{line}(t_2)\boldsymbol{\rho} + v(t_2) \\ ... \\ z(t_m) = \boldsymbol{H}_{line}(t_m)\boldsymbol{\rho} + v(t_m) \ . \end{cases} \tag{6.9}$$

With enough time samples of varying power, we now have an overdetermined equation system that can be solved. If we formulate a matrix of vectors $\boldsymbol{H}_{line}$ at $m$ points in time, then:

$$\boldsymbol{H} = \begin{bmatrix} \boldsymbol{H}_{line}(t_1) \\ \boldsymbol{H}_{line}(t_2) \\ ... \\ \boldsymbol{H}_{line}(t_m) \end{bmatrix} \tag{6.10}$$

and

$$\boldsymbol{z} = [z(t_1) \ z(t_2) \ ... \ z(t_m)]^T \ , \tag{6.11}$$

the solution for estimating relative errors, $\boldsymbol{\rho}$, is as follows

$$\hat{\boldsymbol{\rho}} = [\boldsymbol{H}^T\boldsymbol{H}]^{-1}\boldsymbol{H}^T\boldsymbol{z} \ . \tag{6.12}$$

This formulation is known as a least squares solution that will minimise the sum of the squares in the residuals.

We have the relative errors but, depending on the amount and quality of input data, there are uncertainties associated with the calculation. A combination of low measurement noise, major variations in measured power and a large amount of data will reduce these uncertainties.

According to the least squares theory, for example [45], the variance of the estimated relative errors, $\boldsymbol{\rho}$, can be found in the diagonal elements in the covariance matrix, $\boldsymbol{C}_{\boldsymbol{\rho}}$, calculated according to:

$$\boldsymbol{C}_{\rho} = \sigma^2[\boldsymbol{H}^T\boldsymbol{H}]^{-1}. \tag{6.13}$$

The true measurement error variance, $\sigma^2$, is estimated as the variance of the measurement vector $\boldsymbol{z}$ according to:

$$\sigma^2 \approx \ \frac{\sum_{i=1}^{m}(z(t_i) - \boldsymbol{H}_{line}(t_i)\hat{\boldsymbol{\rho}})^2}{m-n} \ . \tag{6.14}$$

In our case, the statistical degree of freedom $m - n$ is the number of measurements used, minus the number of estimated parameters.

### 6.2.2 Kalman filtering formulation

It is possible to use the least square method described above but there are some advantages to reformulating the problem by using Kalman filtering instead to find the relative errors. Two main advantages deserve to be pointed out:

- The Kalman filter is recursive and the calculations can be updated as data becomes available. After each iteration, the current states are stored and there is no need to store old data.
- The Kalman filter has the "innovation" feature, which is an efficient way of discarding poor-quality data. It is also useful as an alert for finding malfunctioning equipment.

With a Kalman filter, it is possible to process very long time series continuously without major memory being needed and still produce the same (or higher) accuracy than with the least squares calculation. All the results are updated after each new time sample. This makes the Kalman filter ideal for continuous online supervision of measuring systems.

The theory is well described in [46]. Below the steps in calculating each new time sample of measurement data are outlined.

The Kalman gain, $\boldsymbol{K}$, is calculated according to:

$$\boldsymbol{K} = \boldsymbol{C}_\rho^- \boldsymbol{H}_{line}^T / (\boldsymbol{H}_{line} \boldsymbol{C}_\rho^- \boldsymbol{H}_{line}^T + R) \ . \tag{6.15}$$

$\boldsymbol{C}_\rho^-$ is the last updated covariance matrix for the relative error vector (6.8). In (6.15), $R$ is the true measurement error variance. An estimate can be obtained according to (6.14).

With new data, the sum of the measurements, $z_k = z(t_k)$, is calculated according to (6.6). A new estimate of the relative errors, $\hat{\boldsymbol{\rho}}$ and an update of the covariance matrix, $\boldsymbol{C}_\rho$ can be calculated according to:

$$\begin{aligned} \hat{\boldsymbol{\rho}} &= \hat{\boldsymbol{\rho}}^- + \boldsymbol{K}(z_k - \boldsymbol{H}_{line}\hat{\boldsymbol{\rho}}^-) \\ \boldsymbol{C}_\rho &= (\boldsymbol{I} - \boldsymbol{K}\boldsymbol{H}_{line})\boldsymbol{C}_\rho^- \ , \end{aligned} \tag{6.16}$$

which uses the latest estimated updates of the relative errors, $\hat{\boldsymbol{\rho}}^-$, and the covariance matrix, $\boldsymbol{C}_\rho^-$. These updates are stored and used for the next iteration of estimates.

The updates of $\hat{\boldsymbol{\rho}}^-$ and $\boldsymbol{C}_\rho^-$, are valid for the case with no dynamical change in $\boldsymbol{\rho}$ over time for, say, data from shorter durations. For processing data across a range of years (in system monitoring), parameters describing a stochastic change in $\boldsymbol{\rho}$ can be included [46].

The Kalman filter algorithm anticipates the start values of $\hat{\boldsymbol{\rho}}_0{}^-$ and $\boldsymbol{C}_{\rho.0}^-$. The diagonal of the first covariance matrix are given such large values that it has no

noticeable influence on the final result, in either the final covariance matrix or the relative errors.

### 6.2.3 Estimating measuring system errors

In the preceding subsections, we estimated the relative measurement error vector, $\hat{\boldsymbol{\rho}}$, that holds all relative measuring system errors, $\rho_i = r_i - r_n$. Additional information is essential for determining the errors, $r$, at reasonably low uncertainty. Based on factory tests of the different components or other calibrations, it is possible to set up a vector of known *a priori* biases, $r_0$, (with zeros for systems with no known bias), plus a covariance matrix, $C_{r_0}$, describing the uncertainties in the *a priori* values.

The relative errors, $\boldsymbol{\rho}$, can be expressed as $\boldsymbol{\rho} = \boldsymbol{A}_{\rho,r}\boldsymbol{r}$, with:

$$\boldsymbol{A}_{\rho,r} = \begin{bmatrix} 1 & 0 & \dots & 0 & -1 \\ 0 & 1 & \dots & 0 & -1 \\ \vdots & \vdots & \ddots & \vdots & -1 \\ 0 & 0 & \dots & 1 & -1 \end{bmatrix} \tag{6.17}$$

and $\boldsymbol{r} = [r_1\ r_2\ ...\ r_n]^T$ being a vector built from each individual measuring system error.

Analogous to the Kalman filter formulation (6.16), it is possible to calculate an error estimate, $\hat{\boldsymbol{r}}$, based on a linear combination of the estimation results, $\hat{\boldsymbol{\rho}}$, and *a priori* values, $\boldsymbol{r}_0$, as:

$$\hat{\boldsymbol{r}} = \boldsymbol{r}_0 + \boldsymbol{K}_{\rho,r}[\hat{\boldsymbol{\rho}} - \boldsymbol{A}_{\rho,r}\boldsymbol{r}_0] \ . \tag{6.18}$$

The "gain", $\boldsymbol{K}_{\rho,r}$, that blends known information with calculated information is then:

$$\boldsymbol{K}_{\rho,r} = \boldsymbol{C}_{r_0}\boldsymbol{A}_{\rho,r}^T[\boldsymbol{A}_{\rho,r}\boldsymbol{C}_{r_0}\boldsymbol{A}_{\rho,r}^T + \boldsymbol{C}_\rho]^{-1} \ , \tag{6.19}$$

where $\boldsymbol{C}_{r_0}$ is the covariance matrix of the *a priori* error values in $\boldsymbol{r}_0$. The error covariance of the $\hat{\boldsymbol{r}}$ estimate is:

$$\boldsymbol{C}_r = [I - \boldsymbol{K}_{\rho,r}\boldsymbol{A}_{\rho,r}]\boldsymbol{C}_{r_0} \ . \tag{6.20}$$

The derivation of (6.19) and (6.20) can be found in [46].

The estimated errors, $\hat{\boldsymbol{r}}$, are now optimal, based on the *a priori* information on both the known errors and measuring system uncertainties. Figure 6.2 shows the Kalman iteration process and error estimation process.

### 6.2.4 Structure of the known *a priori* covariance matrix

As described in Section 6.2.3, the uncertainties in the *a priori* values $\boldsymbol{r}_0$, contained in its covariance matrix, $\boldsymbol{C}_{r_0}$, have a vital role in finalising the estimates in (6.18).

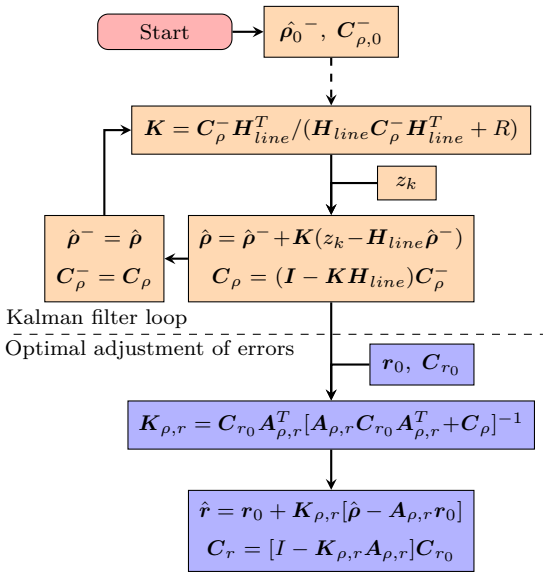


**Figure 6.2:** Schematic description of how the Kalman filter loop and optimal adjustment of errors are performed.

Large diagonal values for a system will give its *a priori* values less influence (as large off-diagonal values also do).

The total random errors, $e_t$, in the *a priori* values can be written as $e_t = r_0 - r$. Each measuring system consists of three main components, the voltage transformers, the current transformers and the energy meter. This means that $e_t$ for the system may be seen as a sum of random terms from each component. For the case with no shared components between the systems, these random terms can be assumed to be uncorrelated between the two systems $i$ and $j$. In other words, $E[e_{p,i}e_{q,j}] = 0$ for the components $p$ and $q$. This results in a covariance matrix with zero off-diagonal elements:

$$C_{r_0,i,j} = \begin{cases} E[e_{t,i}e_{t,j}] = E[e_{t,i}^2] = \sigma_{t,i}^2 & \text{, if } i = j \\ = 0 & \text{, if } i \neq j \ . \end{cases} \tag{6.21}$$

However, if the two systems share a voltage transformer (as indicated for measurements $P_{m,4}$ and $P_{m,5}$ in Figure 6.1), its random error, $e_{u,ij}$ is common to the two systems. With $e_{t,i} = e_{u,ij} + e_{r,i}$ and $e_{t,j} = e_{u,ij} + e_{r,j}$ ($e_r$ from the remaining components), we get $E[e_{t,i}e_{t,j}] = E[e_{u,ij}^2] = \sigma_{u,ij}^2$ when $i \neq j$ and a covariance matrix with non-zero off-diagonal elements:

$$C_{r_0,i,j} = \begin{cases} E[e_{t,i}e_{t,j}] = \sigma_{t,i}^2 & \text{, if } i = j \\ E[e_{u,ij}^2] = \sigma_{u,ij}^2 & \text{, if } i \neq j \ . \end{cases} \tag{6.22}$$

As an example, the covariance matrix would have the following elements:

$$\boldsymbol{C}_{r_0} = \begin{bmatrix} \sigma_{t,1}^2 & 0 & 0 & 0 & 0 \\ 0 & \sigma_{t,2}^2 & 0 & 0 & 0 \\ 0 & 0 & \sigma_{t,3}^2 & 0 & 0 \\ 0 & 0 & 0 & \sigma_{t,4}^2 & \sigma_{u,45}^2 \\ 0 & 0 & 0 & \sigma_{u,54}^2 & \sigma_{t,5}^2 \end{bmatrix} , \tag{6.23}$$

for a substation, as described in Figure 6.1, in which measuring systems 4 and 5 share the same voltage transformers. Note that $\sigma_{u,45}^2$ and $\sigma_{u,54}^2$ are identical.

### 6.2.5 Formulation for handling non-linear errors

The above theory will provide the "optimal" error estimation solution, provided the model of the errors is correct. We have assumed constant, linear, relative errors, which is reasonable for a voltage transformer operating within a relatively small span of voltage variation. However, for the current transformers (and energy meters), the errors vary depending on the operating point. Under certain conditions, this has been shown to create small but unnecessary errors in the estimate. To overcome this problem, it is possible to model a piecewise, linear error curve that will be closer to the real-world errors, as indicated in Figure 6.3.

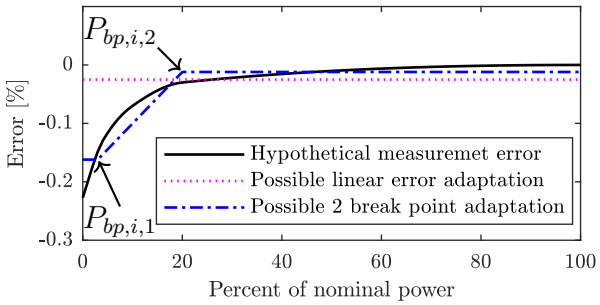


**Figure 6.3:** Piecewise, linear error curves between breakpoints will adapt to a non-linear error curve better than a constant linear error.

One solution to the problem is to split each metering system into two (or more) "fictive meters". Let us define two power breakpoints, $P_{bp,i,1}$ and $P_{bp,i,2}$, in the working area for each of the measuring systems. A piecewise, linear error $r_i$ is built according to:

$$r_i = (1 - \alpha_i) r_{i,1} + \alpha_i r_{i,2} , \tag{6.24}$$

where $r_{i,1}$ and $r_{i,2}$ are the errors at the breakpoints and

$$\alpha_i = \begin{cases} 0 & , \text{if } P_{bp,i,1} > |P_{m,i}| \\ \frac{|P_{m,i}| - P_{bp,i,1}}{P_{bp,i,2} - P_{bp,i,1}} & , \text{if } P_{bp,i,1} < |P_{m,i}| < P_{bp,i,2} \\ 1 & , \text{if } P_{bp,i,2} < |P_{m,i}| \end{cases} . \tag{6.25}$$

$\alpha_i$ is a linear proportion ($0 \leq \alpha_i \leq 1$) for where the measured power is located between the two breakpoints; 0 below the first breakpoint and 1 above the second

one. The result is a piecewise error curve, as shown in Figure 6.3. Analogous to (6.3) in 6.2.1, a new sum of the measurements is built according to:

$$\begin{aligned}
&\sum_{i=1}^{n} r_i P_i(t) = \\
&\sum_{i=1}^{n-1} r_i P_i(t) + (1-\alpha_n) r_{n,1} P_n(t) + \alpha_n r_{n,2} P_n(t) = \\
&\sum_{i=1}^{n-1} r_i P_i(t) - r_{n,2} \sum_{i=1}^{n-1} P_i + (1-\alpha_i)(r_{n,1} - r_{n,2}) P_n = \\
&\sum_{i=1}^{n-1} (r_i - r_{n,2}) P_i(t) + (1-\alpha_i)(r_{n,1} - r_{n,2}) P_n \ .
\end{aligned} \tag{6.26}$$

A relative error vector is constructed according to:

$$\boldsymbol{\rho} = [\rho_{1,1} \ \rho_{1,2} \ ... \ \rho_{n,1}]^T \ , \tag{6.27}$$

where $\rho_{i,j} = r_{i,j} - r_{n,2}$, $n$ is the number of measuring systems and $j$ is the breakpoint number (1 or 2 in this case), since each measuring system is broken down into two fictive ones.

The $\boldsymbol{H}_{line}$ vector is expanded, analogous to the theory in Subsection 6.2.1 and will now contain $2n-1$ values as follows:

$$\begin{aligned}
\boldsymbol{H}_{line}(t) = [&(1-\alpha_1) P_{m,1}(t) \ \alpha_1 P_{m,1}(t) \\
&(1-\alpha_2) P_{m,2}(t) \ \alpha_2 P_{m,2}(t) \ ... \ (1-\alpha_n) P_{m,n}(t)] \ .
\end{aligned} \tag{6.28}$$

The measured power from each measuring system, $P_{m,i}$, can now be split between the fictive measuring systems, $P_{m,i,1}$ and $P_{m,i,2}$ according to:

$$\begin{aligned}
P_{m,i,1} &= (1-\alpha_i) P_{m,i} \\
P_{m,i,2} &= \alpha_i P_{m,i}
\end{aligned} \tag{6.29}$$

and the $\boldsymbol{H}_{line}$ vector will now look as follows:

$$\boldsymbol{H}_{line}(t) = [P_{m,1,1}(t) \ P_{m,1,2}(t) \ ... \ P_{m,n,1}(t)] \ . \tag{6.30}$$

Note that (6.29) satisfies the requirement that: $P_{m,i} = P_{m,i,1} + P_{m,i,2}$.

The result is an error curve that will imitate real-world behaviour better than a flat linear error. Following the same logic, it is possible to introduce further breakpoints and match reality even more closely. However, using this approach will require enough measurement samples from the various power regions for the uncertainty of all errors in the estimate to become low.

### 6.2.6 Further features of Kalman filtering

In the theory section 6.2.1, a simplification in (6.5) was made. As long as the measurement errors are small, this simplification, $P_i \approx P_{m,i}$, will create small estimation errors. In the least squares formulation, it can be dealt with iteratively, using the estimated errors to correct the measurements and running the estimate again. In the Kalman filter, it is possible to use the estimated errors for each new iteration and correct the measured values. However, this is not usually necessary in practice since the measurement errors in a transmission system are normally very small.

Converging as fast as possible requires a good estimate of the true error variance (6.14). To find this value, the errors must be known but this is not the case at the beginning of the Kalman iterations. Nevertheless, after some iterations the estimated errors start to become stable and can be used to make a good estimate of the true error variance.

One very useful feature is the "innovation". The innovation, $J$, is formulated according to:

$$J = z_k - \boldsymbol{H}_{line}\hat{\boldsymbol{\rho}}^{-} \ , \tag{6.31}$$

where the last term is the expected value of the sum of all measurements. The standard deviation of $J$ is:

$$\sigma_J = \sqrt{\boldsymbol{H}_{line}\boldsymbol{C}_{\rho}^{-}\boldsymbol{H}_{line}^{T} + R} \ . \tag{6.32}$$

If the absolute value of the innovation is larger than a factor, $k$, compared to the standard deviation ($|J| > k\sigma_J$), it is an indication that the anticipated value of $z_k$ differs considerably. This indicates that the measurement data is corrupt or that something has happened. The Kalman filter loop can be skipped for this particular iteration. This avoids using an outlier measurement, which would create unnecessary estimation errors. An alert flag can be set to indicate a potential problem. The factor $k$ can be chosen such that the probability of the sum of the measurements, $z_k$, being out of tolerance is defined. For example, choosing $k = 3$ gives a probability of 99.7% that $z_k$ is experiencing some disturbance. The innovation has proven to be an excellent alert for malfunctioning instrument transformers and for sorting out bad data. As an example, Svk has used the innovation to find intermittent secondary winding short circuits in current transformers.

## 6.3 Results and discussion

To validate the true performance of the Kalman filter algorithm for a real-world situation, real data from calibrated measuring systems should be used. The calibration state of the measuring systems should have an accuracy several times better than the results of the method being used but, in practice, this is not possible. In most cases, the proposed algorithms perform as well or better than the traditional verification method, so the performance of the algorithms cannot be validated by comparing the results between methods. Using synthetic data can provide some proof of performance but it is hard to model all potential problems correctly. The proposal is to use something between these two approaches.

Measured data can be used and then "washed" by correcting the measurements to fulfil the assumption that the sum of the power to the substation is exactly zero. This can be done by subtracting the total error, the sum $z(t)$ in (6.2), from the original data. A good option is to subtract the small total error from the measuring system containing the largest values, because the small residual term, $z(t)$, will have negligible impact on the larger values. There is now a perfect dataset that still contains the main features of the measurements. These main features (like the power variation, correlation in variation and power difference between measurements) will affect the convergence rate and are important to conserve when validating the algorithms.

Arbitrary errors and measurement noise can be added to the perfect, "washed" data. Thus, it is possible to fully test how the algorithm behaves under specific measurement and data quality imperfections, without risking mixing up the performance with the unknown errors in the original dataset. It is also possible to verify the theoretical possibility of estimating errors using a specific dataset.

The legal accuracy requirement for an energy meter is that the measured energy is correct, not the power. In the examples below, hourly energy values were used instead of power readings. This will give a direct response to the issue of energy metering system accuracy. However, if the power fluctuates while it is being integrated, it will introduce small errors because the power (and power errors) will vary during the integration period. For transmission systems like the one in Sweden, the power normally changes slowly and has proved not to create substantial errors.

To use the proposed algorithms for legal accuracy verification, there must be *a priori* information acquired through procedures that meet the demands of legal metrology. The required *a priori* information referred to in the Theory section 6.2 can come from different procedures, like factory testing, site testing, standards or other sources. In the following, it is assumed that this information is available.

### 6.3.1 Perfect world - linear error representation

For simplicity, data from a substation which has three measuring systems and a linear error representation is used. The measured data in question is "washed" and rendered into a perfect state. An error of 0.1 % and measurement noise with a standard deviation of 0.14 MW is added to the data for the third energy meter. Both are typical values that can be observed. The *a priori* $2\sigma$ uncertainty of all measurements is set to 0.3 %. An estimate of five days of hourly energy values will give the estimated errors according to Figure 6.4.

A few observations may be noted in the figure. The measurement M3, which contains the error, is low in power and does not vary substantially. This makes reducing the uncertainty of the estimated error slower compared to the other two measurements. Initially, the algorithm also hesitates regarding the error estimate. As anticipated, when the power starts varying in measurement M3, it is evident that the algorithm is performing better.

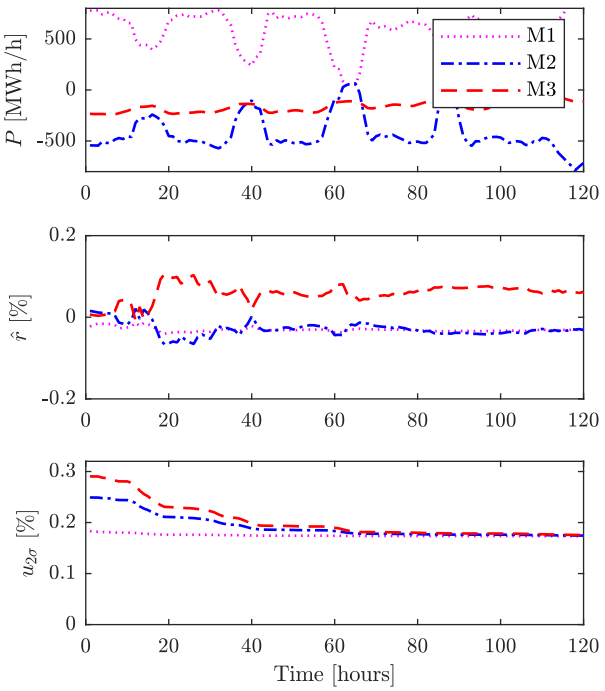


**Figure 6.4:** Top: Hourly values for three real-world measurements. Middle: Error estimate for a theoretical error of 0.1 % on measurement M3 and no errors on M1 and M2. Bottom: Uncertainties in the estimated errors.

After some 70 iterations of hourly energy measurements, both the errors and the uncertainties stabilise. The uncertainties are closing in on around 0.17 %, which is no coincidence. The achievable uncertainty for three uncorrelated measurements with an uncertainty of 0.3 %, measuring the same quantity is $u = 0.3\ \%/\sqrt{3}$. This is the amount that the uncertainties are converging on asymptotically. It will be referred to as the "final uncertainty".

Another thing to point out is that the estimated error for measurement M3 is not 0.1 %; the *difference between* the estimated errors is 0.1 %. That has to do with how the optimal (most likely) adjustment of errors is done. Since there is no *a priori* error information for any of the measurements, the error estimates, $\hat{r}$, are based on the relative errors, $\hat{\rho}$, in a way that minimises all errors based on the stated uncertainties, as per the theory in 6.2.3.

### 6.3.2 Real world - error detection

In this subsection, results are presented based on data with real errors. In one sense, this does not prove the performance of the algorithms because the true errors in the measuring systems are not known. One helpful detail is that, in the dataset used in this example, a capacitor puncture occurred in one of the CVTs connected to measuring system M2. In this particular CVT, a punctured capacitor in the top stack of the CVT will introduce an error of +0.444 % in one phase. This means that the energy measurement error will be approximately one-third of this value since

the power is almost symmetric in all three phases.

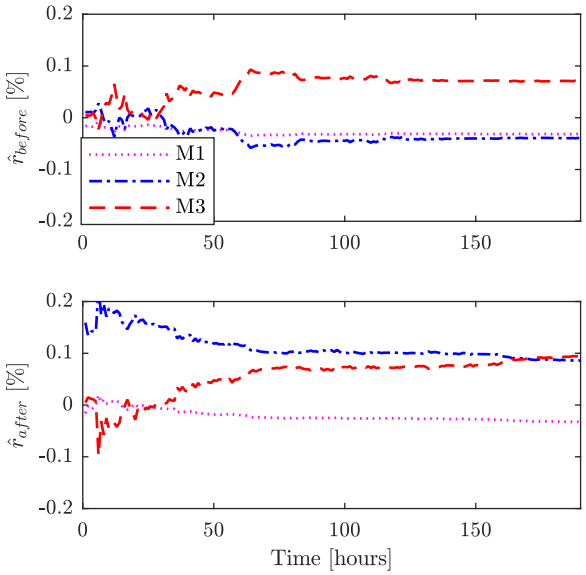


**Figure 6.5:** Estimated measuring system errors before and after a capacitor puncture, in one CVT in measuring system M2. Top graph presents the situation before the puncture event and bottom graph after it.

Figure 6.5 presents the estimated errors before and after the puncture. This puncture was detected using the algorithms presented in [41]. Since the puncture was detected, it was possible to accurately quantify the anticipated error change in the energy measurements as 0.148 %. This value was introduced in the *a priori* information for the specific measuring system. Provided the assumption is correct, doing this means that the anticipated error will not change the error levels for the other measurements. As can be seen in Figure 6.5, only the M2 measurement has changed its error value in the estimate with data after the incident. This confirms that the algorithms perform as anticipated for changes in measurement errors based on real-world data.

An error of this size and in this position in the transmission system causes an incorrect billing of some EUR 26,000 per month. A capacitor puncture will normally be detected during the traditional verification, which is conducted every six years in accordance with legal requirements. This means that such a single error can cause incorrect billing totalling EUR 1.9 million before the measurement error is corrected. This clearly demonstrates the advantage of the algorithms presented in this chapter, if they are used regularly.

### 6.3.3 Perfect world - non-linear representation

At normal operating power, measuring systems are usually highly linear (as they are designed to be). However, at low power, both the measuring instrument and current transformer errors may be non-linear. As long as the measured power for all measuring systems is in the linear region, there will be no erroneous estimates. In cases where the power in any of the measuring systems is often within the non-linear

region, the estimated errors can be contaminated by measurements from the non-linear region. Noticeable (but usually minor) contamination is especially likely if any of the high-power measurements contain non-linear errors and often fall within their non-linear regions. Such contamination is usually at its highest in the low-power measurements. In transmission systems, the low power measurements are often revenue measurement points within which accuracy requirements must be met. Thus, it is important to address the problem. One way of dealing with it is to exclude all measurements from non-linear regions. However, this is not always possible. Another way is to use the theory developed in 6.2.5. This splits the error model into a piecewise, linear error model, as shown in Figure 6.3, which can handle real non-linear errors much better than a flat, linear error model.

To illustrate this problem and its solution, part of the dataset used in 6.3.1 will be washed again to yield a perfect set of measurements with zero errors, as described in Subsection 6.3.1. This perfect data is contaminated with errors in measurement M1. The errors that are introduced are piecewise and linear and start at $-0.2$ % at zero power and ends with 0 % at 200 MWh/h. In the region above 200 MWh/h, the error continues to be 0 %. The middle part of Figure 6.6 shows the results of the estimate based on a pure linear error model. It is important to note that neither M2 nor M3 has been contaminated with errors and that the estimate should indicate zero errors. This is not the case. As can be seen, measurement M3 (the lowest power measurement) is contaminated the most, from the poorly-modelled errors in M1.

When a piecewise, linear model is introduced into the Kalman filter, as described in Subsection 6.2.5 the estimate can adapt to the varying error in the data for measurement M1. The bottom part of Figure 6.6 allows the results of an estimate to be studied, in which the Kalman filter has two breakpoints for measurement M1.

In this case, the error at the low breakpoint is assumed to have twice the uncertainty level of all the other errors (set at 0.3 % with a coverage factor of 2). Given these preconditions, the filter will estimate all errors accurately. It should be noted that the error associated with the low breakpoint for measurement M1 does not change before the power of M1 moves into the region with the varying error.

As stated before, the estimation errors will normally be very small (even without using a piecewise, linear error model in the Kalman filter) but they can easily be avoided if the theory is used and there is enough data to train the filter. Using piecewise, linear error models will require more information about the measuring system. This can normally be found in the calibration and test reports for the energy meter and current transformers.

### 6.3.4 Further discussion

The previous sections have presented the theory and some results that demand wider discussion.

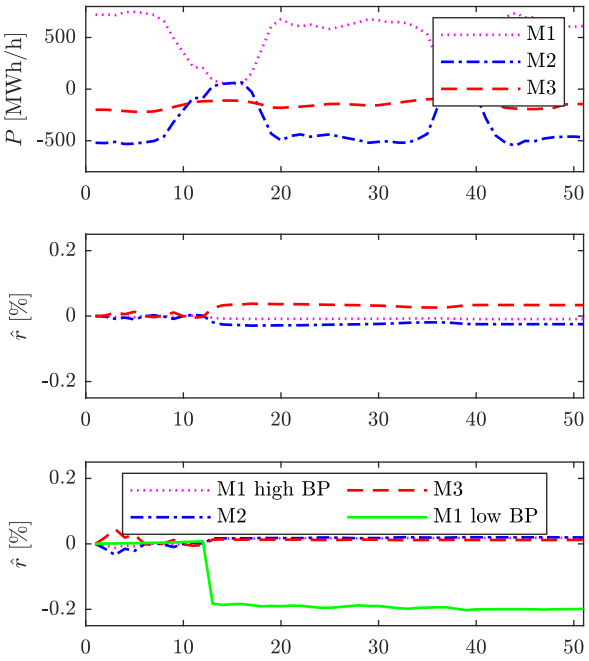


**Figure 6.6:** Comparison between estimates with and without a piecewise, linear error model. The top figure shows the measuring systems' power. The middle one shows the error estimate with a linear model. The bottom one shows the error estimate using a piecewise, linear error model for the M1 measuring system.

#### 6.3.4.1 General discussion

During the commissioning of the energy-measuring systems in a substation, available (*a priori*) information is used to trim the accuracy to be as high as possible. Using best practices, Svk's experience is that the remaining differences in errors between measuring systems are normally below 0.05 %. A "fingerprint" of the system can be obtained at the beginning of its service life. Subsequent verifications aim to prove that no degradation has occurred. One way of describing this is that we rely on factory calibration for the commissioning part and subsequently verify that any change from the original setup is not outside the legal requirements. An evaluation must provide error estimates and method uncertainty. Mathematical algorithms that provide error and uncertainty estimates can replace traditional methods and enable continuous supervision. The algorithm has been developed primarily for verification purposes. If the combination of the errors and uncertainties is too high, then either a different calibration procedure must be conducted or components will have to be replaced.

#### 6.3.4.2 Relationship between errors and the impact of *a priori* information

An important fact to point out is that the algorithms compare all measurement errors to a reference error, $r_n$, as shown in (6.3). However, the algorithms will be

unable to correctly evaluate a common bias in errors (as might appear if a correction for the burden dependence of all voltage transformers was not made during commissioning). The algorithms can only find relative errors and will provide the most probable error estimate for the measuring systems, based on the *a priori* information used in the equations in Subsection 6.2.3.

With the *a priori* values, $\boldsymbol{r}_0$ and $\boldsymbol{C}_{r_0}$, it is possible to distribute the errors statistically according to the equations presented in Subsection 6.2.3. An unexpected error can often be explained and corrected for in the *a priori* information, if its magnitude is known. One example is punctured capacitors in CVTs, as described in Subsection 6.3.2. With a correct *a priori* error value, the other errors are not affected.

If one of several measuring systems is affected by an unknown error, this error will also affect the estimates of the other errors. Table 6.1 contains a theoretical analysis using synthetic data on how the estimates are affected, based on different parameters. All estimates are based on an error of 0.1 % for measuring system number 1. None of the other measuring systems contain any error. The Calculations are made for substations with between three and nine independent measuring systems. For the first four calculations, the uncertainties, $\sigma_t$, according to (6.22), are set at 0.3 % (with a coverage factor of 2, in other words $2\sigma_t$) for all measuring systems. In Calculation 5 the uncertainty for system number 1 is changed to 0.5 % and for Calculations 6 and 7 it is set to 0.1 %.

When the error is unknown, as in Calculations 1-6, it is evident that the algorithms will not find the exact error. It will distribute the errors based on the *a priori* information. Note that the result will be more accurate as the number of measuring systems increases. In Calculation 5, in which the uncertainty is higher for the first system, the estimation errors are all smaller because the measurement of the error is not as "trusted" as the others. In Calculation 6, we can see that a more trusted measurement (lower uncertainty) will make all estimation errors worse. In Calculation 7, the estimate is perfect because the *a priori* error is correct. One thing to point out is that the final uncertainty (achieved when there is sufficient data) will decrease with the number of measuring systems in the substation. It is important to understand that if one of the measurements has a lower uncertainty, as in Calculation 6, it will make the final uncertainty level lower for all measuring systems.

In a real situation, we expect all measuring systems to have small errors. Just as for a single error, as seen in Table 6.1, all errors will introduce estimation errors in all other measurements. This can be seen in the four theoretical examples summarised in Table 6.2. In these examples, there are five independent measuring systems with an uncertainty of 0.3 %. There is no *a priori* error information available, so $r_{0,i} = 0$. Different errors are introduced, as seen from the values in the top row of each example in the table. The estimated errors are shown below.

There are endless possible combinations of errors to explore but the four examples indicate how the algorithm treats various ones. The first calculation indicates that the two positive errors will produce a negative error in their estimate for the three

**Table 6.1:** Impact of uncertainties and error distribution depending on number of measuring systems when one measuring system is experiencing an error of +0.1 %.

| Number of systems | Estimated error system number 1 | | Estimated error remaining sys. | Final uncertainty |
|---|---|---|---|---|
| | error | $2\sigma_t$ | $2\sigma_t = 0.3$ | |
| 3 ($r_{0,i} = 0.0\%$) | 0.067% | 0.3% | -0.033% | 0.173% |
| 5 ($r_{0,i} = 0.0\%$) | 0.080% | 0.3% | -0.020% | 0.134% |
| 7 ($r_{0,i} = 0.0\%$) | 0.086% | 0.3% | -0.014% | 0.113% |
| 9 ($r_{0,i} = 0.0\%$) | 0.089% | 0.3% | -0.011% | 0.100% |
| 9 ($r_{0,i} = 0.0\%$) | 0.096% | 0.5% | -0.004% | 0.104% |
| 9 ($r_{0,i} = 0.0\%$) | 0.047% | 0.1% | -0.053% | 0.073% |
| 9 ($r_{0,1} = 0.1\%$) | 0.100% | 0.1% | 0.000% | 0.073% |

**Table 6.2:** Impact of multiple unknown errors in a substation with five independent measuring systems. The rows represent four different cases with different errors.

| Meas. sys. number | 1 | 2 | 3 | 4 | 5 |
|---|---|---|---|---|---|
| Set errors | 0.05% | 0.05% | 0.00% | 0.00% | 0.00% |
| Estimated errors | 0.03% | 0.03% | -0.02% | -0.02% | -0.02% |
| Set errors | 0.05% | -0.05% | 0.00% | 0.00% | 0.00% |
| Estimated errors | 0.05% | -0.05% | 0.00% | 0.00% | 0.00% |
| Set errors | 0.05% | -0.05% | 0.05% | -0.05% | 0.05% |
| Estimated errors | 0.04% | -0.06% | 0.04% | -0.06% | 0.04% |
| Set errors | 0.05% | 0.05% | 0.05% | 0.05% | 0.05% |
| Estimated errors | 0.00% | 0.00% | 0.00% | 0.00% | 0.00% |

other estimates. The next two calculations show that if the errors are random at around zero, the error estimate will be more accurate. The last calculation shows that the algorithms cannot find a common bias error. This clearly shows the importance of carrying out the commissioning correctly.

As described above, the algorithms will rely more on measuring systems with low uncertainty and "move" any errors to the more uncertain systems. The accuracy of modern energy-measuring systems is pushed to its practical limits and is high. In transmission substations, the equipment used is of the same or similar high quality. Thus, one measuring system is unlikely to be more accurate than the other. This is one reason why it is difficult to "calibrate" the systems using the proposed algorithms. However, under certain circumstances, it is possible to calibrate systems using them. An example is when one measuring system is thoroughly calibrated and has lower uncertainty than the others, as shown in Table 6.1, Calculation 7. This may be achieved when old equipment is changed for new equipment that has been properly calibrated.

The correlation between measurements (such as two measuring systems sharing the same voltage transformers) is taken care of in the covariance matrix, $\boldsymbol{C}_{r_0}$, as described in Subsection 6.2.4. If there is a covariance between measurements, there

is less independent information available for the algorithm to explore. A higher covariance between measurements will result in higher remaining uncertainties. This also means that if a real covariance is omitted in the *a priori* information, the algorithm will present a lower than actual uncertainty. On the other hand, in a transmission system this information is always available and should be included in the calculations to ensure correct results. This means that the impact will not be large. For example, in a substation with three measuring systems, two of which share the same voltage transformers there will be non-zero, off-diagonal elements in the covariance matrix $\boldsymbol{C}_{r_0}$. If the total uncertainty of all the measurements is 0.3% and the uncertainty of the voltage measurements is 0.2%, the final uncertainty will change from 0.173% to 0.194%. With an increased number of measuring systems in the substation, these differences will decrease.

The *a priori* information is available from different sources and is always used when commissioning an energy-measuring system in the Swedish transmission system. For more correct results, it must also be used when deploying the proposed algorithms.

#### 6.3.4.3 Performance validation

The algorithms have been used in parallel with the traditional verification procedures in more than 40 substations. On almost all these occasions, the results between the verification methods were close to identical. This is not a validation of the algorithms but does serve as a good indication that their performance is very promising.

During the initial work, the algorithms have reached a high degree of maturity and are ready for real-world implementation. Even if they perform perfectly on a theoretical level and are found to work well with measurement data from a real substation, there are still be various practical challenges that need to be addressed before these algorithms can be incorporated into an accredited method for verifying the accuracy, as required by law.

Below are a few examples of real-world challenges that can produce estimation errors that must be thoroughly explored:

- Hourly energy measurements are an average of power over the course of an hour. The variation in power will introduce estimation errors when non-linear errors are present.
- Time synchronisation errors between measurements will produce measurement noise. This noise is not normally "white" and will, therefore, produce estimation errors [16].
- Variation in errors due to, say, temperature dependence.
- Large power differences between the measuring systems may have a particularly negative effect on the error analysis of the lower power measurements.

Exploring how the performance of the algorithms degrades under the influence of non-ideal conditions like the challenges described above has started. So far, no unacceptable degradation has been found and it seems possible to calculate the ad-

ditional uncertainty for each dataset that may be added to the main result. Further challenges may well emerge during future work.

## 6.4 Conclusions

Algorithms that estimate measurement errors with associated uncertainties in energy metering systems have been developed. This is the foundation of the ability to introduce data analysis within accredited verification procedures. Using automatic data analysis dramatically reduces the cost of verification and can be carried out much more frequently. Measuring system errors can be detected faster than before and, thus, incorrect measurements and billing can be reduced.

The introduction of unconventional instrument transformers and process buses in DSs introduces new verification problems that may potentially be reduced or eliminated by using the algorithms that have been developed.

Further steps have been carried out by the Swedish NMI (RISE), which has developed an accredited verification procedure based on the presented algorithms. The algorithms have been used for online monitoring purposes between traditional verifications, which have have discovered energy measurement errors valued at over EUR 1 million per year. More recently, the accredited verification process has been used on a regular basis in the transmission system.

# Chapter 7

# $SF_6$ gas leakage

## 7.1 Introduction

$SF_6$ gas is widely used in high-voltage switchgear thanks to its excellent electrical properties. Unfortunately, it is also the most potent greenhouse gas known today, with 1 kg of $SF_6$ equivalent to approximately 25 tons of $CO_2$. Therefore, it is important to monitor equipment that contains $SF_6$ to find and repair any leakages as early as possible.

This chapter discusses practical challenges and provides a novel algorithm that can be used for automatic, early $SF_6$ gas leakage detection in CBs. The work is based on laboratory and field tests in three substations in the south of Sweden.

The tests were carried out with two different types of digital $SF_6$ gas sensors: a density sensor and a pressure sensor. The core of the early $SF_6$ gas leak detection algorithm is that it detects very small changes in gas content by comparing the varying pressures between circuit breakers. The algorithm detects leaks of the order of 0.1 %/year within 2-3 weeks based solely on absolute pressure readings. The total installation cost is approximately EUR 750 per sensor.

The purpose of this chapter is to propose a methodology for sensitive and quick $SF_6$ gas leakage detection. The specific contributions of this chapter are:

- Section 7.5.1. Identification of a practical challenge concerning the selection of suitable sensors, that has not been previously described in the literature.
- Section 7.6. Development of an early leakage detection algorithm that can be used successfully for continuous monitoring of small $SF_6$ leakages in high-voltage applications.
- Section 7.7.4. Derivation of a cost estimate for installing $SF_6$ gas sensors in a context similar to that of the Swedish transmission system.

## 7.2 Field test installations

### 7.2.1 Installation conditions

Most of the CBs in the Swedish transmission system are provided with service panels for handling $SF_6$ gas. The service panel is mounted at a suitable working height on the foundation of the CB and has four gas connections. It is basically a distribution block with four standardised gas connection ports. The first connection is allocated to the CB, which is connected to the service panel through a 1.5 m tube 5 mm in diameter. The second connection is dedicated to the traditional mechanical sensor with two pressure switches, as described in Section 7.3. The third and fourth connections are spares that can be used for gas handling or any other purpose.

One reason for having a service panel at working height is that it is easier to check the dial on the traditional pressure sensor. A second reason is that gas handling is easier when filling or emptying the CB. A third, positive effect is that the vibrations when manoeuvring the CB are much lower in the CB's foundation than in the CB itself. This may be important for sensors on CBs that are manoeuvred frequently, such as shunt capacitors or reactors. This is because repeated high levels of vibration may degrade a sensor more quickly.

The sensors used in this work were all installed in parallel, with the ordinary mechanical sensor attached to spare connection number three, leaving the fourth connection on the service panel available for gas handling.

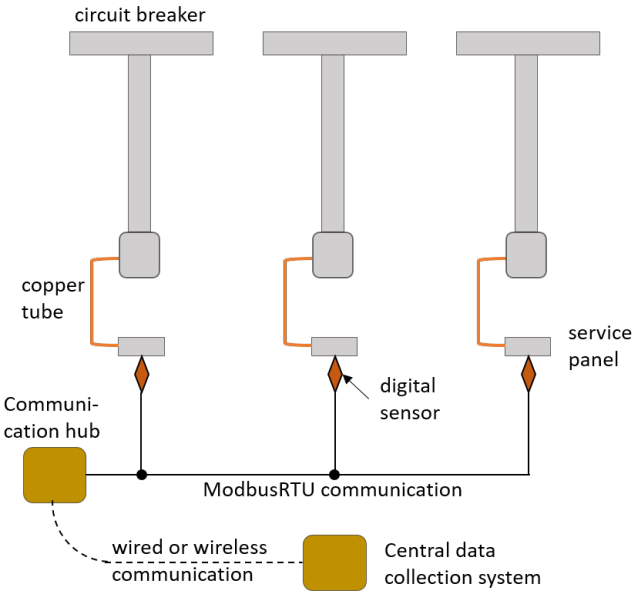


**Figure 7.1:** Schematic connection diagram of a setup of three circuit breakers, including digital sensors and data acquisition.

### 7.2.2 Communication

The digital sensors have a ModbusRTU interface that enables digital communication. It allows the retrieval of multiple data values from each sensor and uses less cabling

than an analogue interface.

The installations were either fixed or temporary. In the fixed installations, prefabricated signal cables are laid in the cable ducts, while the communication hub is placed in an existing cabinet. This cabinet serves a group of three CBs, connected to one busbar in a single bay, providing power and signals to the CBs. For the temporary installations, the communication hub was placed in a small, prefabricated cabinet mounted on the foundation of one of the three CBs. The signal cables were slung above head height between the CBs' foundations.

For all installations, one communication hub serves three sensors. The communication hubs were either RS485-I/Os connected to a programmable logic controller (PLC) via optical fibre, or remote terminal units (RTUs) communicating over the telecommunications network via SIM card. Figure 7.1 shows a schematic of the installation.

### 7.2.3 Test installations

The work included installations of 57 sensors in three different substations on four different occasions. The different installations of sensor batches can be summarised as follows:

- Batch 1: 18 digital density sensors in substation A.
- Batch 2: 6 digital pressure sensors in substation B.
- Batch 3: 30 digital pressure sensors in substation A.
- Batch 4: 3 digital pressure sensors in substation C.

#### 7.2.3.1 Installation of sensor batch 1

The first batch of fixed installation of 18 digital density sensors was put into service on 15th September 2021, at Substation A. The six RS485 communication hubs, one per three sensors, communicate via optical fibres to central data collection hardware in the control building. All sensors are polled once per minute for density, temperature, absolute pressure and pressure at 20 °C. The active installation time for the sensors and data collection hub was about an hour per sensor. Installing the optical fibres between the data collection hubs and central data collection hardware took over an hour per sensor.

#### 7.2.3.2 Installation of sensor batch 2

The second batch of six digital pressure sensors was installed and commissioned on 22nd February 2023, in substation B. This installation concentrated on testing a concept of temporary leakage detection. In this case, an RTU communicates through the ordinary telecommunications network, using secure SIM cards via a VPN tunnel to a similar RTU located in the offices of the Swedish TSO. The RTU there is connected to data collection hardware that reads temperature, absolute pressure and pressure at 20 °C from each sensor every 10 minutes. The active installation time for sensors, cabinet and cabling for each of the two sets of three CBs, was

around nine hours, or 1.5 hours per sensor.

#### 7.2.3.3 Installation of sensor batch 3

The third batch of 30 digital pressure sensors was installed and commissioned on 11th May 2023, in substation A. The communication hubs are fixed, RTU-type installations. The total installation was completed in one day and took some 30 man hours, or one hour per sensor.

#### 7.2.3.4 Installation of sensor batch 4

The fourth batch of three digital pressure sensors was installed and commissioned on 1st June 2023, in substation C, due to a suspected leak in this newly-built substation. This installation was temporary and of the same type as batch 2.

## 7.3 Sensor technology

### 7.3.1 Gas density, pressure and temperature dependence

An ideal gas behaves according to the ideal gas law:

$$pV = nRT \ , \tag{7.1}$$

where $p$, $V$ and $T$ are the pressure, volume and absolute temperature, $n$ is the number of particles and $R$ is the ideal gas constant. Equation (7.1) indicates that the pressure will increase linearly with temperature if the number of gas particles inside a fixed volume is constant. This suggests that if both the pressure and temperature are measured, it is possible to investigate whether the number of gas particles (molecules) are decreasing in the constant volume of a CB. One common way to do this is to normalise the actual pressure to what it would be at 20 °C. The *pressure at* 20 °C is constant if the number of gas molecules inside the breaker is conserved.

Since the mass depends on the number of gas molecules, the density (the mass divided by the volume) is another value that can be used to investigate whether a leak is present. By rearranging (7.1) the following expression is obtained:

$$\frac{p}{T} = \frac{nR}{V} \propto \frac{m}{V} = \rho \ , \tag{7.2}$$

where $m$ is the mass. This means that the density, $\rho$, is proportional to the pressure divided by the absolute temperature in the ideal case. It is common for there to be a mixture of different gases in a CB. Dalton's law of partial pressure implies that the density of a mixture of ideal gases of different molecular weights is still proportional to the pressure divided by the absolute temperature. This assumption only applies if the gas is completely mixed throughout the total gas volume.

Thanks to its electrical properties, $SF_6$ is the gas most used in CBs, as its performance is better at high pressure. At elevated pressures, $SF_6$ gas gets closer to its condensation point. Gas condensation is a problem in CBs, especially at low temperatures [29]. Thus, to lower the condensation temperature and reduce the

amount of $SF_6$ needed [22, 23, 47], other gases can be mixed with $SF_6$. Two common gases used in conjunction with $SF_6$ are nitrogen ($N_2$) and carbon tetrafluoride ($CF_4$). At close to the condensation point and with a mixture of gases, the ideal gas law ceases to apply [48] and cannot be used to accurately calculate the pressure at 20 °C. Various equations are available to calculate the pressure or density at 20 °C for real (non-ideal) gases more correctly and provided the gas composition is known, a correct result can be obtained.

### 7.3.2 $SF_6$ gas sensors

This work relates to three main types of $SF_6$ gas sensors:

- The traditional mechanical sensor with a dial indicator and electrical pressure switches.
- The digital pressure sensor with a ModbusRTU communication interface.
- The digital density sensor with a ModbusRTU communication interface.

The traditional sensor is a mechanical sensor with a membrane mechanically connected to a dial indicator and two electrical pressure switches. As indicated in Section 7.3.1, the pressure will vary substantially with the temperature variations during a day and over a season. To reduce this variation, the mechanical sensor compensates for temperature changes and the dial shows the pressure at 20 °C. This makes the mechanical sensor remarkably accurate and reliable but it still suffers from the same effects as the electronic sensors, as described in Section 7.5.

The digital pressure sensor measures the absolute pressure and temperature. It calculates both the density and pressure at 20 °C, based on the specific gas composition. In the conducted test, one factory-programmed sensor and another, field-programmable one was used. The field programmable sensor produces slightly less measurement noise but is more expensive.

The digital density sensor works differently from the pressure sensor, by measuring dynamic viscosity. The viscosity is estimated based on the frequency difference between two quartz oscillators, one in the gas and the other in a vacuum. That viscosity is then converted to density using a robust, non-linear equation [26, 49]. The density can be used to assess a leakage, but the pressure at 20 °C is more commonly used and so the sensor also calculates the pressure at 20 °C.

The digital sensors used in the test both had ModbusRTU communication interfaces. Thus, it was possible to communicate with the sensor and retrieve different types of information, such as temperature, density, pressure and pressure at 20 °C. Values given in different units, like MPa, Bar, °C or Fahrenheit can also be supplied by the sensor.

## 7.4 Currently used $SF_6$ leakage detection

### 7.4.1 Manual supervision

The functional properties of a CB depend on the gas density. A mechanical sensor is therefore always installed and connected to each CB to monitor the gas. Traditional mechanical sensors have a dial indicator and two digital signal switches connected to the protection and control system. The first signal indicates low pressure, while the second one indicates critically low pressure (which will normally block the CB from manoeuvring). These two digital signals will cause notifications or alarms to the operators in the control centre. The CB will have lost a substantial amount of gas before the first signal notifies the operator. For example, a CB can be filled to a level of 0.70 MPa and the first indication of low pressure will appear at 0.62 MPa. This means the CB will have lost over 10 % of its gas content without a problem being signalled. Consequently, digital pressure switch signals are unsuitable for early leakage detection [26].

In the Swedish transmission system, dial indicators are checked several times a year and, thus, leakages can be detected. However, it is often very hard to get an early warning because manual gas readings will differ from person to person and the information is not organised to allow efficient analysis. Thus, it is difficult to monitor small leakages using traditional mechanical sensors. It usually takes well over a year to accurately detect a leakage rate of 1 %/year.

### 7.4.2 Continuous computerised supervision

With the rapid developments in sensor technology, communications and data analysis, it is increasingly common to install a gas density monitoring system that can be used to detect leakage. The main advantages of this are:

- No visits to substations to monitor gas pressure are required.
- Gas pressure readings are taken more frequently and are not sensitive to the human factor.
- The information is organised in a database and potential leakages can be evaluated automatically.

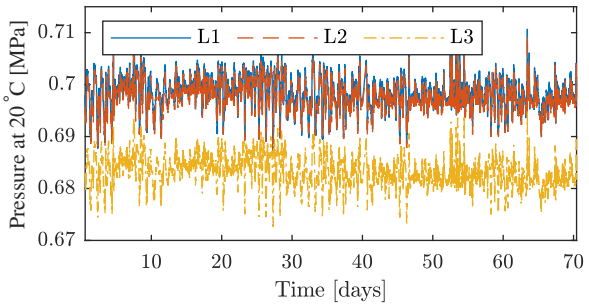


**Figure 7.2:** Sample pressure readings at 20 °C from a group of three circuit breakers connected to one busbar, in one bay.

When gas escapes from a CB, the density (and thereby pressure) will be affected. Therefore, it is straightforward to analyse the pressure and find a leak by introducing an alert limit. As discussed in Section 7.3.1, using a calculated value for the pressure at 20 °C allows a more stable value to be obtained despite varying temperatures in the substation. Figure 7.2 shows the calculated pressure at 20 °C for three CBs connected to one busbar, in one bay. Over a 70-day period, phase L3 CB has lost approximately 0.2 % of its gas content, which is very hard to see in the graph. Thus, early leakage detection based on an alert limit for the pressure at 20 °C, will perform very poorly. There is evidence in the literature to support a detection time of between eight months and seven years for a leak rate of 0.5 %/year [24, 30].

## 7.5 Practical challenges

Our goal is to be able to detect leaks as quickly as possible using a digital pressure or density sensor. A number of challenges have emerged in seeking to accomplish this target. These have been handled during this research project and the most important ones are briefly described and discussed below.

### 7.5.1 Gas mixing challenge

#### 7.5.1.1 Measurements

If the mixture of different gases is not the same throughout the entire volume, it can cause poor measurement results. If there is residual air remaining in the sensor following the mounting procedure, it will affect the measurement until the gas is properly mixed. This was especially pronounced when installing the digital density sensor on the service panel, which is connected to the CB by a thin tube. It will take a great deal of time before the small amount of air is properly mixed with the gas inside the CB. Also, internal density differences in, say, a mixed-gas circuit breaker (which arise during gas filling) will affect the measurement until the gas is properly mixed across the entire volume.

Figure 7.3 shows several filtered density values from the batch 1 installation in substation A. Note that all but two of the values increase slowly over time (solid lines). Naturally, this is incorrect since none of the CBs are filled with any additional gas. This is caused by a small amount of air inside the sensor (introduced during installation) slowly mixing with the heavier $SF_6$ gas inside the CB. The mixing process is greatly extended in time due to the aforementioned tube between the service panel and the CB. The signals increase over 180 days. In the same figure, two signals are declining over time. The lower declining signal (dotted line) in the figure is actually a leak, while the upper one (dashed line) is most likely an internal mixing problem between the horizontal breaker chambers and the vertical insulation column of the CB. This is because the leakage rate appears to slowly decrease over time.

Even if the density signal is fairly stable, there will be small variations in it. This may be because the temperature inside the gas volume is not the same across all parts of the system. If the temperature is not constant inside the gas volume, there

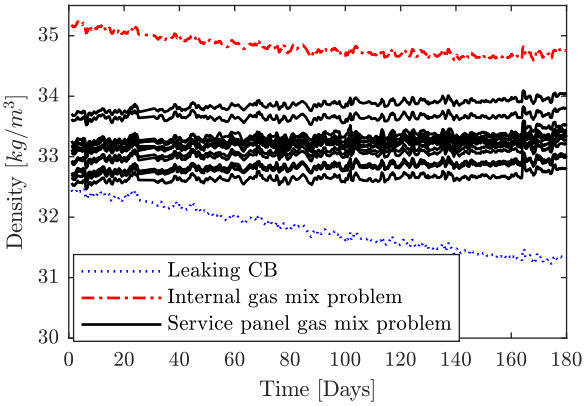


**Figure 7.3:** Filtered density readings from installation batch 1 in substation A. The lower line is a leaking CB and the upper line is a CB with internal mixing problems. The rest of the lines are slowly increasing, indicating a mixing problem caused by the thin tube between the CB and the service panel.

will also be density variations within it. Temperature differences can arise from internal resistive heating and external heating from such things as solar irradiation and outside temperature, as described in the literature [20, 24, 26, 49].

#### 7.5.1.2 Lab test

To check that the problem of slowly increasing density is due to the thin tube between the service panel and the CB, an indoor laboratory test was conducted. In it, a service panel was installed on a CB. One digital density sensor was placed on a reference volume (a gas bottle) located close to the CB. This sensor had been stabilised over several weeks. Another density sensor was placed directly onto the CB. One digital density sensor and one digital pressure sensor were installed on the service panel. To compare the signal, pressure at 20 °C was collected from all sensors. All measured signals can be seen in Figure 7.4.

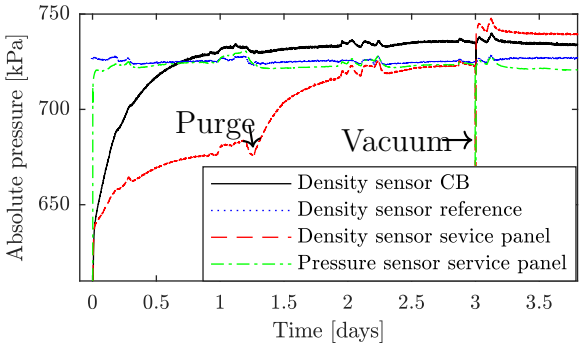


**Figure 7.4:** Laboratory measurements taken to help understand the mixing problem.

The pressure in the reference volume is stable. The small daily changes come from small temperature changes in the lab. The digital pressure sensor responds rapidly

and stabilises within a few hours. However, the digital density sensor mounted on the CB takes a few days to stabilise. This is because of a filter inside it that slows the gas exchange between the sensor and the CB. An identical density sensor positioned on the service panel has an even slower response, which does not come solely from the sensor filter.

After approximately 1.2 days, the tube between the service panel and the CB is purged to eliminate the small amount of air that enters the system while mounting the sensors on the service panel. The sensor now reaches the correct final pressure more quickly.

After three days, a vacuum is created in the tube and service panel to fully emptying the system of residual air. Pure $SF_6$ gas from the CB was then used to refill the system. After this, all sensors are stable at their final pressure values. The small pressure differences are due to the static errors in the sensors. From this laboratory test, it was concluded that it takes a long time for the air left in the sensors from mounting to mix with the $SF_6$ gas in the CB. This is because of the tube between the service panel and the CB, a problem previously unreported in the literature.

A possible solution to this problem could be to install two tubes between the CB and the service panel. The gas can then circulate between the CB and the service panel, achieving a continuous "purging" of the tubes and service panel. Such circulation can be enhanced by ensuring that differing solar irradiation causes the two tubes to have slightly different temperatures. This is speculative and must be tested. The resource consumption to rebuild existing installations would be excessive. For this reason, Svk decided to exclude the digital density sensor from future installations in the Swedish transmission system.

### 7.5.2 Mounting position and gas composition problems

As mentioned in Section 7.3.2, the pressure-based sensors will recalculate the measured absolute pressure to a pressure at 20 °C. This pressure will theoretically be constant, as long as the CB does not leak.

Figure 7.5 allows the variation in pressure versus temperature over two days to be investigated. With a temperature change of approximately 15 °C, the absolute pressure will change by some 0.04 MPa, or 6 %. Keeping in mind that a modern circuit breaker should not leak more than 0.1 %/year [23], these pressure swings make it very hard to quickly find small leaks.

The pressure at 20 °C is constant if the breaker is not leaking and it should be possible to find a small leak relatively quickly. Figure 7.5 also allows the calculated pressure at 20 °C to be studied. As shown in the figure, this signal also varies considerably but not as much as the absolute pressure.

If the gas composition in the breaker is well-known, it is possible to make a more accurate calculation. Indeed, in Figure 7.5, the sensor uses a non-ideal gas calculation, taking the gas composition into account. The signal still varies with temperature and there are some potential reasons for this:

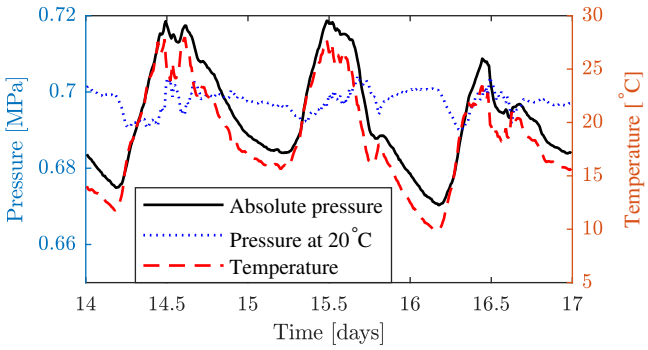


**Figure 7.5:** Example of pressures versus temperature for a 400 kV circuit breaker.

- The gas composition in the circuit breaker differs from the programmed values in the sensor [29, 49].
- The non-ideal gas equation does not perfectly describe reality.
- The temperature in the circuit breaker is not measured correctly.

Our tests suggest that the temperature error is the main contributor to these variations. This is due to the sensor (in which the temperature is measured) being placed away from the CB and not correctly representing the temperature inside it. This is especially true when a circuit breaker is heated up by solar irradiation or when the surrounding air cools it. These shortcomings are documented in the literature [20, 21, 26, 29].

## 7.6 Comparison algorithm for early leakage detection

As stated previously, early $SF_6$ gas leakage detection will help when planning grid maintenance activities. It will also facilitate faster leak repairs, leading to less $SF_6$ escaping into the atmosphere.

Substantial work has been carried out to solve the problems described in 7.5.2. In this subsection, an algorithm that is less sensitive to these problems is introduced. This algorithm only compares the absolute pressures of multiple sensors in the substation. A focus on the pressure sensor technology is mainly due to the challenges of gas mixing described in 7.5.1. The density sensor technology is unsuitable for the Swedish setup, because of the thin tube between the service panel and CB.

### 7.6.1 Relative comparison of absolute pressures

As described in Subsection 7.3.1, the absolute pressure varies substantially with temperature and it is difficult to get a stable pressure at 20 °C, as described in Subsection 7.5.2. This is mainly because the temperature in the sensor and circuit breaker will differ during temperature variations. CBs in close physical proximity will be heated and cooled at approximately the same rate, which makes it possible

to compare the pressures between them.

We will first normalise the absolute pressures in the CBs by dividing the time series of absolute pressures by the pressure at a specific time in the substation, according to:

$$p_{norm,n}(t) = \frac{p_n(t)}{p_n(t_0)} \ , \tag{7.3}$$

where $p_n(t)$ is the measured time series of the absolute pressure from sensor number $n$ and $p_n(t_0)$ is the absolute pressure at a specific time, $t_0$, for the same sensor. The pressure, $p_n(t_0)$, can be obtained from one reading, or from an average of several measurements close together in time. If an average is used, some measurement noise effects will be smaller. The normalised pressures, $p_{norm,n}(t)$, will now be close to 1.

We continue to create a quotient of the normalised pressure, with the average of $N$ other normalised pressures in the substation according to:

$$p_{diff,j}(t_k) = (\frac{p_{norm,j}(t_k)}{\frac{1}{N}\sum_{i=1}^{N} p_{norm,i}(t_k)} - 1) * 100 \ , \tag{7.4}$$

where $t_k$ is each time step in the measured series and describes the percentage difference of system $j$ compared to the average of several other systems in the substation at the time, $t_k$.

In Figure 7.6 an evaluation according to the equations (7.3) and (7.4) has been done for a group of three circuit breakers connected to one busbar in one of the bays of substation A. It is clear from the figure that the pressures differ over time. The same sensors and the same time interval are used in Figure 7.2. It is evident that, even if the absolute pressure varies by several per cent, the difference between the pressures is much more stable. This clearly indicates a difference in leakage between the CBs.

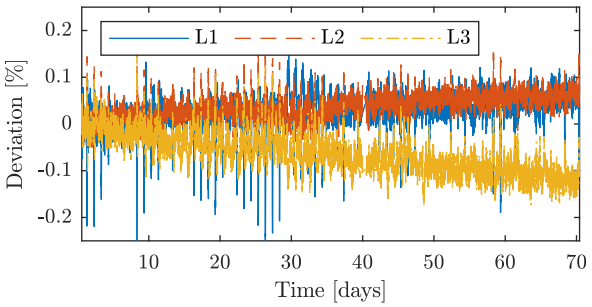


**Figure 7.6:** Example of evaluation of difference in pressure between a group of three circuit breakers connected to one bay in a substation.

### 7.6.2 Relative comparison of pressures at stable temperatures

Even if there is a clear change of pressure between the breakers they are not straight lines, as would be expected if there is a steady, constant leak. The "spikes" in

Figure 7.6 indicate that the pressures do not change at the same rate in the three CBs, meaning that they do not heat up or cool down at the same rate. Even if the CBs are positioned within a few meters of each other, there is a chance that the solar irradiation is not the same on all CBs. This can happen if, say, any of the units are shaded differently from each other because of other structures in the substation. A difference in internal resistive heating from the currents through the CBs can also play a role. Luckily, the currents in a high-voltage substation are normally symmetric. Thus, in a group of three CBs connected to the same busbar in the same bay, the currents (and thereby the internal heating between the CBs) are similar.

As described in [20, 24, 30], it is best to evaluate data from the night, when solar irradiation is absent or low. In Figure 7.7, daily data from 10 p.m. to 5 a.m. was used. Now, the data "spikes" have disappeared and the deviations are mostly measurement noise.

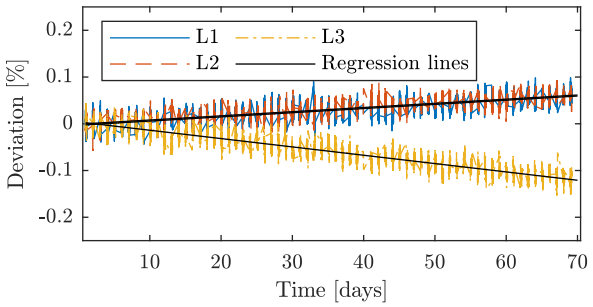


**Figure 7.7:** Example of evaluation of pressure difference between a group of three circuit breakers connected to one bay in a substation. The used absolute pressure values are taken from 10 p.m. to 5 a.m. to avoid problems with external heating by differences in solar irradiation.

It is now possible to use a linear regression algorithm to find the linear representation of the deviations from the average pressure. The regression lines are also shown in Figure 7.7. By comparing the line with the highest (positive) slope, phase L1 in this case, and the lowest (negative) slope, phase L3 in this case, it is possible to find how much more the CB on phase L3 is leaking compared to the one on phase L1.

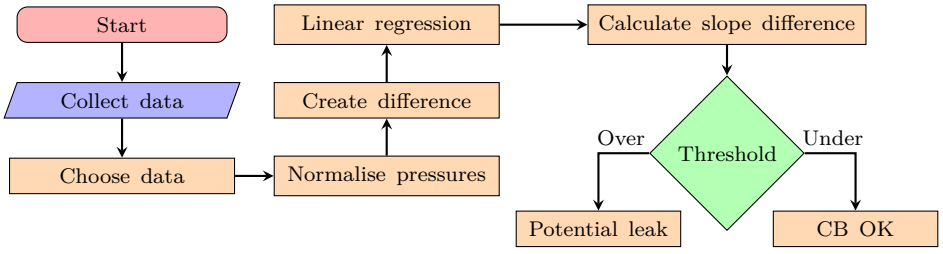


**Figure 7.8:** Calculation flow diagram.

A proposed calculation flow can be studied in Figure 7.8.

### 7.6.3 Leakage detection time

Some CB manufacturers offer products with a specified maximum leakage rate of 0.1 %/year [23, 27]. It would, therefore, be opportune if it is possible to securely detect potential leaks with an accuracy of under 0.1 %/year. So, how quickly can this be achieved?

The algorithm detects the difference between the highest and lowest slopes of the linear regression. The uncertainty of these slopes is determined using a standard regression algorithm. This allows the combined uncertainty between the highest and lowest slopes to be calculated. As more data became available, the leak rate difference and leak rate uncertainty over a 70-day period were calculated. Figure 7.9 shows the combined $2\sigma$ uncertainty (95 % confidence interval) as a dotted line. For this case, the uncertainty will fall below 0.1 %/year after 22 days.

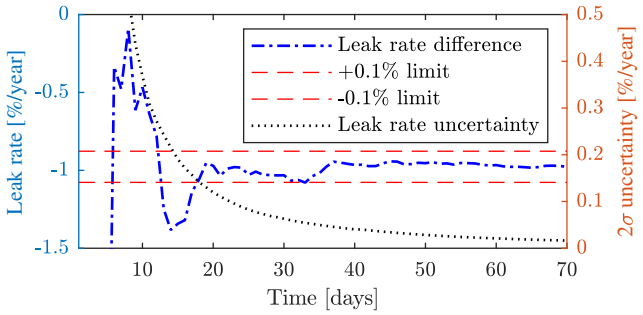


**Figure 7.9:** Example of linear regression evaluation of how the difference in normalised pressure between two CBs change over a 70-day period.

Figure 7.9 also shows the leak rate difference and a ± 0.1 %/year limit, based on the last calculated leak rate. In this case, the leak rate will stabilise to within the ± 0.1 %/year limit after 18 days.

It is important to recognise that the linear regression slope and uncertainty estimates are only valid if the leak rate is constant, which is represented by a straight line. It does seem to be happening in this case but, sometimes, the leak rate will change over time and is not represented by a line. Accordingly, the results must be interpreted with caution.

### 7.6.4 Proposed versus state-of-the-art method

The most common method of detecting leaks today is to use the alert signal from the switches on the traditional mechanical sensor. Unfortunately, this method comes with a major drawback; a relatively large amount of gas escapes the circuit breaker before any notification is made. Thus, as indicated in 7.4.1, this method is unsuitable for early leakage detection.

Another method of finding leaks is to manually read the mechanical sensor dial several times a year and analyse the results. This method is labour-intensive and its quality is personnel-dependent. In Svk's experience, it is difficult to detect a leak smaller than 1 % more rapidly than a year.

An increasingly common state-of-the-art method is to install digital sensors connected to a computerised analysis system. As stated in 7.4.2, the detection time for finding a leak of 0.5 %/year is between eight months and seven years.

The proposed algorithm is faster and more accurate, as it has the potential to detect a leak rate of 0.1 %/year safely within a few weeks. This is clearly an improvement on the current state-of-the-art method. In addition to its rapid detection time, the method only requires pressure values to perform a detection. This will make installation costs more attractive. The algorithm is simple to implement and straightforward to use, which is an additional advantage.

## 7.7 Results and discussion

### 7.7.1 Sensor selection

The conducted tests suggest that the main contributor to the errors in pressure at 20 °C is the temperature discrepancy between the sensor and the measured volume. This problem is pronounced during rapid temperature changes.

Both types of digital sensors used in the test are performing well. The resolution of the measurements is high and the long-term stability also seems high. In the beginning of the work the density sensor was used but, unfortunately, discovered that in the type of installations Svk have in the Swedish transmission system, the density sensor is not a suitable candidate. The digital density sensor seems to works best in installations where the sensor is mounted without any piping between the CB and the sensor.

In this work, two types of digital pressure sensors were examined. One that has less measurement noise and the option of programming the gas mixture composition and a less costly one with more measurement noise, which needs to be ordered alongside the gas mixture specification. The more expensive sensor is flexible and does not have to be ordered with any specifications. This is positive in terms of such things as keeping spare parts. On the other hand, for early $SF_6$ gas leakage detection (as described in this chapter), the gas composition need not be specified because only the absolute pressure is used. If a traditional leak detection algorithm is also used, it is recommended to use a sensor that calculates the pressure at 20 °C and the density as accurately as possible. The price difference between the two sensors is approximately EUR 200.

The more expensive sensor can securely detect a leak faster than the cheaper one because of its lower measurement noise. However, it will only be a few more days before the uncertainties reach the same level. The most important specification for the sensor is its stability over time because any stability problem would show up as a pressure difference. The tests did not specifically study the sensors' stability.

Sensors which have a digital communication interface were used so as to easily collect different types of information from the same sensor. It is more cost-effective to use a digital communication interface than an analogue one. However, the presented

algorithm only requires the absolute pressure value and could be implemented with a single analogue interface.

### 7.7.2 Validation

As pointed out in 7.7.1, accurate results strongly depend on the stability of the sensor. This fact raises two important questions:

1. How can we be sure that the results in this chapter are not due to poor sensor stability?
2. Over a sustained operation time, how can we differentiate between a lack of sensor stability and leakage?

Regarding the first question, several activities were conducted by way of a remedy:

- Using traditional methods, we chose substations in which Svk suspected leaking CBs.
- We used calibrated sensors to check the pressure more accurately, in conjunction with scheduled CB tests.
- We placed sensors on units that Svk suspected were leaking, as well as on units Svk did not suspect were leaking.
- Svk replaced CBs the developed algorithm identified as leaking. The leaking units were subsequently analysed in a lab and leaks were confirmed. The same sensors were placed on the new CBs that Svk did not suspect were leaking and the algorithm no longer indicated leakage.

So far, all the activities have confirmed the anticipated result.

The research did not aim to validate the stability of the sensors. The detection method was in focus. When using sensors widely, it becomes crucial to solve the second question above. How can we trust our results if the sensor stability degrades over a prolonged operation time? We discussed this issue during the research project and came up with a couple of possible solutions.

One option is to place an extra set of sensors on the service panel and make a parallel investigation if a potential leak is detected. Another option, which we favour, is to permute the existing sensors between the CBs, if a leak is detected. If the subsequent analysis gives the same indication, we can be certain that the sensors are stable and there is a leak. It will only take a few weeks to get a reliable, new indication with the presented method. The permutation of sensors and the new analysis can be done during the planning time needed for replacing or repairing the leaking CB. This option is probably the most cost-effective because the manual activity to permute the sensors only has to be done if a potential leak is detected.

### 7.7.3 Early leakage detection

The algorithm for early leakage detection has proven to be robust and simple to implement. A drawback of it is that it only can find a difference in leaks between the objects. It will not find the absolute leakage rate. This means, if all objects that are compared with each other are leaking by exactly the same amount, no difference will show up. The algorithm may also underestimate the leak rate.

The likelihood that all units in a substation are leaking is low. In the example in Section 7.6, only three sensors were used to create the average normalised pressure. If more sensors were used in the comparison, the algorithm would be less likely to underestimate the leak. Having said that, it is also important to point out that the temperature in a circuit breaker also depends on the internal resistive heating from the current in the CB. This means that, if sensors from different bays are used to average the normalised pressures, there may be fluctuations because the CBs are differently heated due to the difference in current between them. In the investigations, effects have been noticed that the author believe originate from this fact. This is also highlighted as a problem in [26]. Future work will focus on this issue.

In the tests, a good indication of a potential leak is normally achieved within 10 days. The uncertainties in the evaluation are usually lower than 0.1 %/year after 15 to 25 days. The more expensive sensor has lower measurement noise than the cheaper one but this has only marginal impact on how many days it takes to obtain an accurate result from the evaluation.

We expect the algorithm to work worldwide, as there are no climate or function-specific conditions that need to be considered.

### 7.7.4 Installation and material cost estimates

Two different types of gas sensors were used in the tests, the density sensor and the pressure sensor. Due to Svk's circuit breaker setup, described in 7.5.1, we favour using the pressure type. Also two different types of communication infrastructures were used: 1) an installation using optical fibre communication between nodes in the substation; and 2) the RTU with wireless upstream communication via secure SIM cards. We chose the wireless solution because it is more flexible and cheaper to install compared to the optical fibre solution.

The digital pressure sensors used in this project cost approximately EUR 410 for the less accurate sensor and approximately EUR 600 for the more accurate one. The RTU used in the project costs approximately EUR 390. However, there are other RTUs available that are close to half that cost. Pre-fabricated cabling with connectors costs approximately EUR 135 per sensor. Installation takes approximately one hour per sensor, if multiple sensors are installed in a substation. When installing a temporary measurement solution with a smaller number of sensors, the time required is around 1.5 hours per sensor.

The cost of installing one sensor is summarised in Table 7.1. These costs include

**Table 7.1:** Approximate installation cost for one $SF_6$ gas sensor, including communication to central location.

| Item | Temporary installation | Fixed installation |
|---|---|---|
| Cabinet | 100 | - - |
| Communication hub | 130 | 130 |
| Prefabricated cables etc | 135 | 135 |
| Digital sensor | 410 | 410 |
| Installation | 120 | 80 |
| Total | 895 EUR | 755 EUR |

communication to a central location but not the data collection system. However, Svk can repurpose an existing data collection system. Furthermore, the overheads, like ordering equipment, planning the project and travel are also not included in this cost estimate. The costs given are based on purchasing materials to install 30 sensors. There is a large cost-saving potential to be gained by ordering larger amounts of communication hubs, cables and sensors.

Since the communication hubs use SIM-cards there is a cost related to data transport. Reading three registers every ten minutes, from each sensor requires less than 10 MB of data per month for a group of three sensors. The cost for this is EUR 0.5/month. Since the project has concluded that only the absolute pressure is required and that only the nighttime pressure values are important to record, it is possible to drastically reduce the amount of data capacity needed.

### 7.7.5 Other comments

Installing a sensor can potentially introduce a new leak at the sensor connection point. It is important to leak-test the sensor installation itself. We did this by securing a small plastic bag around the sensor and service panel connection point overnight and then checking if any $SF_6$ had entered the bag the next morning.

## 7.8 Conclusions

The conclusions from the work can be summarised as follows:

**Sensor selection**
A digital pressure sensor works well in an early leakage detection system, in a context similar to that of the Swedish transmission system. The most important feature of the sensor is its measurement stability over time.

**Sensor and communication installation costs**
Even in rather small volumes, the cost to install one sensor with communication infrastructure is approximately EUR 750. This number can be reduced for higher volumes.

**Leak detection time**

When using the comparison algorithm, secure detection of small $SF_6$ gas leaks can be accomplished in weeks, rather than the years it takes when using traditional leak detection methods.

# Chapter 8

# Digital measurement platform

## 8.1 Introduction

Introducing the PB in an IEC 61850 digital substation makes accurate measurement a challenge. Svk, the Swedish TSO, is introducing the PB concept in a digital pilot substation. This chapter will discuss some of the challenges concerning accurate measurements utilising the PB, that have been encountered during the substation design process.

There is a limited supply of supporting digital metering products that use PB technology. Moreover, these products do not fully exploit the technology's important features. They cannot provide the data that Svk currently relies on to automatically assess the condition of the substations and grid. To overcome these problems, Svk has developed and tested a proof-of-concept digital measurement platform (DMP) to explore opportunities to extract more value from the PB technology. The DMP virtualises the metering functions.

The purpose of this chapter is to describe the DMP and discuss how it can be used in DSs with PB technology to make the metering infrastructure more efficient. The main contributions of this chapter are:

- In Section 8.1.1 and 8.2, challenges (in terms of accurate metering) of introducing the PB are identified.
- In Section 8.3, the DMP concept is introduced.
- In Section 8.4, a list of advantages that a DMP may provide, adding to the overall efficiency of an accurate metering process in high-voltage substations, is presented.
- In Section 8.5, introduce some preliminary results that show good computational performance and measurement quality for a DMP prototype, both in the lab and in the field.

### 8.1.1 Comments on digital metering using available technology

Studying Section 2.4, it is possible to find various benefits to using the PB for accurate measurement. Some of them are:

- Cable lengths between the ITs and SAMUs are short. This will result in a low voltage drop in the cables, which will improve the voltage measurement accuracy.
- The burden imposed by the measurement cables will be low, which will improve the current measurement accuracy and allow more suitably sized cables to be used.
- There will be no physical summation of currents. This will decrease the uncertainty of the current readings.
- Only one SAMU must be connected to each of the secondary signals from the ITs. This will reduce the burden on the ITs and there will be no increase in that burden, no matter how many instruments subscribe to the SVs on the PB.
- Since no physical voltage selection scheme with relays will be implemented, the burden will not change on the VTs (depending on the circuit breaker operation in the substation).

However, even if the above items are appealing, there are some drawbacks to the available digital metering technology. Some challenges that have appeared during Svk's investigations are:

- In some jurisdictions, the legislation for revenue metering does not allow the use of DEMs. If it is allowed, the legislation sometimes requires a dedicated SAMU used only for a single revenue metering instrument. This will increase the cost of equipment and the burden on the ITs, since an additional SAMU must be connected to them. Fortunately for Svk, this does not apply in Sweden.
- Many of the available SAMUs on the market do not meet the accuracy requirements for use in revenue metering. The temperature dependence of some SAMUs make them unsuitable for use in marshalling kiosks located outdoors in the switch yard.
- The DEMs currently on the market do not support a voltage selection scheme. This requires installation of more VTs in a substation.
- The DEMs currently on the market cannot receive to two SV streams and perform a mathematical summation of the currents to each busbar. If energy metering is required in all bays, this will result in more DEMs in the substation. It will also result in more space being required in the control building and overall higher costs.

- A specific problem in the Swedish TSO context is that DEMs currently on the market cannot supply the same type of data as the traditional energy meters used by Svk. This means the existing automatic supervision, which uses data from the energy meters, will not work in a DS using the available DEMs.

Some of the drawbacks above relate to how Svk designs substations and how the measured data is used. This does not necessarily apply to other TSOss. However, in private discussions with several TSOss, they express concerns and find that digital energy metering is challenging.

Often, specific regulations in different countries and a lack of standards make it difficult or impossible to embrace digital revenue-metering technology. Work is ongoing on different levels but it will likely take some years before regulations and standards are updated and consistent.

The accuracy requirements of PACS are not as stringent as those on revenue metering. This has led to a lack of accurate SAMUs on the market. A SAMU standard has recently been released [50]. This has made it easier to develop and acquire SAMUs that can be used for accurate measurements, plus protection and control. High-accuracy SAMUs are currently emerging on the market.

## 8.2 Increasing efficiency by virtualisation of measurement tasks

Traditional, accurate measurement instruments have their own A/D conversion that converts the analogue signal to digital samples. These instruments are often supplied as separate units, meaning that traditional substations have many (costly) A/D converters. However, this is beautifully solved in DSs, where the A/D conversions are made in SAMUs that can share their SV with as many IEDs and metering instruments as needed, without adding further A/D converters. This efficiency increase is enabled by the PB.

The traditional market model for almost all metering instrument manufacturers is to offer specific instruments for rack installation in the control building. Some protection and control equipment manufacturers have already implemented virtual PMUs and PQMs as software options in various IEDs in their PACS devices. This will increase the computing efficiency since the same computing hardware is used for both measuring and control tasks, allowing the reuse of calculated values from the protection function. As a consequence of the introduction of the PB, some of the actors in the protection and control community are currently promoting virtual protection schemes, in which one device can host all necessary protection functions as software applications [51–54]. This will dramatically increase the efficiency of the computing hardware since standard server technology can be used. Until now, this kind of technology has not been available for metering functionality.

The energy metering manufacturers (and other metering manufacturers) are still using the "one-box-one-measurement approach" even for the new digital technology.

As each "box" must have its own specially designed computing hardware, the only efficiency achieved is that the A/D conversion is shared with multiple metering functions, plus protection and control.

Consistent with the virtual protection schemes, it would be more efficient to host some or all measurement tasks on one device, sharing common computing hardware supported by a wider community. The various measurement tasks can be managed by dedicated software applications (APPs). Svk means that some challenges of introducing the PB could be resolved by such a platform. The only problem is that this kind of platform does not yet exist as a commercial product.

## 8.3 The proposed digital measurement platform

Svk approached several potential industry suppliers within the substation sector to help develop virtual metering but without success. It therefore decided to explore the feasibility of using virtual metering by developing a prototype in partnership with dedicated industry suppliers within and outside the substation sector. We call the virtual metering solution the Digital Measurement Platform.

### 8.3.1 Our definition of a digital measurement platform

The DMP comprises hardware and software and is meant to provide a more flexible and efficient way of acquiring high-quality measurements from substations.

*The DMP* is a standard industrial server, physically connected to both the PB and upstream management and data collection systems, that host a software framework (SF).

*The SF* listens to the PB and collects relevant data, like SV, GOOSE-messages and precision time protocol (PTP) packets. The SF organises the information and provides open-standard interfaces to different APPs. It also provides interfaces to external systems.

*The APPs* are hosted by the SF in secure containers (implemented via the widely-used docker containerisation [55] technology). The APPs can be software measuring instruments like DEMs, PMUs or PQMs. APPs may also be used to implement supervision tasks or other relevant but as-yet unforeseen tasks on the data from the PB supplied by the SF.

The SF interfaces between the APPs and data collection systems. The SF provides an interface to the information that APPs have returned to the framework. This is possible using a universal REST API [56] but the interfaces can also be tailor-made for legacy applications like phasor data concentrators and disturbance recording systems. A simple schematic layout of the SF is shown in Figure 8.1.

### 8.3.2 Software framework and software applications

The SF offers an open API for APP developers. APPs can subscribe to streams and produce their own data streams which are returned to the SF. APPs can

communicate (data) with each other (only) via such streams. This means that multiple APPs can benefit from other APPs' computations. All such communication follows a standardised format and is routed through the SF.

To achieve secure isolation of third-party APPs, publishing and subscribing to streams is the only interoperability between APPs and any software other than the SF. By design, APPs are prevented from sharing data in any other way with each other or the outside world. This aids the re-use and composition of APPs into complex measurement functions as APP developers need not fear anyone unintentionally interacting with their APP.

The SF orchestrates which streams are available and who can access which stream for reading or writing. APPs can share a private piece of the file system with the SF but other APPs have no access to it. APPs also have their own internal file system, some parts of which can be made persistent across planned or unintentional outages.

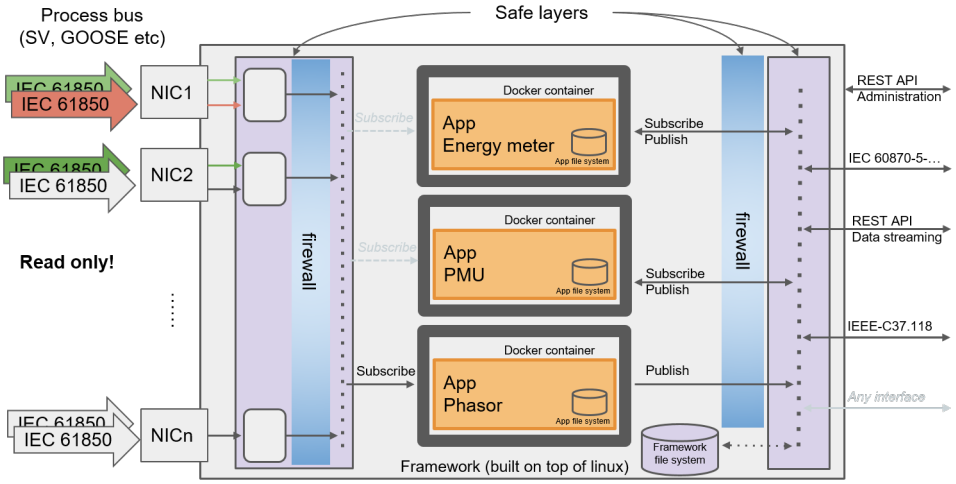


**Figure 8.1:** Example of a conceptual schematic of the software framework.

In Figure 8.1, standard IEC 61850 SV streams produced by SAMUs enter the SF through network interface cards (NICs) and decoding software. The SF acts as a router for these streams, giving access to those APPs that actively subscribe to a stream. Also, APPs cannot directly access the PB network interfaces; they get the parsed data via the SF. Since the framework parses the incoming SV stream, APPs are guaranteed not to be exposed to incorrectly or maliciously formatted data.

External applications can query the SF for results produced by the APPs. The SF also gives access to operation and maintenance protocols through a Web API. Using standard protocols, the outside world can download files, read data streams or query specific published data items through the SF firewall.

Each APP runs in an isolated environment on the DMP. To ensure the security and stability of the DMP, each APP has limited resources and access rights. The containerisation technology in the SF makes it possible for third parties to write APPs using any suitable programming language. The SF's role is to ensure that APP

isolation and lifetime management (startup, stream subscription, stream publishing and shutdown) are orchestrated according to a predefined standard.

## 8.4 Advantages provided by the DMP

The main motivation for Svk developing the DMP is the problem of retaining the valuable data analysis opportunities provided by Svk's traditional energy metering after the PB is introduced. This would not be possible using existing DEM products.

The existing DEM technology simply imitates the standard way of implementing a measurement, without taking specific advantage of any new features of the PB. The challenges indicated in Section 8.1.1 can be reduced by introducing the DMP.

The DMP allows new opportunities provided by the PB to be exploited. These include:

- Fewer measuring instruments in the substation.
- Lower maintenance costs and a more efficient commissioning process.
- Less overall need for computing resources.
- Lower hardware costs.
- Decreased measurement uncertainty.
- Increased time synchronisation accuracy.
- Increased IT security.
- Increased measurement redundancy.
- Increased potential for supervision based on data analysis.
- Increased support for more flexible switch yard designs.
- Cost-effective development and use of virtual measurement functions (APPs).

Figure 8.2 presents a conceptual design layout for a DS using the DMP. Comparing Figures 2.11 and 8.2, it is clear that the number of measuring instruments (hardware units) needed in the control building is drastically reduced in the DMP design.

Below are some clarification examples of the various opportunities presented above.

### 8.4.1 Reduced number of hardware units

As mentioned in Section 2.4.2.1, the number of metering instruments will have to be increased when available digital technology is used. One tangible opportunity of introducing the DMP and using virtual measurement is that the number of hardware units in the substation can be drastically reduced. The need for separate instruments requiring rack space in the control building will essentially be reduced to two servers;

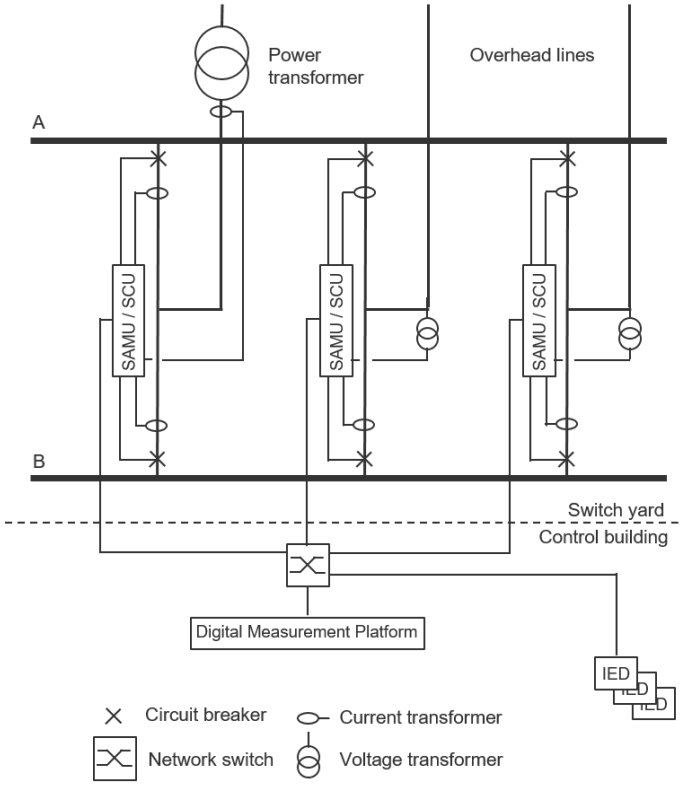


**Figure 8.2:** Digital substation metering conceptual design layout using the Digital Measurement Platform.

a main server and a redundant one. A modern server will require no more rack space than an available DEM.

As there is no need to connect and set up each instrument individually, the overall commissioning process will be much faster. Maintaining the DMP will also need fewer supervision resources as fewer hardware units are installed. The documentation will be reduced according to the number of units installed.

Many specially designed instruments require substantial hardware design resources, the costs of which are high. Using off-the-shelf hardware products like industrial servers, it is possible to exploit higher volume production. The cost of a high-quality commodity computer is a fraction of that of many special metering instruments.

Hardware scalability is possible since the SF is agnostic concerning computer performance. Computers can be chosen that are sized to meet the computational needs of a specific substation. In the development phase, the SF ran successfully on both a Dell XR11 server and a Raspberry Pi. These two platforms are at opposite ends of the computational resource and cost spectrum and consequently support different loads.

### 8.4.2 Measurement quality, redundancy, and supervision

SAMUs are synchronised to an absolute time by accurate clocks using PTP. The achievable time synchronisation accuracy is well below a microsecond. The SV is

supplied with a time stamp, which enables such things as the PMU functionality. Moreover, such functions as PQMs, energy metering, fault recorders and many others will be able to benefit from the fact that the timing is excellent. The synchronisation of any measurement will be superior compared to when the instruments are time stamped by a network time protocol (NTP) server (or worse, when it is time stamped by the data collection system).

When all data is available within the same hardware unit and correctly time-stamped, it is possible to create, say, an average value of all the voltages belonging to one of the three phases. This value will have a lower degree of uncertainty and higher accuracy than each individual voltage value on that phase.

As described in Section 2.4.1, the use of summed currents is prohibited for revenue metering in traditional substations. In a DS, the two currents to the different busbars will be measured separately and a mathematical evaluation and summation can be made. Thus, the uncertainties will be reduced and it may also be possible to use the data for revenue metering.

Once all the data is available within the same hardware unit (the DMP), it is simple to implement redundancy strategies to cope with the loss of an IT or SAMU. If, say, a specific voltage signal is lost in the substation, it is possible to switch over to another voltage signal (the voltage drop in a high-voltage substation is practically zero).

The sum of the power flow in and out of a substation must be zero. If the currents and voltages of all bays in a substation are measured, redundant energy measurement can be generated in one bay, based on the measurements from all the others. It is also possible to supervise, find errors and quantify measurement errors based on the residual sum of all power flows, as demonstrated in [40]. This is easy to do continuously within the DMP, since all information is available and shared within the SF.

Because all data is available to the APPs in the SF, many different types of analysis can be made. For example, the measurement core current of a CT can be compared with the protection core currents. Any larger deviations may indicate a malfunction in the CT. Similarly, the voltage readings from different VTs can also be compared with each other to find a malfunctioning device. One such example of a supervision task that can be performed using data analysis is for punctures in capacitor voltage transformers [41] (which is described in detail in Chapter 5).

### 8.4.3 IT security

IT security vulnerabilities are posing new threats across almost all sectors of society. IT security for the electricity sector has become a top priority. The metering instruments industry currently supplies both software and hardware, which are hard to inspect for vulnerabilities. Even if any are found and patches made available, regularly updating all the software in all units is a massive undertaking. Using a well-developed SF that treats APPs securely will enhance IT security. If APPs have

flaws, the SF can isolate any potential harm. When patching is needed, it also takes fewer resources to patch a limited number of hardware units.

### 8.4.4 Flexible substation design

As mentioned in Sections 2.4.1 and 2.4.2.1, using the double-busbar double-breaker substation design and voltage selection schemes does raise some problems regarding available digital metering products. With the DMP, this problem can be eliminated. Physical summation of measurement grade currents imposes errors; these can be eliminated using a mathematical summation in the APPs. A voltage selection scheme can be implemented in an APP as a logical function, based on the information in the available GOOSE-messages.

### 8.4.5 Computational efficiency and APP development

Since the hosted APPs in the SF can return their calculation results to the framework, other applications can subscribe to the previously calculated information and make further calculations based on the earlier results. This will reduce the overall need for computational resources. For example, most metering applications start by calculating individual phasors for current and voltage. If these phasor calculations are made in one APP and the results returned to the framework, other APPs (like energy meters, PMUs and PQMs) can subscribe to the same phasors, as they have already been calculated once. This reduces the overall demand for calculations, as can be seen from the test results in Section 8.5.

When, say, a traditional PMU is developed, it requires skills and technology from many different sectors. This requires synchronisation to absolute time from a global navigation satellite system (GNSS). Carefully designed A/D conversions must be implemented and synchronised to the absolute time. Computing hardware and software must be designed. Hardware casings must be designed, EMC tests run and other duties dealt with, all of which makes this a substantial undertaking. If a DMP is available in a DS with a PB, almost all these features come "free of charge" when developing new measurement functionality. Time is synchronised in a SAMU, that carries out A/D conversion and supplies the time-stamped SV. Hardware design and EMC testing have already been implemented on the components in the system. The only missing piece is the APP. The algorithms can be found in books or on the Web and often as open-source code.

Since the infrastructure is already present, there will be a much lower threshold for developing computing software than for a complete product. If a DMP is available, it will be cost-effective to develop both measurement and supervision functions that will be useful for important tasks. Once developed, APPs can be copied and there is no longer a need to limit the number of measuring instruments to meet cost, burden or space requirements.

There is an obvious need for the various metering and supervision functions that the industry currently supports. Since the threshold for developing new APPs is low, the platform will surely provide a basis for innovative new functions in the future.

## 8.5 Some results from lab and field test

The DMP prototype was developed to explore whether the proposed DMP concept is viable. During the development process, the following foreseeable issues were primarily explored:

- What is the decoding rate limit of SV?
- Can data be distributed fast enough within the server?
- Are there any severe computational limits?

The configuration of the DMP prototype used in the laboratory and field test is shown in Figure 8.3. The SF and APPs have mainly been written in the Erlang [57] functional programming language. While interpreting the results below, it is important to acknowledge that there has been little emphasis on optimising the code. This means that it should be possible to increase the performance substantially via further code optimisation.

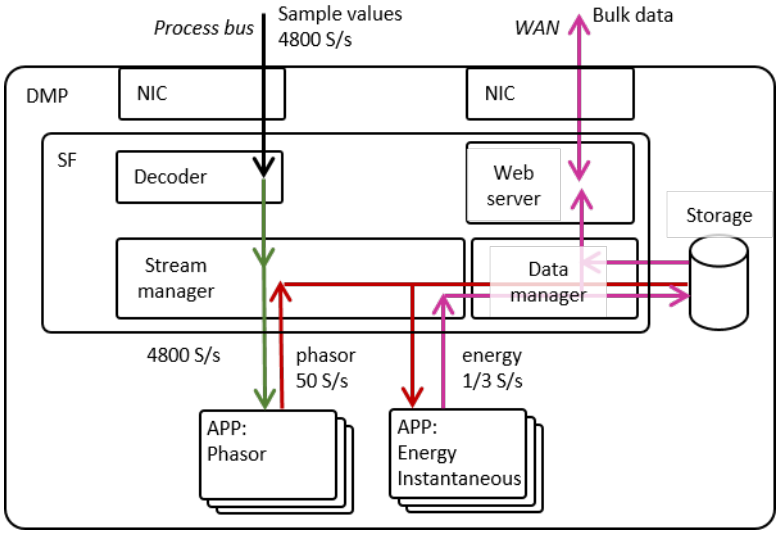


**Figure 8.3:** DMP configuration layout for laboratory and field tests.

Two different APPs have been implemented:

- **Phasor APP**: Calculates phasor data, that is, fundamental amplitude and absolute phase angles. For the calculations the PMU P-class reference algorithm presented in Annex D of the IEC/IEEE 60255-118-1 international standard [58] is used. The phasors are calculated once per nominal cycle (in this case 50 Hz) using a window of two consecutive cycles.
- **Energy and instantaneous value APP**: The energy meters calculate energy using the phasors, updating four registers (for imported and exported active and reactive energy) every three seconds. The instantaneous values are a down-sampling of the phasor values to 1/3 samples/s.

The SV data streams enter the DMP through a dedicated NIC. In the laboratory

tests, an emulator that produced different types of SV streams was used, while in the field test, two SAMUs that produced three F4800S2I4U4 streams each was implemented. The SV follows the IEC 61850-9-2 [59] and IEC 61869-9 standard [60].

The SF decodes the data into an internal stream format. These streams are sent to phasor APPs that, after calculations, return a phasor stream of 50 samples/s for each channel. As an example, an F4800S2I4U4 will result in eight phasor streams, four current and four voltages. (The fourth voltage and current are normally superfluous since the power and energy are calculated based on the three phases. The fourth signal can be used for other supervision purposes).

The Energy and instantaneous value APP will subscribe to a three-phase set of current and voltage phasor streams (six phasor streams in total). The calculated data is sent back to the SF and stored on disk. The user can retrieve measurement data from the DMP using a Web API.

Svk's design goal is that one standard server with 48 logical CPU cores will be able to handle a substation with 13 bays (which is the largest substation in the Swedish transmission system). With Svk's substation layout, as discussed in 2.4.1, there is a total of six current measurements in each bay, two for accurate measurements and four for protection. Using the Parallel Redundancy Protocol (PRP) will duplicate the amount of SVs recieved by the SF. Svk intend to use F4800S2I4U3 SV streams which results in sample value data of some 47 Mbit/s per bay or 614 Mbit/s for a 13-bay-substation.

Below, a few results that have been achieved during the development are presented.

### 8.5.1 Laboratory stress tests

Figure 8.4 shows how the prototype implementation of the DMP scales in CPU load, given four different configurations and as the number of SV streams increases. The experiment was conducted on a Dell XR12 machine with a Intel® Xenon® Gold 6312U CPU @ 2.4 GHz. The machine has 48 logical cores and 250 GB of internal memory.

In the first configuration, the DMP receives and decodes F4800S2I4U4 SV streams. The designation F4800S2I4U4, means that the update rate of SV-packets is 2,400 per second, with two application service data units (ASDUs) in each packet, with four current values and four voltage values in each ASDU. This means that all voltages and currents are sampled at 4,800 samples per second. In the second configuration, it receives the same streams and sends each one to a dedicated app for producing phasor data. In the third and fourth configurations, one and two energy meters respectively are attached to each collection of phasor streams.

We note that the scaling behaviour of the system is roughly linear with respect to the number of different APPs and number of SV streams. The slight increase in CPU utilisation per SV stream as the number of SV streams increase is attributed to inefficiencies in the prototype's use of communications and containerisation technology, rather than a fundamental issue with the DMP concept or design that can

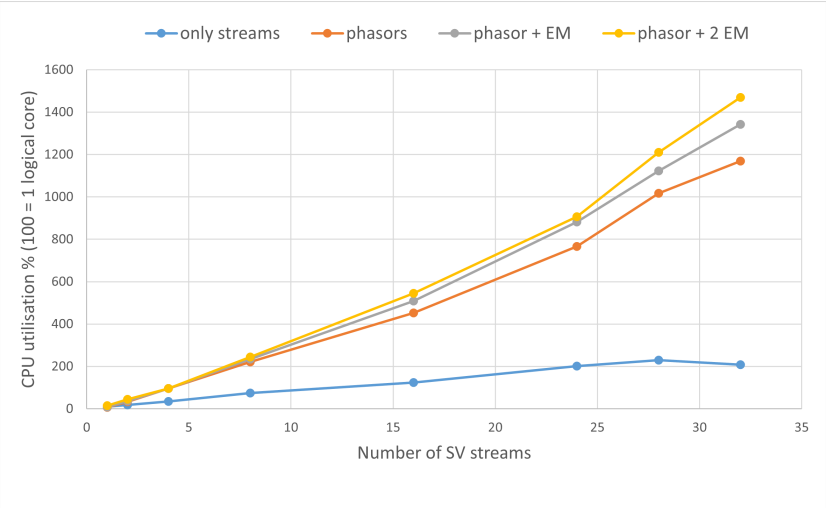


**Figure 8.4:** DMP CPU utilisation scaling behaviour under load in laboratory conditions.

be dealt with during a product development phase of the DMP concept.

The prototype DMP code was written to handle a few SV streams in a field test and not to be able ta handle many SV streams that is present in a large substation. Therefore there are a few things that limits the possibility to handle many SV streams. One such limitation is that the decoding of SV-packets is managed by only one logical core. The code in the DMP was never optimised for lowering the CPU utilisation.

A second stress test was performed on the same machine, but with a software development tool that is more optimised. The optimisation mainly concerns buffering of information to reduce overhead caused by sending many small messages between processes and processing small amount of data many times. The software includes decoding and calculations of phasors, with the same algorithms used in the DMP test. The development tool cannot share streams to several calculations and therefore does not support the use of APPs and plugins, which also reduces CPU utilisation. The code is written in the RUST programming language.

Figure 8.5 presents the result from the stress test with the development tool. In this test up to 160 SV streams of the same type as in the previous test were introduced to the machine, with the exception of using parallel redundancy protocol (PRP). In this test the CPU utilisation is reduced by more than an order of magnitude keeping in mind that the software has to decode double the amount of data per SV stream because of the PRP connection. The limiting factor in this second test was to produce a large number of SV streams.

The main conclusion from the stress tests is that the CPU utilisation scales linearly with the number of SV streams and applications and that modern servers can easily run hundreds of different virtual instruments simultaneously. With code optimisation by, say, a suitable trade off between CPU utilisation and latency in calculations,

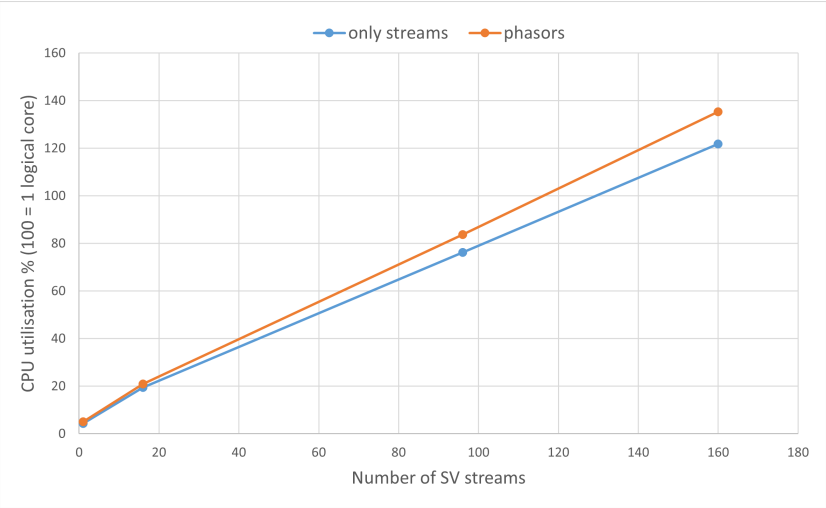


**Figure 8.5:** Development tool CPU utilisation scaling behaviour under load in laboratory conditions.

it will be possible to host all necessary APPs for the largest substation in Sweden within a single DMP.

### 8.5.2 Real-world substation test

Running systems in a lab environment normally creates small problems. However, using systems in a real-world environment often introduces unexpected behaviour. Therefore, an important part of the research project was to test the DMP in a real substation environment.

The DMP is installed in a five-bay substation, in parallel with the traditional energy meters. The substation is equipped with six traditional energy meters since one of the bays contains two energy meters (one for each busbar). For the field test, two multichannel SAMUs, one PTP clock source, one switch and the DMP were all installed. The DMP was set up with six phasor and six energy meter applications, to mirror the traditional setup and compare the DMP with the traditional solution.

The DMP is running stably and no unexpected behaviour was found. By contrast, the algorithms used in the DMP performed better than expected in the real-world environment and showed similar results to those of the traditional metering systems. The real world variations caused by drift in the primary equipment is the same, while there is a small (negligible) difference in reported values due to differences in calibration. As these results are similar, it is hard to know if the DMP or the traditional meters are better. However, one thing stands out about the DMP is the time synchronisation between the measurements in the substation is orders of magnitude better in the DMP compared to the traditional measuring systems. This is an important aspect when it comes to analysing the data with algorithms using data from multiple systems at the same time. A simple algorithm that is used regularly at Svk is a comparison of the voltages (provided in Section 4.3.1). Figure 8.6 examines a comparison of the voltage of one phase compared to the average of

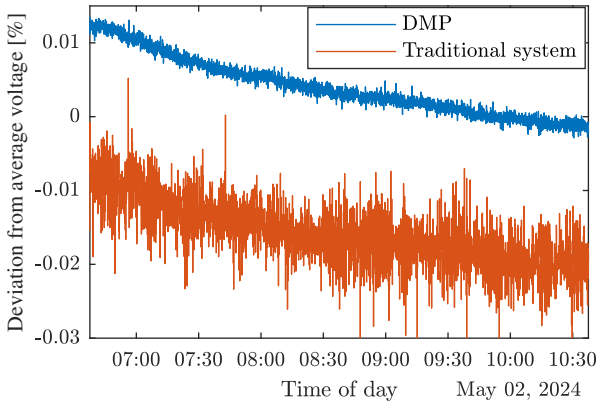


**Figure 8.6:** Comparison of voltage deviation between the DMP and traditional energy meters. The deviation is presented as a relative deviation from the average of all voltages on a specific phase. For clarity, only the results from one bay and one phase are presented.

all voltages on the same phase. The figure shows the deviation (as a percentage) from the average voltage. This representation comes from an average voltage with a window of 200 ms for all systems (traditional meters and the DMP). As can be seen, the noise level is heavily reduced for the DMP values. The variation is 25 times lower for the DMP compared to the traditional measurements. This improvement is mainly due to the measurement values being synchronised properly. This type of improvement makes algorithms converge on an accurate result much faster.

In Figure 8.6, we note a slight offset between the DMP and the traditional measuring system. This is due to slightly incorrect calibration. We also note that there is a slight decrease in the value over the four hours of collected data. Both the DMP and traditional meter experience the same change because the stability of the individual VTs in the switchyard is different. The changes are very small compared to the overall accuracy requirement.

A prototype installation always involves some time-consuming activities, as it is done only once and the process is not developed based on multiple prior installations. In our case, we installed the SAMUs and antenna for the PTP clock prior to installing the DMP, PTP clock and communication switch. From the arrival at the substation and until the equipment was installed and commissioned took less than an hour. Commissioning of six traditional energy meters in a substation normally takes several hours. This indicates a small but important efficiency gain when using a DMP, compared to a traditional setup including multiple meters.

## 8.6 Further opportunities for increased accuracy in digital substations using process bus

Apart from the improvements described in Chapter 3.3, there are interesting new improvements that can be made in a DS.

### 8.6.1 Average of voltage measurements

There is nothing to stop us from subscribing to all SVs in the DS. This means that it is, for example, possible to average all available VT values in the substations. According to GUM, an average of several measurements of the same quantity will lower the total uncertainty, as described in (3.11).

### 8.6.2 Independent current measurements to the busbars

As discussed in 2.3.2.1, the summation of currents cannot be used in revenue energy metering systems because it is impossible to know the power factor of the individual currents into the two busbars (see Chapter 2.4.1). Since the two secondary currents from the CTs (which are connected to the different busbars) will no longer be connected in parallel but measured instead by separate SAMUs, the summation of the power or current will be done mathematically. This will introduce several positive effects:

- Depending on the situation, there may be a small residual current in the branch even if the breaker is in the open position. Since the circuit breaker position will be continuously supervised via GOOSE messages on the PB, it is possible to mathematically make the current zero when the breaker is open.
- It is possible to continuously monitor that large currents are not transmitted between busbars (which reduces the accuracy in the current supplied to the measured object).
- Since a sum or average of multiple independent measurements will create a lower uncertainty according to (3.11), the uncertainty of the sum of the two currents can be reduced by a factor of $1/\sqrt{2}$.

### 8.6.3 Measurement redundancy

It is safe to assume that the voltage in the substation is the same in all bays and that the sum of both currents and the power is zero within a substation. Since all bays in a DS are measured and supply SV, it is possible to create measurement redundancy in the substation. If, say, a voltage measurement was to be lost, it is possible to use any other voltage reading in the substation. If a current reading in a bay is lost , it is possible to temporarily use any of the other cores in the CT. If all measurements in a bay are lost, it is also possible to recreate voltages, currents and power using the measurements from the other bays.

### 8.6.4 Supervision of measuring systems

As stated in Section 3.3.3, many different things can degrade the performance of a measuring system over time. Some (detected) problems are listed below:

- Capacitor punctures in CVTs. For various reasons, one or more capacitors in CVTs can puncture (short circuit). The CVT will still work but a voltage measurement error will be introduced. It is possible to supervise the voltage readings and detect all punctures, as described in [41].

- The electrical connection in the secondary voltage circuit can degrade through such things as bad screw connections or an oxide layer on fuses. The result is often a voltage reading reduced by several kV.
- An internal short circuit in secondary CT winding. This is a potentially dangerous situation and creates very large measurement errors.
- A broken energy meter (or SAMU) creates a loss of measurements.

If the measurements are continuously supervised and problems detected, then they can be rapidly solved. In the time up to when the measuring circuit is repaired, it is possible to switch over to a redundant measurement source.

## 8.7 Discussion

In many countries, the legislation surrounding revenue metering introduces difficulties when technology changes. Such legislation is not normally technology-agnostic and points to different standards. In such cases, the challenge comes when new technical solutions are required, like when the PB is introduced. Thus, virtualising measurements is too innovative and, in many countries, may require changes to both legislation and standards. Fortunately, Sweden is a notable exception.

When it concerns new technologies, standards and regulations are always lagging behind and it takes time before they become synchronised. For new technologies to be usable, legislators need to write technologically agnostic requirements. There are many ways to satisfy requirements and the author believe legislation should be concerned with what requirements should be satisfied, rather than how it should be accomplished.

In any case, the author argue that the DMP and virtualisation of the measuring instruments is a useful development that makes accurate metering more efficient when the PB is introduced into a substation. The protection and control industry is currently developing virtualised protection and control, which is very similar to what is proposed here. It is much broader in scope and virtualised metering has the potential to become an element of such developments. However, there is a problem in that metering and protection most often involve different people, from different departments and with different needs [36]. For protection and control plus metering to reside within the same hardware and software, there is a need to work more closely together. At Svk, the protection and control and metering personnel are in the same department. This is very helpful as we develop common solutions for the future.

In a fully DS, the metering function needs a subset of the components required by the protection and control functions. Thus, one can argue that the accurate metering part of a substation only needs to add the DMP to its installation. This is a cost-effectiveness measure. In developing the DMP prototype, we found other advantages that could also be used in traditional substations. Therefore, Svk is currently investigating the possibility of converting only the metering part of a traditional

substation into a virtual digital solution. This is not as financially favourable as introducing the DMP in a fully DS, as the DMP is not the only thing that must be installed. SAMUs, a time server and a communication switch must also be installed. This will make the solution less attractive but other valuable advantages are gained.

## 8.8 Conclusions

The technology for accurate measurements used in fully DSs is not mature. We are seeing a gradual improvement of necessary components but no changes which strive to exploit the PB and make the accurate measuring infrastructure more efficient.

During the research, a functional prototype of a DMP has been developed. Important, foreseeable issues were solved during the development process. The results are positive and no major obstacles emerged during the development. Quite the opposite; all aspects seemed to fall into place.

During the development phase, the work was primarily focused on small substations with three to five bays. The lab tests suggested that a single server could also host all necessary metering functions for large substations and still have enough computing power left to support valuable new measurement and supervision functionality. The substation field test further supports our thoughts on how value can be added when using a PB.

One major issue is that legal requirements differ in various parts of the world and virtual metering could be problematic in many countries for some time to come. Sweden has legislation to support the introduction of new technology, such as a DMP.

## 8.9 Future work

Svk has decided to continue developing the DMP well past its current research prototype stage. The DMP will be used in the digital pilot substation, which will be in full operation by mid-2026. Some of the forthcoming activities will focus on:

- Developing further functionality and a more advanced user interface for the SF.
- Securing the overall stability of the DMP.
- Gaining more practical field experience in real substations.
- Further developing APPs to secure the necessary accuracy to meet the legal requirements of revenue metering.

# Chapter 9

# Discussion

## 9.1 General discussion

Using measurements to supervise equipment is definitely not a new idea for transmission grids. Likewise, remote data collection from substations has been practised for decades. What might be considered a novel trend for transmission grids, is the collection of more data and enhanced use of automatic analysis on that data to make the supervision more efficient.

When relevant data becomes available, the practice of in person substation visits to verify the condition of equipment can be reduced or abandoned. A person might manage two physical substation visits per day. However, if the relevant data is available, that same person can virtually inspect many more without leaving the office. Using ACM, all substations can be inspected several times a day and the monitoring system does not tire or make human mistakes.

It is highly advantageous if equipment degradation can be detected well before it poses a threat to the operation, as is having the freedom to plan maintenance activities. Other advantages include the fact that automatic supervision can be conducted continuously without human interaction or the need to visit substations.

High-voltage substations are constructed in such a way that problems seldom occur but since almost every serious problem in a high-voltage substation brings major risks and high cost, it is worthwhile being able to find and correct problems before they get serious. One obvious achievement from the research is how to find punctured capacitors, which might ultimately lead to explosions, substantial repair bills, danger to personnel and potential instability in the grid. Finding problems before they develop into serious events helps maintenance planning, reduces risks and is proven to be cost-effective.

Less serious events, like accuracy degradation in a measurement system, can be ongoing for years without being noticed. This type of problem does not necessarily entail physical risks but substantial sums can be incorrectly billed to customers for years. Finding these types of problems early will create a fairer industry and greater

trust between actors.

## 9.2 Specific observations

While working with data analysis to support ACM activities, some specific observations have been made:

- Time synchronisation of measurement values is more important than the effort normally expended on it.
- Collecting more data, at a higher update rate and storing it for longer than might seem necessary has proven to be valuable.
- Organising diverse data collection to facilitate access for data analysis purposes has also proven valuable.
- Working on real-world substation measurement data (rather than synthesised data) during the development of supervision algorithms will take a long(er) time but creates better supervision functions.
- Understanding accuracy and uncertainty will become more important in the future.

### 9.2.1 Time synchronisation

As mentioned in Section 2.2, time synchronisation is extremely important in making algorithms efficient but is, unfortunately, often neglected. The efficiency of the algorithms can be orders of magnitude higher when time is correctly stamped. Details are important; it is not enough for the equipment to just be correctly timed. Careful design must be practised when constructing measurement values. A measurement value is always some type of "average" (over a longer or shorter period). The author wishes that all time stamps could be placed (precisely) in the middle of that range. If this is not done, unnecessary "noise" will degrade the performance of any algorithm, whenever a diversified quantity of data is used. Moreover, the author also wishes that we could all agree to use the same time-base. Coordinated Universal Time (UTC) is commonly used as an international time base and can be translated to different local time bases. Using UTC creates fewer mistakes and less confusion but still has some inherent problems with leap seconds. It might even be better to use International Atomic Time (TAI), which will always be incremented. Time representation creates more confusion than might be realised.

### 9.2.2 Diverse collection of data in the same system

Historically, different measuring equipment has been introduced for specific tasks, with measurement data collected and used by different systems and stored at different locations. This scattering of data makes it hard to conduct some types of analysis. Having a diverse collection of measurement data available for analysis within a single system makes the ACM effort much easier. For example, if weather data is available at the same location as the substation measurements, this affords the

opportunity to differentiate more efficiently between corona losses and measurement error. Alternatively, having $SF_6$ gas pressures measurements at the same location as the substation electric measurements enhances the internal heating estimate by using the currents running through the CB.

### 9.2.3 Real-world substation measurement data

Using real-world measurements instead of synthesised data when developing algorithms will take longer. The advantage is that, if real-world data is used from the start when algorithms are being developed, there is a chance that the algorithms may be suitable for ACM. Since substation measurement data can be sensitive (from a privacy perspective), it is difficult for the transmission systems owner to share such data with those outside the company. I would encourage our industry and universities to enable students to work with real substation measurements during their studies. That would create far better data analysts for the future.

### 9.2.4 Accuracy and uncertainty

Accuracy plays a vital role when measurements are used for economic settlement. High accuracy creates trust between actors. Moreover, measurements are often used to make decisions that end up being acted upon. Without knowing the uncertainty in the measurement, it is impossible to know the quality of a decision.

There is more emphasis on using measurements to make operations more efficient. Many young data analysts are entering the industry with no clear understanding of the quality of the data that they are working on. If analysts are to automatically evaluate the uncertainty of their results to aid decision-makers in taking value-adding actions, then every measurement value needs to be automatically accompanied by its uncertainty.

# Chapter 10

# Conclusions and future work

## 10.1 Conclusions

Not surprisingly, the main conclusion in this thesis is that ACM is a helpful tool for quickly finding different types of problems that were previously impossible to find or which cost substantial sums to detect. It is hard to quantify the sums saved because when a problem is found and corrected before it creates a more serious event, that event will not happen. And to add to the complexity, perhaps it would not have happened anyway.

One surprising result was our finding several problems we previously did not know existed. At least, not occurring as often, as we have now seen. Examples are: Corrosion in connectors and fuses that cause voltage drops in the secondary measuring circuit and thereby measurement errors. Missing earth connections in energy meters, causing an undefined neutral point for the measured voltages. Short circuits in the secondary measuring circuit of CTs. Mechanically mixed-up parts between VTs in newly built substations. Another unanticipated overall result is the scale of the efficiency increase and increased precision in troubleshooting gained through ACM. A third turn-up is that at the beginning of the work, it was unclear how much the excellent quality of our data increased the opportunities for developing sensitive algorithms.

### 10.1.1 CVT punctures

This thesis presents algorithms that specifically detect individual punctures in CVTs. One puncture in a CVT does not constitute an increased risk but introduces a substantial measurement error (that can be corrected for). Further punctures increase the risk of explosion and, at some point, it is necessary to exchange the unit. The punctures can now be monitored, which was not the case earlier. Each time a unit can remain in service, Svk will save planning resources and a replacement costing in the order of EUR 50,000. Svk has detected over 74 punctures in the Swedish transmission grid so far, and in October 2024, monitors 59 active punctures daily.

### 10.1.2 Remote calibration

It is possible to continuously monitor the accuracy of the energy-measuring systems using the developed algorithm. That will make the metering more accurate in the transmission system which creates trust between actors. There is a legal requirement to verify the accuracy of each revenue metering system every six years. The traditional way of meeting this requirement required a substation visit costing over EUR 10,000 for each substation. Since the algorithm is part of an accredited verification process that could be performed without substation visits, a majority of these traditional costs can be saved in the future. Svk needs to verify over 200 substations every six years and is planning to build around 200 more in the coming decades. Consequently, there are both substantial sums to be saved and an increased accuracy gain by using the algorithm. Furthermore, the algorithms introduce a possible solution to the upcoming problem of verifying the accuracy in LPITs during operation. Today, this is only possible through a costly calibration procedure (that cannot be used during full operation).

### 10.1.3 Gas leakage

A fast and accurate $SF_6$ gas leakage detection algorithm is introduced in conjunction with a cost estimate based on actual installations. The research indicates that a yearly leak rate of 0.1 % can be detected already within 15-25 days for a CB (which is probably a world record). This can be done at an installation cost of approximately EUR 750 for each sensing point; a low sum compared to what the market offers.

### 10.1.4 Digital measurement platform

The proposed DMP is probably the most exciting research included in this thesis. It is a real game-changer when it comes to accurate substation metering. It has been possible to incorporate everything we have learned about ACM in the past into the new development. The solution is (much) less costly. It will eliminate some problematic issues of implementing process buses in Svk's substations and provide many value-adding opportunities in terms of analysis. It will save a substantial amount of money in each substation, thanks to lower hardware costs, lower maintenance costs and space-saving. The indications are that a single DMP can collect and organise all information flowing on the process bus whilst hosting all accurate metering and data analysis functions, even in Svk's largest substations with 13 bays.

## 10.2 Future work

The introduction of the instantaneous three-second values from all substations greatly improved the prospects of conducting ACM, since a lot of useful data was collected by one system and accessing the data is simple. The data has to be transported to a central location to be analysed because it is collected from many different measuring instruments. This brings new challenges, like communication bandwidth needs and the management of multiple instruments and data collection servers.

The development of the DMP will change this situation in several ways:

- There will be more relevant information available for analysis, leading to totally new analysis opportunities.
- All information from one substation will be available in one unit, leading to the possibility of locally analysing the information. This, in turn, limits the need to transfer a vast amount of data.
- There will be fewer instruments and other equipment in the substations, leading to more efficient maintenance.

A prototype DMP is currently running in one substation, from which Svk is gathering experience. Svk has started a new project, in which the prototype will be developed into a production version. Several different APPs are being produced simultaneously. The goal is to install a fully functional DMP hosting many virtual instruments when Svk's fully digital pilot substation is brought into operation in mid-2026.

Many other interesting opportunities are gradually emerging as Svk develops and uses the prototype DMP. The focus of future developments regarding ACM will probably revolve around the DMP in the coming years.

Svk's journey with ACM has just begun and will probably never end...

# Bibliography


[1] Z. Feng, F. Ling, J. Jinyang, Z. Jiaming, D. Jie, C. Yingying, and Z. Huayong, "State assessment of measuring error and analysis of risk early warning technology for operating cvt," in *2019 IEEE 4th Advanced Information Technology, Electronic and Automation Control Conference (IAEAC)*, vol. 1. IEEE, 2019, pp. 1877–1880.

[2] C. Zhang, Z. Meng, M. Chen, Y. Jiao, Q. Chen, and H. Li, "Monitoring the ratio error drift of cvts connected to the same phase along with kde-pca," in *2019 IEEE International Instrumentation and Measurement Technology Conference (I2MTC)*. IEEE, 2019, pp. 1–6.

[3] B. Kasztenny and I. Stevens, "Monitoring ageing ccvts practical solutions with modern relays to avoid catastrophic failures," in *2007 Power Systems Conference: Advanced Metering, Protection, Control, Communication, and Distributed Resources*. IEEE, 2007, pp. 187–208.

[4] M. Freiburg, E. Sperling, and F. Predl, "Capacitive voltage transformers-electrical performance and effective diagnostic measures," in *2016 International Conference on Condition Monitoring and Diagnosis (CMD)*. IEEE, 2016, pp. 20–23.

[5] A. Lindskog, E. Viberg, and T. Lindquist, "Online monitoring of capacitive voltage transformers using energy meters," in *CIGRE SESSION 47, Poster session A3, Transmission and distribution equipment, Paper A3-207*. Cigré, 2018.

[6] A. Korhonen *et al.*, "Verification of energy meters using automatic meter reading data," Master's thesis, School of Electric Engineering, Aalto University, Espoo, Finland, 2012.

[7] X. Kong, X. Zhang, N. Lu, Y. Ma, and Y. Li, "Online smart meter measurement error estimation based on ekf and lmrls method," *IEEE Transactions on Smart Grid*, vol. 12, no. 5, pp. 4269–4279, 2021.

[8] L. Ye, G. Li, G. Yang, Q. Yanan, Z. Xin, M. Yuying, and K. Xiangyu, "Method for solving electric energy meter error of low-voltage station based on big data," in *2018 China International Conference on Electricity Distribution (CICED)*.

IEEE, 2018, pp. 1036–1040.

[9] L. Fangxing, H. Qing, H. Shiyan, W. Lei, and J. Zhengsen, "Estimation of smart meters errors using meter reading data," in *2018 Conference on Precision Electromagnetic Measurements (CPEM 2018)*. IEEE, 2018, pp. 1–2.

[10] L. Zhang, H. Chen, Q. Wang, N. Nayak, Y. Gong, and A. Bose, "A novel on-line substation instrument transformer health monitoring system using synchrophasor data," *IEEE Transactions on Power Delivery*, vol. 34, no. 4, pp. 1451–1459, 2019.

[11] P. Gupta and S. A. Soman, "Calibrating cvts of a substation from local pmu data: An svd approach," *IEEE Transactions on Power Systems*, 2020.

[12] A. Pal, P. Chatterjee, J. S. Thorp, and V. A. Centeno, "Online calibration of voltage transformers using synchrophasor measurements," *IEEE Transactions on Power Delivery*, vol. 31, no. 1, pp. 370–380, 2016.

[13] C. Zhang, H. Li, J. Yang, M. Chen, and Y. Jiao, "Detecting measurement error drifts of a capacitor voltage transformer on-line and its field application," *Measurement Science and Technology*, vol. 30, no. 10, p. 105109, 2019.

[14] C.-j. Zhang, H.-b. Li, and Q. Chen, "Detection of the ratio error drift in cvt considering avc," *Measurement*, vol. 138, pp. 425–432, 2019.

[15] Z. Zhang, Q. Chen, C. Hu, H. Li, and M. Chen, "Evaluating the metering error of electronic transformers on-line based on vn-mwpca," *Measurement*, vol. 130, pp. 1–7, 2018.

[16] A. Korhonen, "Verification of energy meters using automatic meter reading data," Master's thesis, Aalto University. School of Electrical Engineering, 2012. [Online]. Available: http://urn.fi/URN:NBN:fi:aalto-2020122858745

[17] Ž. Nakutis and P. Kaškonas, "A contemplation on electricity meters in-service surveillance assisted by remote error monitoring," *Energies*, vol. 13, no. 20, p. 5245, 2020.

[18] X. Kong, Y. Ma, X. Zhao, Y. Li, and Y. Teng, "A recursive least squares method with double-parameter for online estimation of electric meter errors," *Energies*, vol. 12, no. 5, p. 805, 2019.

[19] M. J. Lin, "To research on application and maintenance of sulfur hexafluoride (SF6) circuit breaker," *European Journal of Electrical Engineering and Computer Science*, vol. 7, no. 3, pp. 1–5, 2023.

[20] P. Cheetham, A. Hellany, and S. Jones, "Density monitoring of high-voltage SF6 circuit breakers," *IEEE Electrical Insulation Magazine*, vol. 31, no. 2, pp. 6–13, 2015.

[21] P. Kaur and T. Choudhury, "Early detection of SF6 gas in gas insulated

switchgear," in *2016 7th India International Conference on Power Electronics (IICPE)*. IEEE, 2016, pp. 1–6.

[22] Y. Siregar, H. Zulkarnain, and M. F. S. Yesa, "The dielectric power of mixed gas insulation of SF6-CO2 and SF6-N2," in *2022 International Seminar on Intelligent Technology and Its Applications (ISITIA)*. IEEE, 2022, pp. 355–359.

[23] E. Yedinak, K. Lentijo, and I. C. Kizilyalli, "Eliminating SF6 from switchgear," in *Direct Current Fault Protection: Basic Concepts and Technology Advances*. Springer, 2023, pp. 409–427.

[24] M. Tatemi, H. Inami, T. Rokunohe, and M. Hirose, "Study on field demonstration of high-sensitivity SF6 leakage detection method for gas insulated switchgear," *Electrical Engineering in Japan*, vol. 214, no. 1, pp. 35–41, 2021.

[25] J. Owens, A. Zhang, J. Bonk, and M. DeLorme, "Review of health and safety data on leading SF6-alternative gas mixtures," in *2022 IEEE International Conference on High Voltage Engineering and Applications (ICHVE)*. IEEE, 2022, pp. 1–4.

[26] L. Graber, "Improving the accuracy of SF6 leakage detection for high voltage switchgear," *IEEE Transactions on Dielectrics and Electrical Insulation*, vol. 18, no. 6, pp. 1835–1846, 2011.

[27] P. Widger and A. Haddad, "Evaluation of SF6 leakage from gas insulated equipment on electricity networks in great britain," *Energies*, vol. 11, no. 8, p. 2037, 2018.

[28] M. Schulz and D. Kourkoulas, "Regulation (eu) no 517/2014 of the european parliament and of the council of 16 april 2014 on fluorinated greenhouse gases and repealing regulation (ec) no 842/2006," *Off. J. Eur. Union*, vol. 2014, no. 517, p. L150, 2014.

[29] W. Yang, Z. Liu, B. Li, and B. Dou, "Simulation test and analysis of defects for SF6/CF4 mixed gas circuit breaker," in *2021 4th International Conference on Energy, Electrical and Power Engineering (CEEPE)*. IEEE, 2021, pp. 178–182.

[30] M. Kawada, T. Minagawa, E. Nagao, M. Kamei, C. Nishida, and K. Ueda, "Advanced monitoring system for gas density of gis," in *2008 International Conference on Condition Monitoring and Diagnosis*. IEEE, 2008, pp. 363–368.

[31] M. Schulz and D. Kourkoulas, "European union commission. proposal for a regulation of the european parliament and of the council on fluorinated greenhouse gases, strasbourg, france, 2022, amending directive (eu) 2019/1937 and repealing regulation (eu) no 517/2014," *European commission, Strasbourg*, 2022.

[32] X. Jin, Z. Liujun, H. Xiaoguang, L. Liang, and Z. Lei, "Development of on-line monitoring system for SF6 circuit breaker," in *2011 6th IEEE Conference on*

*Industrial Electronics and Applications*. IEEE, 2011, pp. 537–541.

[33] R. Wang, Y. Li, W. Zhang, F. Kang, D. Chen, and Y. Qi, "Design scheme of multifunctional electric energy meter based on distributed sampling method," in *2020 IEEE Sustainable Power and Energy Conference (iSPEC)*. IEEE, 2020, pp. 1817–1823.

[34] W. Wu, X. Mu, Q. Xu, X. Mu, F. Ji, J. Bao, and Z. Ouyang, "Effect of frequency offset on power measurement error in digital input electricity meters," *IEEE Transactions on Instrumentation and Measurement*, vol. 67, no. 3, pp. 559–568, 2017.

[35] W. Xia, X. Qin, W. Lu, J. Liang, and J. Ou, "Remote calibration of digital input electricity meters," in *2022 IEEE 5th International Conference on Electronics Technology (ICET)*. IEEE, 2022, pp. 128–132.

[36] CIGRE WG B5.41, "Improved metering systems for billing purposes in substations," *CIGRE Technical Brochure, No. 789*, 2020.

[37] Y. Chen, E. Mohns, M. Seckelmann, and S. de Rose, "Precise amplitude and phase determination using resampling algorithms for calibrating sampled value instruments," *Sensors*, vol. 20, no. 24, p. 7345, 2020.

[38] J. JCGM, "100:2008 (gum 1995 with minor corrections) evaluation of measurement data-guide to the expression of uncertainty in measurement," *Joint Committee for Guides in Metrology*, vol. 19, 2008.

[39] ——, "101:2008 evaluation of measurement data–supplement 1 to the "guide to the expression of uncertainty in measurement"–propagation of distributions using a monte carlo method," *International Organisation for Standardisation, Geneva*, 2008.

[40] A. Lindskog, P. Jarlemark, and S. Svensson, "In situ calibration of transmission system power grid energy meters using energy measurements and kalman filter," *IEEE Transactions on Power Delivery*, 2022.

[41] A. Lindskog, T. Thiringer, and T. Lindquist, "A data driven approach for monitoring puncture events in capacitor voltage transformers," *IEEE Transactions on Power Delivery*, 2021.

[42] H. Saadat, *Power System Analysis. 3rd edition.* PSA Publishing, 2010, pp. 439–442.

[43] G. Rietveld, M. Fransen, N. V. Blanc, and E. So, "Design and testing of a setup for on-site power measurements in high-voltage grids," in *2019 IEEE 10th International Workshop on Applied Measurements for Power Systems (AMPS)*. IEEE, 2019, pp. 1–5.

[44] D. Jie, C. Yingying, Y. Huaxiao, H. Jianming, Z. Feng, and X. Ji, "The electricity measuring system and calibration technology in the new smart substations,"

in *2017 IEEE 2nd Advanced Information Technology, Electronic and Automation Control Conference (IAEAC)*. IEEE, 2017, pp. 1902–1905.

[45] S. A. Van De Geer, "Least-squares estimation," *Encyclopedia of Statistics in Quality and Reliability*, vol. 2, 2008.

[46] R. Brown and P. Hwang, *Introduction to Random Signals and Applied Kalman Filtering*. John Wiley & Sons, New York, 1997, pp. 439–442.

[47] Z. Qin, C. Zhang, Y. Zheng, W. Zhou, and S. Yang, "Insulation properties of SF6/N2 gas mixtures under high pressure and low ratio," in *2017 IEEE Electrical Power and Energy Conference (EPEC)*. IEEE, 2017, pp. 1–4.

[48] L. W. Kui, Z. X. Min, L. Z. Jie, Y. Y. Qi, S. K. Ke, W. Y. Liang, and G. Y. Hang, "Analysis and experimental study on liquefaction characteristics of SF6/CF4 mixture gas," in *2017 4th International Conference on Electric Power Equipment-Switching Technology (ICEPE-ST)*. IEEE, 2017, pp. 305–309.

[49] T. A. Paul, M. Porus, B. Galletti, and A. Kramer, "SF6 concentration sensor for gas-insulated electrical switchgear," *Sensors and Actuators A: Physical*, vol. 206, pp. 51–56, 2014.

[50] IEC, "Instrument transformers – Part 13 Stand Alone Merging Unit (IEC 61869-13)," https://www.iec.ch, 2021.

[51] R. D. F. Ferreira and R. S. de Oliveira, "Cloud iec 61850 a case study of a software defined protection, automation & control system," in *2018 IEEE 23rd International Conference on Emerging Technologies and Factory Automation (ETFA)*, vol. 1. IEEE, 2018, pp. 75–82.

[52] Y. Ji, M. Yuan, Y. Huang, L. Huang, H. Wan, X. Liu, and Q. Li, "Design and development of intelligent substation cluster measurement and control device based on virtualization technology," in *2021 6th International Conference on Power and Renewable Energy (ICPRE)*. IEEE, 2021, pp. 401–406.

[53] Q. Wang, Z. Bo, Y. Zhao, Y. Zhu, L. Wang, X. Ma, and M. Zhang, "Novel protection & control architecture based on virtual devices in digital substation," in *2016 IEEE Power and Energy Society General Meeting (PESGM)*. IEEE, 2016, pp. 1–5.

[54] A. Rahman, O. Yilmaz, O. Vaze, and A. Mandal, "Smart substation control and protection facilitating the virtualization of multiple protection and control," in *2023 IEEE International Conference on Energy Technologies for Future Grids (ETFG)*. IEEE, 2023, pp. 1–6.

[55] J. Turnbull, *The Docker Book: Containerization is the new virtualization*. James Turnbull, 2014.

[56] D. Miller, J. Whitlock, M. Gardiner, M. Ralphson, R. Ratovsky, and U. Sarid, "Openapi specification v3. 1.0," https://swagger.io/specification/, 2022.

[57] “Erlang official homepage,” https://www.erlang.org, 2024.

[58] IEC/IEEE, “Part 118-1: Sychrophasor for power systems - Measurements (IEC/IEEE 60255-118-1),” https://www.iec.ch, 2018.

[59] IEC, “Part 9-2: Specific communication service mapping (SCSM) - Sampled values over ISO/IEC 8802-3 (IEC 61850-9-2:2011/A1:2020),” https://www.iec.ch, 2020.

[60] ——, “Part 9: Digital interface for instrument transformers (IEC 61869-9),” https://www.iec.ch, 2016.